VASCULAR MECHANISMS OF AD PATHOGENESIS:

THE PUTATIVE ROLE OF A DEFECTIVE BLOOD-BRAIN BARRIER, SERUM Aβ42, AND NEURON-BINDING AUTOANTIBODIES

by

HENYA GROSSMAN

A Dissertation submitted to the

Graduate School-New Brunswick

Rutgers, The State University of New Jersey

in partial fulfillment of the requirements

for the degree of

Doctor of Philosophy

Graduate Program in Psychology

written under the direction of

Louis Matzel, Ph.D.

and approved by

_____

_____

_____

_____

New Brunswick, New Jersey

October, 2010

ABSTRACT OF THE DISSERTATION

Vascular Mechanisms of AD Pathogenesis: *The Putative Role of a Defective Blood-Brain Barrier, Serum Aβ42, and Neuron-Binding Autoantibodies*

By HENYA GROSSMAN

Dissertation Director:

Louis Matzel, Ph.D.

Mounting evidence suggests that cerebrovascular damage may play a significant role in disease progression of AD, including findings demonstrating consistent morphological evidence of BBB dysfunction in AD brains. Furthermore, recent research has provided support for the critical contribution of intraneuronal accumulation of Aβ peptide to AD pathology. However, while several studies have indicated preliminary evidence that Aβ peptides in the AD brain may originate in the blood via chronic BBB leak, this source has not yet been directly and systematically tested. To address this possibility, we developed an experimental mouse model combining chronic application of pertussis toxin and introduction of soluble Aβ42 into the venous blood to empirically test whether long-standing disruption of BBB integrity can trigger the appearance of pathological features simulating AD. Mice dually exposed to pertussis toxin and soluble Aβ42 on a chronic basis were found to demonstrate clear evidence of perturbation of the BBB and manifested an associated cascade of pathological features, including extravasation of plasma Aβ42 and IgG and entry into the brain parenchyma, neuronal binding of IgG,

neuronal as well as synaptic Aβ42 binding, and intracellular accumulation of Aβ42. Importantly, regional deposition and intracellular internalization of Aβ42 conformed to a selective pattern of distribution analogous to human AD and was generally co-localized with regions of neuronal IgG binding, suggesting that the two may be mechanistically linked, as well as markers of astrocytic activation and subtle signs of dendritic and synaptic degradation suggesting early inflammatory and adverse neuro- functional repercussions of neuronal deposition of Aβ42 and IgG. With respect to cognitive functioning, animals subjected to this manipulation displayed a pattern of variable disruption of the acquisition of learned behaviors, a more consistent and preferential deficit in the capacity for long-term retention, and an increased susceptibility to interference in selective attention. Regarding unlearned behaviors, treated animals exhibited a mild up-regulation of emotionality and altered stress reactivity. Taken together, neuropathological sequelae of BBB disturbance converge with those manifested in the behavioral and cognitive domains, in corresponding to a common, emergent, phase of AD- like pathology. Collectively, these results indicate that chronic disruption of the BBB and the resulting influx of exogenous Aβ42 and anti-neuronal autoantibodies from the blood can mimic the pathological events of AD, and thus provides compelling evidence implicating the blood as a likely source of amyloid that deposits in AD brains via chronic BBB dysfunction and anti-neuronal autoantibody-induced endocytosis as a likely means of entry into neurons.

ACKNOWLEDGEMENTS

I would like to thank the members of my dissertation committee, Dr. Robert Nagele, Dr. Tracey Shors, and Dr. Alexander Kusnecov, for their time and helpful suggestions. In particular, I am especially grateful to Dr. Robert Nagele for his valuable guidance, and to my advisor, Dr. Louis Matzel, for his constant encouragement, and, above all, for always challenging me to think critically about the design and interpretation of experiments and about science in general.

TABLE OF CONTENTS

LIST OF FIGURES

GENERAL INTRODUCTION:

Alzheimer's disease (AD) is a neurodegenerative disorder characterized by widespread destruction of neurons and their synapses in the cerebral cortex, entorhinal area, hippocampus, ventral striatum and basal forebrain resulting in a loss of memory and eventual dementia (Braak and Braak, 1991; Felician and Sandson, 1999). This condition is accompanied by a number of pathological features, including reactive gliosis, inflammation, amyloid plaques (APs) and neurofibrillary tangles (NFTs) in the brain parenchyma. Among these, the latter two are considered to be pathognomic and constitute a collective hallmark of this disease. These changes in the brain are associated with a progressive, severe decline in cognitive functioning that is initiated and dominated by a striking deterioration of memory function. Recent increases in the average lifespan have led to a dramatic rise in the incidence of AD, with an incidence approaching 40% in individuals over the age of 85 years, in an illustration of the fundamental link that is repeatedly evidenced between aging and this disease (Hebert et al., 2003).

In an attempt to determine the pathogenic course of AD and ascertain which pathological features are responsible for driving its development, investigations have addressed a range of potential factors such as neuropathological components including amyloid plaques and NFTs, neuroinflammation, and vascular pathology. While this question is hotly contested, spawning a plethora of conflicting theories, one recurring theme that is common to many theories concerns the prominence and therefore likely role of the β amyloid (Aβ) peptide in the pathogenesis of this disease. Thus, despite differences in specific mechanisms proposed, a pivotal role for these peptides in

development of AD has become accepted among many (LaFerla et al., 2007, Hardy & Selkoe, 2002). Amyloid plaques principally contain amyloid $\beta_{1\text{-}42}$ (Aβ42), a self-assembling peptide composed of 42 amino acid residues. This Aβ peptide is derived from cleavage of the amyloid precursor protein (APP) through the combined, sequential actions of β - and γ-secretases, which comprise one of two competing alternative pathways of APP processing known collectively as the amyloidogenic pathway (Koo and Squazzo, 1994; Wilson et al., 1999). This pathway produces two forms of Aβ42: $\beta\text{-A}_{40}$ (Aβ-40) a shorter peptide that is much more prevalent in the healthy human brain (~90%), and $\beta\text{-A}_{42}$ (Aβ-42), the form that has been implicated in AD pathology, in which 2 additional amino acids impart the ability to oligemerize more readily and thereby give rise to the pathogenic qualities of Aβ (Verdile, 2004). Processing of APP and production of the Aβ peptides is regulated in part by presenilins, transmembrane proteins that function as a part of the γ-secretase protease complex, which help determine which form of Aβ is produced (Verdile, 2004). The localization of AD-causing genetic mutations to genes expressing APP, presenilin 1 (PS1) and PS2, all of which confer their pathogenic effects by promoting increased production or accumulation of Aβ42, has prompted the view that accumulation of Aβ peptides is a primary factor in AD pathogenesis (Hsiao et al., 1996; Price et al., 2000; Hardy et al., 1992; Oddo et al., 2003). This notion was supported as well by the localization of the APP gene to chromosome 21 (Schellenberg et al., 1992), in the context of AD neuropathology manifesting in individuals with trisomy 21 (Down Syndrome; Heston, 1977). Thus, increased production of Aβ42 and its deposition in the brains of patients with early onset, familial AD caused by mutations in APP and presenilin genes as well as in certain transgenic

mice have confirmed correlations among expression of these genes, Aβ42 levels, formation of plaques and cognitive deficits in both AD patients and older transgenic mice (Games et al., 1995; Citron et al., 1997; Moechars et al., 1999; Oddo et al., 2003; Heston, 1977). In particular, correlations have been observed between the distribution of amyloid plaques, synaptic loss and degenerating neurons, as well as between Aβ42 levels and severity of dementia (Hsiao et al., 1996; Johnson- Wood et al., 1997; Nalbantoglu et al., 1997). The key role of peptides has been corroborated by work on transgenic mice which overexpress both mutant human tau as well as mutant human APP, in which these mice exhibited expedited and increased formation of tau-positive NFTs , coupled with largely unaltered amyloid deposition (Selkoe, 1998; Oddo et al., 2003). A potential mechanism for the influence of amyloid on NFT development was illustrated in studies in which it was explicitly demonstrated that injection of amyloid into cells led to hyperphosphorylation of tau, resulting in its aggregation and NFT formation through a number of specific signaling pathways, including MAPK, MASK, and tck-5 (Rank et al., 2002; Ferreira, 1997). All of these studies underscore the incidence of a phenomenon in which increased Aβ42 peptide production and/or an age-dependent accumulation of this material result in pathology and cognitive deficits resembling AD.

Despite these efforts, however, the precise nature of the contribution of Aβ42 to the disease process remains elusive, warranting the need for further research to determine whether it is extracellular Aβ42 deposition and/or intracellular Aβ42 accumulation that initiates the disease process. In particular, the means by which Aβ42 is deposited within plaques and consequently the putative contribution of these plaques to AD pathogenesisis largely unresolved and controversial. In the prevailing theory known as the amyloid

cascade hypothesis, it is posited that plaques arise from gradual, extracellular deposition of Aβ42 at "seeding sites" in the brain parenchyma and lead to a series of events that culminate in synaptic and neuronal destruction (Younkin, 1995; Selkoe, 1998). According to this theory, genetic and environmental influences (i.e. APP, PS1 and PS2 mutations) cause a dysregulation in APP processing resulting in an over-production and accumulation of the Aβ42 peptide, which coalesce into deposits of loosely arranged peptides known as diffuse plaques (Verdile, 2004). The formation of these plaques is hypothesized to result in a sequence of pathological events, initiated with an inflammatory response consisting of microglial activation and cytokine release, astrocytosis, acute phase protein release and complement activation. These in turn lead to oxidative stress and damage, and disruption of neuronal and metabolic functioning. Subsequently, tau, which is normally present in an unphosphorylated or phosphorylated state and regulates microtubule formation and stability, becomes hyperphosphorylated. This causes it to accumulate, aggregate, and form neurofibrillary tangles, while the cellular microtubules are depolymerized and disrupted, ultimately leading to neuronal degeneration and resulting disruption of synaptic transmission, and eventual widespread synaptic and neuronal loss. These changes result in increasingly profound cognitive impairment, as there is a progressive breakdown in synatic transmission, followed by neuronal death, which manifest collectively as dementia (Verdile, 2004).

However, more recently, a growing number of researchers have challenged this theory and begun to shift attribution for initiation of this cascade of events from extracellular amyloid plaques to intracellular accumulation of Aβ42. In contrast to the

classic ascription of AD pathogenesis to amyloid plaques, they credit the former alternatively to the actions of soluble Aβ42 located within individual neurons of the brain and regard the appearance of amyloid plaques as a secondary event in the development of AD. Mounting evidence from a number of studies demonstrates that a substantial amount of Aβ42 accumulates intracellularly in neurons of AD brains and in mutant transgenic mice overexpressing AD-relevant genes older than 12 months (Chui et al., 1999; Gouras et al. 2000; D'Andrea et al., 2001; Nagele et al., 2002). Investigations in AD-relevant transgenic mice have revealed that intraneuronal Aβ42 accumulation invariably precedes the appearance of plaques and temporally coincides with loss of synapses, the appearance of cognitive deficits and, in a triple transgenic mouse model characterized by overexpression of mutant tau, APP, and presenilin (i.e., 3xTg-AD), the development of tangles (Oddo et al., 2003; 2006). Parallel to this, a number of studies have demonstrated that intraneuronal Aβ42 accumulation precedes plaque formation, particularly in early stages of AD, and primarily targets pyramidal neurons in the cerebral cortex and hippocampus (D'Andrea et al., 2001; Nagele et al., 2002; Wang et al., 2004). Importantly, one study has shown an inverse correlation between synaptic density and intraneuronal levels of Aβ42 in APP transgenic mice and in brains from individuals with AD (Lue et al., 1999). Other studies have demonstrated that exposure to soluble Aβ42 induces oxidative stress, electrophysiological changes indicative of neuronal injury, and inhibition of LTP in neuronal cells (Walsh et al., 1999; Hartley et al., 1999). Thus, converging evidence from these studies indicates that massive intracellular deposits of Aβ42 can accumulate selectively in certain neuronal subtypes prior to the appearance of amyloid plaques in AD patients, individuals with Down syndrome, and AD-relevant

transgenic mouse models. Collectively, this body of evidence suggests that intraneuronal Aβ42 accumulation is likely an early, crucial step in a disease process that eventually leads, either directly or indirectly, to neuronal and synaptic loss, the appearance of amyloid plaques and neurofibrillary tangles and associated neurological sequellae. Based on this, some researchers have proposed that the gradual deposition of Aβ42 within vulnerable neurons might progressively impair the ability of these cells to structurally and functionally support their extensive dendrite arbors and synapses, thus precipitating a dendrite collapse that ultimately leads to deterioration of cognition and memory (Nagele et al., 2002). Nevertheless, very little has been conclusively ascertained thus far concerning how and why Aβ42 accumulates selectively in certain types of neurons, why aging predisposes these neurons to do so, and how this accumulation might induce its potential effects on neuron structure and function.

Several studies have demonstrated that regions in AD brains with abundant intracellular Aβ42 accumulation exhibit signs of neuronal lysis, leading to dissemination of the formerly *intra*cellular Aβ42 among other cytoplasmic contents into the surrounding extracellular compartment, from which amyloid plaques are formed (D'Andrea, 2001; Bahr, 1998). Together with numerous cytoplasmic proteins, lysosomal enzymes, and neuronal mRNAs within plaques, a nuclear remnant has been found at the dense core of many of these plaques, providing evidence that each amyloid plaque represents the end product of a single neuronal cell lysis (D'Andrea et al., 2001). This possibility is further suggested by the restriction of amyloid plaques to regions of pyramidal neurons with excessive Aβ42 accumulation, the inverse relationship between amyloid plaque density and pyramidal neuron density in regions of the AD brain, and the

absence of amyloid plaques in brain regions which lack neuronal perikarya (D'Andrea et al., 2001). Additional support for this possibility is derived from the close relationship between the size of amyloid plaques and the size of surrounding pyramidal neurons, as well as the finding that cells that show signs of undergoing recent lysis manifest selectively in brain regions containing amyloid plaques as well as neurons with excessive intracellular Aβ42 (D'Andrea et al., 2001). Taken together, these findings suggest that neurons and activated astrocytes burdened with excessive Aβ42 accumulations eventually undergo lysis, which results in the radial dispersal of their cytoplasmic contents, including accumulated Aβ42, into the surrounding extracellular space, and that this leads to formation of a single, spherical dense-core plaque containing Aβ42 in the place previously occupied by a neuron (D'Andrea et al., 2001; Nagele et al., 2002; 2003; 2004). This also likely represents a mechanism of neuronal loss that occurs in AD, contributing to the prevalence of the latter in AD brains, and accounts for the inverse correlation that has been found between intracellular and extracellular Aβ42 in brains of individuals with Down syndrome (Mori et al. 2003).

Although this provides an account for the formation of amyloid plaques that demonstrates their likely derivation from intracellular Aβ42 and supports the possibility of a more central and primary role for the latter in driving AD pathogenesis, the original source and mechanism for initial accumulation of Aβ42 in the neuronal cell is not addressed by these findings. Thus, it is not clear from this account whether Aβ42 initially accumulates within neuronal cells through entry of extracellular Aβ42 into pyramidal neurons, or as a result of de novo production of Aβ42 and its gradual accumulation inside pyramidal neurons. Although several studies have suggested that

Aβ42 can accumulate in neurons gradually through slow intraneuronal production,a number of findings in other studies (e.g. Nagele et al., 2003, D'Andrea et al., 2001) favor the latter possibility. In particular, the reported prevalence of uniformly small granules in which Aβ42 and cathepsin D are co-localized within pyramidal cells of brain regions with low amyloid plaque density (presumably representing an earlier stage of AD pathogenesis) in one study (D'Andrea et al., 2001) indicates that Aβ42 first selectively accumulates in the perikaryon of pyramidal cells as discrete granules that likely represent lysosomes. This finding highlights the probable existence of an entry mechanism for Aβ42 into pyramidal cells that entails endocytosis, which by definition implies that the origin of at least some of the Aβ42 that accumulates within cells is extracellular. This type of mechanism would require that Aβ42 possesses binding affinity for a receptor or other surface protein that is found on the plasma membranes surrounding the perikaryon and/or dendritic tree of pyramidal neurons.

A potential candidate was provided by a recent series of studies which revealed that Aβ42 binds with high affinity to the alpha-7 nicotinic acetylcholine receptor (α7nAChR), suggesting the possibility that binding to this receptor may play a key role in intracellular accumulation of Aβ42 and the ensuing pathological events, particularly in the context of the prevalence of these receptors in pyramidal cells which are especially involved in AD neuropathology (Wang et al., 2002; Nagele et al., 2003; D'Andrea and Nagele, 2006). Other studies have supported this possibility by demonstrating that substantial intraneuronal Aβ42 accumulation is restricted to cells that express relatively high levels of the α7nAChR, and that α7nAChR is consistently co-localized with

intracellular Aβ42 both within the perikaryon of neurons in AD brains and the cytoplasm of α7nAChR-transfected cultured cells (Nagele et al., 2002). In addition, transfected neuroblastoma cells that express elevated levels of this receptor were shown to exhibit more rapid binding, internalization and accumulation of exogenous amyloid Aβ42, which actions were subsequently blocked by alpha-bungarotoxin (BTX), a selective α7nAChR antagonist (Nagele et al., 2002). Converging with this, exposure to Aβ42 resulted in rapid depletion of cell surface-associated α7nAChR and a redistribution of this receptor to intracellular Aβ42-positive deposits (Nagele et al., 2002). Overall, these results provide strong support for the notion that the high affinity interaction between α7nAChR and Aβ42 may be an important early step leading to gradual accumulation of Aβ42 and subsequent neurodegeneration in neurons of AD brains. By concentrating soluble Aβ42 in the brain parenchyma on the surfaces of neurons that are abundantly endowed with this receptor, this interaction may provide a gateway for Aβ42 entry into neurons and facilitate internalization and selective pathological accumulation therein (Wang et al., 2000; Nagele et al.,2002; Wang et al., 2002).

While this provides a potential route via which Aβ42 can be internalized from the extracellular environment, it remains unresolved where in the extracellular environment Aβ42 originates. One potential source, suggested by levels of Aβ42 normally present in healthy individuals, is the blood. In normal healthy brains, the soluble Aβ peptide levels within the interstitial space and CSF are generally extremely low (Andreasen and Blennow, 2002; Seubert et al., 1992). In contrast, it is well established that Aβ40 and Aβ42 are present in the blood (Citron et al., 1994) at levels that are ten-fold greater than in the interstitial fluid of the brain and in the CSF (Ghiso et al., 1997), which increase

further yet with age (Ghiso et al., 1997). This disparity raises the possibility that the blood may serve as a source of exogenous soluble Aβ peptides that eventually accumulate within neurons and deposits in the AD brain (Zlokovic et al., 1993). This possibility is suggested as well by reports of subsequent development of amyloid plaques in the direct vicinity of brain injuries that result in bleeding (de la Torre, 2001). Furthermore, cerebral amyloid angiopathy, a condition that involves increases in plasma levels of Aβ peptides and deposits of amyloid in the neurovasculature, is frequently co- morbid with AD (Verdile et al., 2004). Interestingly, while plasma Aβ40 and Aβ42 levels are elevated in some patients during earlier stages of AD, they usually decline thereafter (Mayeux et al., 2003). In accordance with this possibility, a number of studies have provided evidence that the blood can contribute Aβ peptides to the brain (Deane et al., 2004; Zlokovic, 2004, 2005). However, in order to be plausible, this scenario would require a compromise in integrity of the blood-brain barrier (BBB) in AD patients, given that access of blood-borne Aβ peptides to brain tissue under normal conditions is effectively blocked by the integrity of the blood–brain barrier (BBB) (Kandimalla et al., 2005; Poduslo et al., 1999).

Importantly, in light of the growing body of evidence ascribing to AD a robust link with and possible origin in cerebrovascular disease, this latter possibility is particularly compelling. Thus, epidemiologic studies have demonstrated that nearly all of the reported risk factors in AD are common to vascular dementia (VaD) as well, all of which share a mutual theme of vascular dysfunction, particularly cerebral hypoperfusion and/or impaired vascular nitric oxide, suggesting that the presence of such vascular-related risk factors in the elderly tends to reduce cerebral blood flow to a level that may ultimately generate metabolic, cognitive and eventually neurodegenerative changes in the

brain (Breteler, 2000; Buee et al., 1997; Kalaria et al., 1996). Furthermore, evidence that cerebral infarction increases the incidence of AD by 50% when compared with non-stroke subjects, and that chronic cerebral hypoperfusion and oxidative stress can trigger hypometabolic, cognitive and neurodegenerative changes characteristic of AD, lends support to a cerebrovascular role in AD pathology (de la Torre, 2004). This link is further attested to by the finding that preclinical detection of AD is reliably achieved through evaluation of regional cerebral blood flow and glucose uptake, observations of cerebrovascular pathology in nearly all AD brains, and evidence of parallel cerebrovascular and neurodegenerative pathologic markers including amyloid plaques and neurofibrillary tangles in both AD and VaD brains post-mortem (de la Torre, 2004; Kalaria et al., 1996). Consequently, on the basis of this converging evidence, it has been proposed that at least some forms of AD may develop primarily from cerebrovascular changes (de la Torre, 2004).

In particular, one crucial anticipated consequence of these changes would likely be a compromise of BBB integrity; consistent with this, there is an array of evidence documenting the presence of a compromised blood brain barrier in AD. For example, immuno-histochemical analyses of post-mortem human brain tissues in a recent study (Clifford et al., 2007) illustrate that extravasation of plasma components including Aβ42, IgG and complement C1q from the microvasculature is extremely common in AD brains, as demonstrated by the presence of perivascular leak clouds, in contrast to age-matched controls. In a similar fashion, in vivo studies examining the ratio of CSF albumin to serum albumin have demonstrated a significant perturbation in this ratio which correlates with the severity of the dementia, providing evidence that BBB breakdown is common in

the brains of living AD patients (Skoog et al., 1998; Wada, 1998). Consistent with a putative role in driving development of AD pathology, increased BBB permeability has been demonstrated early in the progression of the disease in humans, and prior to amyloid plaque formation in Tg2576 mice (Skoog et al., 1998; Ujiie et al., 2003). Collectively, these findings indicate that defects in the BBB are associated with AD, providing a potential mechanism by which Aβ peptides circulating in the blood but normally barred from the brain could enter into the interstitial spaces of the brain and access neurons, possibly allowing internalization therein. In a recent study which examined this possibility more directly (Clifford et al., 2007), fluorescein isothiocyanate-labeled Aβ42 and Aβ40 were introduced via a single bolus tail vein injection into mice with a BBB rendered permeable by treatment with pertussis toxin. Both Aβ40 and Aβ42 readily penetrated the defective BBB and bound selectively to certain neuronal subtypes. Several days following treatment, Aβ42-positive neurons were found in the brain (e.g., particularly among pyramidal neurons in the cerebral cortex), in a very limited subset of which Aβ42 was detected in granules located within the cellular cytoplasm, suggesting that exogenous Aβ42 can be internalized within the same subtypes of neurons that are overburdened with large intracellular Aβ42-rich deposits in human AD brains. By contrast, these actions were blocked by an intact BBB in saline-injected controls. In view of the high incidence of blood-brain barrier compromise in AD patients, these results provide considerable support for the possibility that the blood serves as a source of the soluble, exogenous Aβ that accumulates within neurons and eventually amyloid plaques in AD brains (Clifford et al., 2007), although their predictive capacity is limited by the lack of chronicity in BBB breakdown induced in this study.

Nevertheless, despite implication of blood serum as a potential source of soluble Aβ42 in AD and its high affinity binding to α7nAChR as a potential route of intracellular internalization, little is known about the precise mechanism by which Aβ42 internalization might occur subsequent to α7nAChR binding. One possibility is suggested by results of previously described studies which point to a lysosomal origin of the intracellular granules in which Aβ42 is located, alluding to an initial endocytotic entry into the cell (Nagele et al., 2004). This possibility is further supported by observations that blockade of Aβ42 accumulation in α7nAChR-transfected SK-N-MC cells by pre-treatment with PAO, an inhibitor of endocytosis, indicating that the entry mechanism by which this binding results in Aβ42 internalization appears to be endocytosis (Nagele et al., 2004). However, despite evidence pointing to this mechanistic possibility, the identity of potential triggers of endocytosis remains unknown.

Given that binding of antibodies to cells is known to trigger internalization of antibodies through endocytosis (He et al., 1998; Noseworthy et al., 2000), one interesting possibility is suggested by the recent discovery of binding of immunoglobulin (Ig) to the surfaces of the same cortical neurons that exhibit AD pathology. In the context of the known endocytotic actions of neuron-bound Ig, this finding raises the prospect that the presence of neuron-binding Ig in AD may contribute to AD pathogenesis by facilitating Aβ42 internalization (D'Andrea, 2003). In a recent study (Nagele et al, 2010), this possibility was further explored by using human IgG as a primary antibody for immunohistochemistry on sections of AD brains, allowing for detection of anti-neuronal antibodies in human sera. Neurons were found to be intensely immunostained, with selective Ig binding in a subset of individuals restricted to the same neurons in the

hippocampus, entorhinal cortex and temporal cortex that are vulnerable to AD-related pathological changes, particularly those prone to intracellular accumulation of Aβ42**.** Immunoprecipitation and Western analyses of sera and solubilized brain fractions from AD brains revealed that one target of these autoantibodies is the GluR2 subunit of the AMPA receptor complex, which has been shown to be a double-stranded (ds) DNA molecular mimic. This autoantibody has already been linked to profound memory and cognitive decline often exhibited in elderly patients with systemic lupus erythematosus (DeGiorgio et al., 2001; Kowal et al., 2004).

Based on these studies, it appears that these and other neuron-binding antibodies may be present in the blood throughout life, and that their access to the brain parenchyma may be generally restricted by the integrity of the blood-brain barrier in normal healthy individuals. However, in aged individuals who have undergone changes in vasculature associated with vascular disease, the integrity of the blood-brain barrier is likely to be compromised, conferring access to the brain parenchyma to these neuron-binding antibodies and thereby potentially allowing them to subsequently play a key role in disease pathogenesis. Thus, the prevalence of these neuron-binding antibodies in the blood may account for the observed abundance of neuron-bound Ig in AD brains. Based on results of these studies, individuals with specific neuron-binding autoantibody profiles (i.e. resulting in selective binding to neurons that accumulate intracellular Aβ42), may generally be more at risk for AD than are those lacking these autoantibodies, given the potential role of the latter in AD pathogenesis.

The apparent specificity of these antibodies for targeting the same neurons that also exhibit AD-related pathological changes (e.g., intraneuronal Aβ42 accumulations

and cell death) has led to the suggestion that binding of these antibodies to neuronal cell surfaces may contribute to events at neuronal cell surfaces leading to internalization of surface-bound Ig and Aβ42, by initiating an endocytotic process in target cells that is aimed at clearing bound Ig from their surfaces. Specifically, it is postulated that this Ig-induced clearance mechanism may result in the passive deletion of other cell surface membrane components, including membrane proteins and receptors as well as cell surface-bound Aβ42, resulting in internalization of the latter into the cell. The proposed combination of chronic and excessive Aβ42 deposition within neurons and the continuous cell surface receptor stripping due to enhanced endocytic activity might account for common symptoms of memory and cognitive loss (e.g., mild cognitive impairment) in AD patients that precede considerable amyloid plaque formation and significant synaptic and neuronal degeneration. In support of this possibility, a recent study (Nagele et al., in preparation) demonstrated that Ig derived from individual human sera that intensely immunolabel neurons in sections of AD brain tissue also promote internalization of exogenous Aβ42 in neurons *in vitro* in mouse organotypic brain slice cultures and *in vivo* in mouse brains subjected to stereotaxic injections of human serum with or without purified Aβ42 peptide. Thus, in light of these actions of Ig, specific profiles of neuron-binding autoantibodies (i.e., resulting in selective binding to neurons that accumulate intracellular Aβ42) may play a pivotal role in executing the above theorized chain of pathogenic events in AD. Based on the combination of previously described findings, it is proposed that one potential route of pathogenesis of AD, particularly in patients that exhibit concomitant symptoms of vascular disease, may entail the combination of two processes: A) a compromised blood-brain barrier enabling chronic access of neuron-

binding autoantibodies and soluble exogenous Aβ42 to selective brain neurons and B) neuronal binding of these autoantibodies triggering and/or facilitating the internalization and accumulation of cell surface-bound Aβ42 in vulnerable neurons via their natural tendency to clear surface-bound autoantibodies through endocytosis.

To address this possibility, the following study was designed to investigate the pathological and cognitive consequences of a chronically compromised BBB coupled with entry of Aβ42 (i.e., and accompanied by other associated plasma components including autoantibodies) into the brain parenchyma. In examining these potential consequences and whether they are linked, emphasis was given to elucidating the putative role of the latter phenomena as an aging-linked trigger which can drive the observed intraneuronal accumulation of Aβ42 that is endemic to AD brains. In order to test empirically whether this combination of senescence-dependent events can account for the development of AD pathology, an experimental animal model was developed in which emergently senescent animals were chronically treated with pertussis toxin to compromise the integrity of their BBB, in concert with repeated venous introduction of soluble Aβ42 to augment their serum reserves of Aβ42. In three separate control groups, injections of saline, pertussis toxin alone or Aβ42 peptide alone were administered.

Following treatment, animals were assessed cognitively and histopathologically to ascertain whether these potentially pathogenic manipulations resulted in manifestation of neuropathological features and cognitive deficits associated with AD pathology. In addition to helping determine the likelihood of these proposed pathogenic mechanisms, this approach afforded the collateral and unprecedented benefit of illuminating the impact of BBB compromise on cognitive and/or behavioral function. Thus, animals were

subjected to a range of cognitive tasks relying on distinct neural systems as well as a number of unlearned measures of sensory/motor function, general locomotion, exploration and anxiety tasks to rule out potential confounds. Following completion of behavioral testing, the presence of neuropathological features was assayed as well, to facilitate investigation of the putative contribution of the latter to behavioral and/or cognitive alterations characteristic of AD as potentially triggered by the above pathogenic processes.

MATERIALS AND METHODS:

Subjects:

A sample of 48 male CD-1 mice (Harlan Sprague Dawley) were ~10 months old at the start of experimentation. Animals were assigned to each of four experimental groups controlling for body weight, with 20, 8, 12, and 12 mice assigned respectively to groups treated with combined pertussin toxin (PT) and Aβ42, solely Aβ42, solely PT, or saline, according to treatment conditions described below. Animals were trained and tested in four independent replications (n = 13), each of which was generally comprised of roughly equal numbers of animals from each group. Two of these replications were separated by two days and run concurrently through behavioral testing, following the completion of which the remaining two groups were run concurrently, and again separated by two days. For some tests, the number of mice was reduced because of two mortalities and, in several instances, apparatus malfunction. Animals were acclimated to our laboratory for 7 days prior to the initiation of any treatment, and were handled for 90 sec/day during this period. This handling ensured that differential stress responses to the experimenters, and any associated effects on learning were minimized. Animals were individually housed in clear boxes with floors lined with wood shavings in a humidity- and temperature-controlled vivarium adjacent to testing rooms. A 12hr/12hr light/dark cycle was maintained.

Drug Treatment:

In four separate groups, tail vein injections of saline; PT and saline; Aβ42 peptide and saline; or Aβ42 peptide and PT were administered according to the following time intervals and concentrations for each of these respective treatments. In order to

effectively achieve lesioning of the BBB, two groups of mice, (i.e., mice exposed to PT and Aβ42 or, in a corresponding control, to PT and saline), were treated with PT (300 ng in 100 μl 0.9% saline) for 3 months via tail vein injection, which has been demonstrated to induce BBB compromise reliably in prior work (Clifford et al., 2007). Comparable to previous protocols, injections occurred on days 0, 3, 17, 33, 47, 61, and 75 of the 3 month injection period. To augment plasma reserves of Aβ42, soluble Aβ42 peptide was administered via tail vein injection (100 microliters of 6.9 micromolar in 0.9% saline;), which according to previous protocols occurred on days 7, 11, 14, 18, 21, 25, 28, 32, 35, 39, 42, 46, 49, 53, 56, 60, 63, 67, 70, 74, 77, 81, 84, 88, 91, and 95 during the same 3 month period, in a series that generally followed up each individual PT treatment with 4 consecutive Aβ42 treatments. Given inherent levels of Aβ42 peptide present in mice, which under conditions of BBB breach can potentially enter the brain parenchyma and bind to neurons, a subset of PT- Aβ42 treated mice (n=12) were treated with a form of Aβ42 conjugated to a fluorescent moiety, fluorescein isothiocyanate (FITC) so as to permit direct tracking of the fate of injected Aβ42 and to distinguish injected Aβ42 from that which may be inherently present in the mouse throughout the course of the treatment. In the remaining subset of mice dually treated with PT and Aβ42 (n=8), animals were administered unlabeled Aβ42 peptide to verify the validity of findings observed with FITC-labeled Aβ42 and to address the possibility that the addition of the FITC moiety to the Aβ42 peptide might somehow modify its behavior and/or fate in the animal. Controls for Aβ peptides and for pertussis toxin were injected with similar volumes of saline (100 μl of 0.9% saline) with or without Aβ peptides. Following completion of one month of treatment, behavioral testing was initiated.

Prior to administering, Aβ peptides (Fluorescein isothiocyanate (FITC)-labeled Aβ42, Anaspec, San Jose, CA; unlabeled Aβ peptides, Biosource, Camarillo, CA) were solubilized to the monomeric form according to the method described by Zagorski et al. (1999). Briefly, Aβ peptide was solubilized (1 mg/ml) in trifluoroacetic acid (TFA), followed by removal of TFA under a slow, steady stream of N2(g). This was followed by three sequential solubilizations in 1,1,1,3,3,3-hexafluoroisopropanol (HFIP) followed by removal of HFIP under N2(g) each time. Stock solutions (50.0 μM) were prepared in 0.5× PBS, 250.0 mM HEPES buffer, pH 8.5. Working solutions were diluted in 0.9% NaCl to 6.9 μM and used for tail vein injection. Protein concentrations were confirmed using the Pierce Micro BCA Assay (Rockford, IL). Working solutions of PT (Sigma-Aldrich, St. Louis, MO) were diluted in 0.9% saline to 3.0×10−3 μg/μl prior to use in tail vein injection. Protein concentrations were confirmed using the Micro BCA Assay (Pierce; Rockford, IL).

Behavioral Training and Testing Procedures

Animals were trained and tested in four separate replications. All animals were tested on four learning tasks (passive avoidance, Lashley Maze, spatial water maze, and odor discrimination; see a detailed description, below) and 12 measures of unlearned performance and fitness. The learning tasks were explicitly designed and included in the test battery so as to impinge on different sensory, motor, motivational, and information processing systems. In our previous work, five learning tasks were used to assess the general learning abilities of individual animals (Matzel et al., 2003); here, a subset of four learning tasks was selected for use, with the addition of an independent cognitive task assessing selective attention abilities. Animals were first tested in an open field to

assess activity and exploratory tendencies, followed by testing in four learning tasks initially assessing acquisition and subsequently long-term retention (i.e., with the latter occurring after completion of initial acquisition in all tasks), a test of selective attention, and lastly, on all remaining tasks designed to assess sensory and motor function, stress and pain reactivity, fear, and additional exploratory tendencies. Between each successive test of learned behaviors, animals received a day of rest.

Tests of Unlearned Behaviors and Sensory/Motor Function:

Each of the following tests was administered with one day intervening between the completion of one test and the start of the subsequent test. Open field testing was conducted two days prior to the start of tests of learning; all other tests were administered beginning two days after the completion of the tests of learning. In all but several instances, tests of unlearned behaviors and sensory/motor function were completed in a single day. Many of the tests yielded several different measures of performance such that seven variables were assessed that are relevant to balance, strength, coordination, general activity, pain sensitivity, anxiety, stress reactivity, and exploratory tendencies. The apparatus and parameters that are described below were chosen based on pilot work in which they were determined to be adequate to capture variations in performance between animals. As most of these tasks are in common use, detailed descriptions of apparatus are provided only in those instances where the task or dependent variable is novel. The tests were conducted in the following order: rod suspension, pain sensitivity, balance beam, dark/light test, shock-induced freezing.

Measures of Motor Strength/Coordination:

1. *Balance Beam.* Animals were placed on a 40 x 0.7 x 2 cm (l x w x h) beam

suspended 30 cm above the ground. Movement along the beam is the variable of interest, in addition to latency to fall, as movement is presumed to interact with balance. In a 4 min test, mice exhibited wide variability in the amount of movement along its length.

2. *Rod Suspension.* Animals were hung from their front paws from a 4 mm rod coated with black rubber (shrink tubing). The rod was suspended 30 cm above ground. Latency to drop from the rod (an index of grip strength) was recorded.

Measure of Anxiety and Stress Reactivity:

Shock-induced freezing. Freezing after the offset of an unsignaled shock is often interpreted as a measure of fear. Mice were acclimated for 20 min to a 25-cm square chamber (60 Lux) with a stainless steel grid floor. On the subsequent day, they were returned to the chamber, where after 10 min a 0.6-mA, 500-ms constant-current scrambled footshock was administered through the floor. The shock was delivered on the command of the experimenter, who initiated the shock when each subject was located near the center of the chamber with all paws on the grid floor. Using this method, the actual delivery of the shock typically occurred between 10–10.5 min. During, and for a brief time (500 ms) following the shock, the mice exhibit a burst of activity, after which they exhibit freezing, a presumed index of fear. Mice were assessed for the amount of movement (number of grid squares crossed) exhibited in a period of 20 s following the shock as a function of the amount of movement (number of grid squares crossed) exhibited in the 20 s prior to the shock. In addition, the duration of freezing (the latency for the rear paws of the mice to move 20 cm) served as a dependent variable.

Measure of Pain Sensitivity:

Hot plate. Upon being placed on a 52.6° C aluminum plate, animals' latency to

raise a hind paw and to either lick or shake the paw serves as the index of pain sensitivity.

Measures of General Activity, and Exploration:

1. *Open Field Exploration*. A square field (46 x 46 cm) with 13 cm high walls was constructed of white Plexiglas and located in a brightly-lit room (400 Lux) with a background noise of 65 dB_c. The field was conceptually divided into a grid comprised of 6 x 6 7.65 cm quadrants, where 20 of the quadrants abut the outer walls of the field (i.e., "wall" quadrants), and 16 quadrants are displaced from the walls and comprise the interior (i.e., "open" quadrants) of the field. Animals were placed in the center of the field. After 20 sec elapsed (during which the animals self-select a starting location), the animals' behavior was monitored for 4-min. Throughout this time the animal's entries into walled and open quadrants were recorded. An entry was recorded whenever both front paws cross the border of a quadrant. Both total activity (i.e., quadrant entries regardless of category) was recorded as was the percentage of entries into unwalled (open) quadrants of the field. Lastly, the bolli deposited by each animals was recorded as a potential measure of emotionality. It should be noted that a 4-min test was explicitly chosen (based on pilot work) because changes in behavior (e.g., that which accompanies habituation) were *not* detectable over time. Thus we presume that open field performance is most sensitive to *unlearned* behavioral tendencies.

2. *Dark/ Light Test.* A 10 X 36 chamber divided along its length into two equal-sized compartments was utilized. One compartment was brightly lit (100 Lux), with a clear plastic top and white-lined bottom, and the other compartment was dim, with a dark plastic top and black-lined bottom. The two compartments were divided by a center wall with a 3 cm square opening that joins the dark and light compartments. Animals were

placed in the dark compartment of the chamber and allowed to explore for 4 minutes. Generally, entries into the brightly light compartment are considered aversive and stressful to mice, thus measures in this test provide indices of exploratory behavior similar to exploratory measures in the open field and elevated plus maze. The number of visits into the light compartment, i.e. crossings between compartments, and the percentage of time spent in this compartment have been shown to be the most reliable indices in this apparatus. These measures were assessed in the present test.

Tests of Cognitive Function.

The order of testing was designed so as to provide a temporal separation between any two tasks that are motivated by either food or water deprivation (to prevent excessive physical strain and to minimize any potential cross-task influences due to motivational factors). In addition, the testing order was designed to separate tasks based on similar processes or motor requirements (e.g. mazes of a similar nature, activity vs. passivity), again so as to minimize any potential transfer between tasks. All animals were tested in the following tests: Lashley maze, passive avoidance, odor discrimination, spatial water maze, selective attention.

Prior to testing on any task, the test chambers were "primed" by exposing two nonexperimental animals to the apparatus and procedures. This is intended to standardize the apparatus such that the first animals in a test cycle encountered a chamber that was nominally identical (e.g., in odor) to that experienced by subsequently tested animals.

The surfaces of every piece of apparatus were cleaned with a mild alcohol solution following removal of every subject from the apparatus, or between successive trials when multiple training/test trials were employed.

For the three learning tasks that require food deprivation, *ad lib* food was removed from the animals' home cages at the end of the light cycle approximately 40 hours prior to the start of training (and thus encompassing the "rest" day between successive tasks). During the deprivation period, animals were provided food in their home cages for 90 min/day during the last 2 hrs of the light cycle, and thus were approximately 16 hrs food-deprived at the time of training or testing. This deprivation schedule has been deemed "mild" (animals typically lost less than 8% of their free-feeding body weight during this period in previous experiments), but sufficient to maintain stable performance on these tasks. In the one task that requires water deprivation, the same schedule was followed except that free access to water will be limited to 60 min per day.

So that the time of day does not differentially impact animals' performance, all animals were trained and tested during the middle 7 hrs of the light cycle, and procedures were administered to animals with as little temporal dispersion as possible. All animals were trained and tested under nominally identical conditions.

Lashley III Maze. The Lashley III maze consists of a start box, four interconnected alleys, and a goal box containing a food reward. Over trials, the latency of rats to locate the goal box decreases, as do their errors (i.e., wrong turns or retracing). Here, the Lashley III maze was scaled for mice, and parameters have been developed that support rapid acquisition. The maze was constructed of black Plexiglas. A 2 cm wide x 0.1 cm deep white cup was located in the rear portion of the goal box, and 45 mg BioServe (rodent grain) pellets served as reinforcers. Illumination was 80 Lux at the floor of the maze. The maze is isolated behind a shield of white Plexiglas to prevent the

use of extra-maze landmark cues.

Food-deprived animals were acclimated and trained on two successive days. On the day prior to acclimation, all animals were provided with three food pellets in their home cages to familiarize them with the novel reinforcer. On the acclimation day, each mouse was placed in the four alleys of the maze, but the openings between the alleys were blocked so that the animals could not navigate the maze. Each animal was confined to the start and subsequent two alleys for 4 min, and for 6 min in the last (goal) alley, where three food pellets are present in the food cup. This acclimation period promotes stable and high levels of activity on the subsequent training day. On the training day, each animal was placed in the start box and allowed to traverse the maze until it reached the goal box and consumed the single food pellet present in the cup. Upon consuming the food, the animal was returned to its home cage for a 25 min interval (ITI), during which the apparatus is cleaned. After the ITI, the mouse was returned to the start box to begin the next trial, and the sequence repeated for five trials. Both the latency and errors (i.e., a turn in an incorrect direction, including those which result in path retracing) to enter the goal box were recorded on each trial.

To estimate capacity for long-term retention in this task, following a 30-day retention interval from completion of training, animals were placed in the start box and allowed to traverse the maze again for two trials. The ratio of errors on the first trial following the retention interval to average errors on the last two trials during acquisition training was calculated for each animal and served to index long-term retention in this task.

One-Trial Passive Avoidance. Animals learned to suppress movement to avoid

contact with aversive stimuli. This "passive avoidance" response is exemplified in step-down avoidance procedures, where commonly, an animal is placed on a platform, whereupon stepping off of the platform it encounters a footshock. Following just a single encounter with shock, animals are subsequently reluctant to step off of the safe platform. The animals' reluctance to leave the platform is believed to *not* reflect fear, because typical fear responses are not expressed in animals engaged in the avoidance response (Morris, 1974; Bolles, 1969). Upon stepping off the platform, animals were exposed to a compound of bright light and loud oscillating noise rather than shock, so as not to duplicate stimuli between tasks (see fear conditioning, below). Like more common procedures, our variant of this task supports learning after only a single trial (i.e., subsequent step-down latencies are markedly increased).

A chamber illuminated by dim (< 5 fc) red light was used for training and testing. Animals were confined to circular ("safe") chamber (10 cm diameter, 8 cm high). The walls and floor of this chamber were white, and the ceiling was translucent orange. The floor was comprised of plastic rods (2 mm diameter) arranged to form a pattern of 1 cm square grids. A clear exit door (3 CM square) was flush with the floor of the safe compartment, and the door could slide horizontally to open or close the compartment. The bottom of the exit door was located 4 cm above the floor of a second circular chamber (20 cm diameter, 12 cm high). This "unsafe" chamber had a clear ceiling and a floor comprised of 4 mm wide aluminum planks that formed a pattern of 1.5 cm square grids oriented at a 45^{o} angle relative to the grids in the safe compartment. When an animal stepped from the safe compartment through the exit door onto the floor of the unsafe compartment, the compound aversive stimulus comprised of a bright (550 Lux)

white light and "siren" (60 dBc above the 50 dB background) was initiated.

Animals were placed on the platform behind the exit blocked by the Plexiglas door. After 4 min of confinement, the door was retracted and the latency of the animal to leave the platform and make contact with the grid floor was recorded. Prior to training, step-down latencies typically range from 8-20 sec. Upon contact with the floor, the door to the platform was lowered and the aversive stimulus (light, noise, and vibration) is presented for 4 sec, at which time the platform door was opened to allow animals to return to the platform, where they were again confined for 5 min. At the end of this interval, the door was opened and the latency of the animal to exit the platform and step onto the grid floor (with no aversive stimulation) was recorded. The ratio of post-training to pre-training step-down latencies was calculated for each animal and served to index learning. It has been determined that asymptotic performance is apparent in group averages following 2-3 training trials; thus performance after a single trial reflects (in most instances) subasymptotic learning.

Odor Discrimination and Choice. Rodents rapidly learn to use odors to guide appetitively-reinforced behaviors. In a procedure based on one designed by Sara (Sara, Roullet, & Przybyslawski, 2001) for rats, mice learned to navigate a square field in which unique odor-marked (e.g., almond, lemon, mint) food cups were located in three corners. Although food was present in each cup, it was accessible to the animals in only one cup (e.g., that marked by mint odor). An animal was placed in the empty corner of the field, after which it explored the field and eventually retrieved the single piece of available

food. On subsequent trials, the location of the food cups was changed, but the accessible food was consistently marked by the same odor (i.e., mint). On successive

trials, animals required less time to retrieve the food and made fewer approaches (i.e., "errors") to those food cups in which food was not available. Using an adapted procedure for mice, errorless performance is typically observed within 3-4 training trials. Control procedures (where the target odor is not consistent) indicate that odor is the principal determinant of animals' discrimination (i.e., performance does not improve under conditions for which the target odor is changed across trials).

A black Plexiglas 60 cm square field with 30 cm high walls was located in a dimly lit (10 fc) testing room with a high ventilation rate (3 min volume exchange). Three 4 x 4 x 2.0 cm (l, w, h) aluminum food cups were placed in three corners of the field. A food reinforcer (30 mg portions of chocolate flavored puffed rice) was placed in a 1.6 cm deep, 1 cm diameter depression in the center of each cup. The food in two of the cups was covered (1.0 cm below the surface of the cup) with a wire mesh so that it was not accessible to the animal, while in the third cup (the "target" cup), the food could be retrieved and consumed.

A cotton-tipped laboratory swab, located between the center and rear corner of each cup, extended vertically 3 cm from the cups' surface. Immediately prior to each trial, fresh swabs were loaded with 25 μl of either lemon, almond, or mint odorants (McCormick flavor extracts). The mint odor was always associated with the target food cup. (It should be noted that in pilot studies, the odor associated with food was counterbalanced across animals, and no discernible differences in performance could be detected in response to the different odors.)

On the acclimation day, each food-deprived animal was placed in the field for 20 min with no food cups present. At the end of that day's light cycle, three pieces of

chocolate flavored puffed rice that serve as the reinforcer in this task were placed in each animal's home cage to acquaint them with the reinforcer. On the subsequent test day, animals received four training trials in the field with three food cups present. On each trial, an animal was placed in the empty corner of the field. On Trial 1, the reinforcing food (rice) was available to the animal in the cup marked by mint odor. An additional portion of food was placed on the top surface of the same cup for the first trial only. The trial continued until the animal retrieved and consumed the food from the target cup, after which the animal was left in the chamber for an additional 20 sec and then returned to its home cage to begin a 5 min ITI. On Trials 2-4, the location of the food cups were re-arranged, but the baited cup remained consistently marked by the mint odor. Both the corner location of the mint odor and its position relative to the remaining odors was changed on each trial. On each trial, the latency to retrieve the food and errors were recorded. An error was recorded any time that an animal made contact with an incorrect cup, or its nose crossed a plane parallel to the perimeter of a incorrect cup. Similarly, an error was recorded when an animal sampled (as above) the target cup but did not retrieve the available food.

Spatial Water Maze. For this task, animals were immersed in a round pool of opaque water from which they could escape onto a hidden (i.e., submerged) platform. The latency for animals to find the platform decreased across successive trials. In this task, performance of animals can improve across trials despite the animals beginning each trial from a new start location. Such a procedure mitigates against egocentric navigation and promotes the animals' dependence on extramaze spatial landmarks. As demonstrated by Morris (Morris, 1981), rats' performance in the water maze does not

rely on fixed motor patterns (i.e., performance improves despite the animal's irregular starting location) or the presence of discernable cues within the maze (e.g., visual, tactile, or olfactory signals). Instead, performance is dependent on the stability of extra-maze cues, or "landmarks", and is said to reflect the animals' representation of its environment as a "cognitive map".

We have developed a protocol in which mice exhibit significant reductions in their latency to locate the escape platform within ten training trials. In our protocol, animals were confined in a clear Plexiglas cylinder on the safe platform for 5 min on the day prior to training. Second, a considerably longer ITI (10 min) was used than is typical (c.f., 90 sec). Lastly, the maze, surround, and water were black; visual cues were constructed of patterns of lights.

A round black pool (140 cm diameter, 56 cm deep) was filled to within 24 cm of the top with water made opaque by the addition of a nontoxic, water soluble, white paint. A hidden 11 cm diameter perforated white platform was in a fixed location 1.5 cm below the surface of the water midway between the center and perimeter of the pool. The pool was enclosed in a ceiling-high black curtain on which five different shapes (landmark cues) were variously positioned at heights (relative to water surface) ranging from 24-150 cm. Four of these shapes were constructed of strings of white LEDs (spaced at 2.5 cm intervals) and included an "X" (66 cm arms crossing at angles 40^{o} from the pool surface), a vertical "spiral" (80 cm long, 7 cm diameter, 11 cm revolutions), a vertical line (31 cm) and a horizontal line (31 cm). The fifth cue was constructed of two adjacent 7 W light bulbs (each 4 cm diameter). A video camera was mounted 180 cm above the center of the water surface. These cues provide the only illumination of the maze, totaling 16 fc at

the water surface.

On the day prior to training, each animal was confined to the escape platform for 360 sec. Training was conducted on the two subsequent days. On Day 1 of training, animals were started from a unique location on each of five trials. (The pool was conceptually divided into four quadrants, and two starting points were located in each of the three quadrants that do not contain the escape platform. The starting point on each trial alternated between the three available quadrants.) An animal was judged to have escaped from the water (i.e., located the platform) at the moment at which four paws were situated on the platform, provided that the animal remained on the platform for at least 5 sec. Each animal was left on the platform for a total of 20 sec, after which the trial was terminated. Trials were spaced at 10 min intervals, during which time the animals were held in a warmed (27.5^{o} C) opaque (5 Lux) box lined with wood shavings. On each trial, a 90 sec limit on swimming was imposed, at which time any animal that had not located the escape platform was placed by the experimenter onto the platform, where it remains for 20 sec. Animals were observed from a remote (outside of the pool's enclosure) video monitor, and animals' performance was recorded on video tape for subsequent analysis. Day 2 of training proceeded as did Day 1.

To estimate capacity for long-term retention in this task, animals were tested with a "probe" trial following a 30-day retention interval from completion of acquisition training. On the probe test, the escape platform was removed from the pool, and all animals were started from the first position for that day. A 60 sec test was conducted in which the animals' time searching in the target quadrant (that in which the escape platform was previously located) and non-target quadrants were recorded; this measure

served to index long-term retention in this task.

Selective Attention

For this task, animals were trained and tested in two contexts. The first was the same black Plexiglas box used in the odor-guided discrimination task. The second box was identical in all respects except for the addition of white stripes that were placed on the inside walls. Each of these boxes was equipped with 10 cm wide flat panels (constructed of black Plexiglas) placed behind the food cup in each corner. The panels traversed the height of the box. These flat surfaces were backlit by a single white led (1100 mCandle) and had holes drilled into them to form three 6 cm shapes: A circle (O), an X, and two horizontal lines (=). These patterns of light served as visual cues (which produced a 30 Lux above background illumination, measured from the center of the test box). The food cups at the bottom of each panel contained cotton wading (to which odorants could be loaded) covered by a metal screen. All parameters such as lighting conditions, ITI, and deprivation schedule were identical to those used in odor discrimination. In the box previously used for odor discrimination, the cotton in the food cups was loaded with the previously described odors (almond, lemon, or the target odor, mint) and mice were trained to associate the mint odor with accessible food in the previously described manner. The remaining cup also contained food, but it was not accessible to the animals (i.e., it was located under the screen in the bottom of the cup). During odor discrimination training, the lights behind the flat surfaces were not illuminated, and the unlit visual stimuli randomly cycled between the odors, insuring that in this odor discrimination box, these stimuli had no discriminative role in localizing the food. Animals received eight days of training (five trials/day) in this task, at which time,

no animal committed more than three errors across the final four trials.

After completion of the initial odor discrimination training, mice began training for the visual discrimination in the box with white stripes. Here the unique visual pattern on each flat panel was illuminated, creating visual cues for the mice to follow. There were no odorants on the cotton in the food cups. A chocolate flake was accessible to the animal in the cup located under the circle (O) visual cue; the two remaining cups contained inaccessible chocolate flakes. Training proceeded in exactly the manner used for training in the odor discrimination box. Animals received eight days of training (four trials/day) in this task, upon the completion of which animals were required to meet the training criteria of no more than three errors across the final four trials, in order to continue on in this task (one animal from each group was terminated from this task as a result of failing to meet these criteria). Following completion of the initial training in the odor and visual discriminations, animals were "overtrained". For this, and to adapt animals to alternating between the two tasks, mice began alternating between days (for six days, six trials/day) in the two tasks, followed by four days of training where they performed one of the discrimination tasks (four trials) during the first half of the light cycle and one discrimination during the second half of the light cycle. The order of the discrimination tasks within a day alternated across days.

Following completion of training, animals were subjected to the test of selective attention, where they were first placed in the odor discrimination box with both odor cues (the relevant targets) and illuminated visual cues (the task-relevant distracters) present. (For this task, the target odor cue [mint] was always present in a cup other than the one marked by the relevant visual cue [O]). To perform effectively in the task, the animals

were required to inhibit their approach to visual cues and selectively attend to odor cues in order to efficiently locate the accessible food.

Fifteen minutes after testing in the odor discrimination box, animals were placed in the visual discrimination box with both visual cues (the relevant targets) and odor cues (the task-relevant distracters) present. (For this task, the target visual cue [O] was always present in a cup other than the one marked by the relevant odor cue [mint]). To perform effectively in the task, the animals were required to inhibit their approach to odor cues and selectively attend to visual cues in order to find food. Animals then continued to alternate between boxes and were tested in this manner until they had been tested for performance in each box four times (for a total of eight test trials). The number of errors accumulated over the eight test trials served as the index of selective attention.

Immunohistochemistry and Tissue Preparation

Animals were euthanized using pentobarbital (200 mg/kg) administered intraperitoneally. Following euthanization, brains were removed rapidly and fixed in 4% paraformaldehyde in PBS at 4 °C, for 7 days. From each animal brain, a total of ~11 tissue blocks were generated for purposes of immunohistochemistry (IHC), including the cerebral cortex (from multiple locations), hippocampus and cerebellum. Following fixation, tissue was either paraffin embedded or frozen. Paraffin-embedded tissues were sectioned at a thickness of 5.0 μm, floated on a gelatin-glazed water bath (47°C), and placed on Superfrost® Plus glass slides (48311-703, VWR, Bridgeport, NJ), previously coated with Poly-LLysine (P8920, Sigma-Aldrich, St. Louis, MO). Slides were allowed to dry and then baked at 60°C for a period of 1 hour to ensure tissue was fully adherent. Following fixation, tissue to be used for freezing was sucrose infiltrated with 10% and

then 30% sucrose (in a PBS solution also containing 1.0% Paraformaldehyde, pH 7.4) at 4 °C under constant gentle agitation. Specimens were subsequently placed atop a solid 4.0% gelatin matrix that was previously heated to dissolve in Hanks Balanced Salt Solution (HBSS) (21-021-CV; Cellgro, Herndon, VA), and the resulting tissue/collagen blocks were consequently snap frozen in liquid nitrogen and stored at −80 °C until cryosectioning. Sectioning of frozen tissue was performed using a Leica CM1850 Cryostat (Deerfield, IL). Tissue was sectioned at 12.0 μm, placed on Superfrost® Plus glass slides (48311-703, VWR, Bridgeport, NJ), then equilibrated to room temperature to allow adherence of tissue. Subsequent to this melting step, tissue was stored in a dry container at 4 °C until use in immunostaining.

Immunohistochemistry was carried out on paraffin-embedded tissues as described previously (D'Andrea et al., 2001; Nagele et al., 2002). Briefly, after removal of paraffin with xylene and rehydration through a graded series of decreasing concentrations of ethanol, protein antigenicity was enhanced by microwaving sections in Target Buffer (Dako, Carpenturia, CA) for 2 min. Alternatively, frozen sections was treated for 2 min in acetone and again air-dried. Following a 30 min incubation in 0.3% H2O2, sections were treated for 30 min in normal blocking serum and then incubated with primary antibodies at appropriate dilutions for 1 h at room temperature. After a thorough rinse in PBS, a secondary biotinlabeled antibody was applied for 30 min. Immunoreactions were treated with the avidin–peroxidase-labeled biotin complex (ABC, Vector Labs, Foster City, CA) and visualized by treatment of sections with 3-3-diaminobenzidine-4 HCl (DAB)/H2O2 (Biomeda, Foster City, CA). Sections were lightly counterstained with hematoxylin, dehydrated through a graded series of increasing concentrations of ethanols, cleared in

xylene and mounted in Permount. Additionally, a subset of frozen sections from mice treated with PT-FITC-AB42 were washed in PBS and mounted using 4',6-diamidino-2-phenylindole, or DAPI (H-1500, Vector Laboratories, Burlingame, CA), then stored flat at 4 °C, prior to examination via fluorescence (darkfield) microscopy to assess the presence of FITC-conjugated peptides. All other specimens were examined and photographed with a Nikon FXA microscope, and digital images were recorded using a Nikon DXM1200F digital camera and processed using Image Pro Plus (Phase 3 Imaging, Glen Mills, PA) imaging software.

Effects of the treatment manipulations on BBB integrity; influx, neuronal binding, and intraneuronal accumulation of specific plasma components; dendrite and synapse integrity; and the number, distribution and/or activity of other local cells types, was evaluated by using a panel of cell type- and protein-specific immunomarkers assessing a number of cellular components and proteins. In particular, immunohistochemical analyses were performed using the following antibodies, for which the specificity of each was confirmed by Western blotting or ELISA. Two anti-Aβ42 antibodies (polyclonal, AB5078P Chemicon International, Temecula, CA; polyclonal 556501 Pharmingen, San Diego, CA), were used to assess the degree of Aβ42 load within neurons (Aβ42; Millipore (Temecula, CA). In addition to Aβ42, immunoglobulin was employed to detect indices of blood-brain barrier defects and leakage (anti-mouse IgG; Millipore, Temecula, CA). Glial fibrillary acidic protein (anti-mouse GFAP; Millipore (Temecula, CA) was used to monitor the local inflammatory response of these cells to the injections and any developing pathological changes (Nagele et al., 2003; 2004). Antibodies directed against F480 (Millipore (Temecula, CA), were used to monitor activation of phagocytic

microglia and the immigration of macrophages from the blood into the brain, and thus served as an assay for cellular death. Antibodies directed against synaptophysin, (Millipore (Temecula, CA), a synaptic protein, were utilized in the present study to monitor changes in synaptic density at or near the site of BBB compromise. Anti-microtubule-associated protein-2 (MAP-2; Millipore (Temecula, CA) was employed to evaluate the integrity of neuronal dendrite trees, while anti-NF (Millipore (Temecula, CA) was used to evaluate the integrity of axons as well as dendrite trees.

Statistical Analyses

ANOVAs were utilized to compare behavioral (i.e., including cognitive) performance between groups, as well as to compare the quantitative characterization of neuropathological features observed in each group. On the latter, as well as behavioral tasks with a single dependent measure, the four experimental groups were compared using a one-way ANOVA. Where tasks incorporated multiple trials, a mixed two-factor ANOVA was used to compare the groups' performance, with trials treated as a repeated measure. Planned comparisons were then used to identify specific differences between groups.

RESULTS AND DISCUSSION

Neuropathology Results:

Chronic Pertussis toxin (PT) treatment leads to sustained compromise of BBB integrity and leak of plasma components into the brain tissue

Immunohistochemical detection of mouse immunoglobulins (IgG) was used to identify leakage of plasma components from brain blood vessels and to assess the integrity of the BBB in mice treated with PT. This method of detection was found to be effective in identifying all elements of the microvasculature: arterioles, capillaries, and venules, as a result of their internal plasma content, including IgG (Figs. 1a-d; Figs. 2a-e).

Importantly, leaks in the brain vasculature were observed in all PT-treated mice, thus permitting the efflux of blood-borne components that include IgG from local blood vessels into the brain interstitium and thereby providing direct evidence for BBB breakdown induced by chronic PT treatment (Fig. 1; Fig. 2). Notably, where present in both PT-Aβ42 - as well as PT-treated mice, evidence of BBB breakdown was not uniform along brain blood vessels and tended to be relatively variable and unpredictable in location and extent. In particular, vascular leaks found in the brains of PT- Aβ42 treated mice were demonstrable among each of the different vessel subtypes and not limited to or consistently observed along brain blood vessels of a single type. Specifically, in addition to arterioles, individual capillaries, clusters of local capillaries and venules were also involved (Figs. 3c-f, 4a-f). Furthermore, vascular leaks ranged from focal, a small plume of material observed leaking from a single discrete site along

the length of a blood vessel (Figs. 3a- c), to more extensive, occurring along a greater length of the blood vessel and its tributaries (Fig. 4a, e-f) or among several blood vessels within a given region (Fig. 4e-f). Thus, as evidenced by Figs. 1a-c, vascular leak or extravasation of IgG was often visible as a perivascular leak cloud of varying shape and dimensions that either emerged from a distinct, focal point along the length of the vessel or from a greater length of the vessel (Figs. 1a-c). Frequently, a substantial vascular leak in a local arteriole or venule led to widespread diffusion of IgG (as well as other plasma components), with rather sharp lines of demarcation and abrupt diminution of IgG immunoreactivity seen as a fairly well-defined interface (see dashed line in Fig. 1d). These observations are consistent with the notion that BBB leaks were highly variable in extent, most likely reflecting the extent of compromise of the endothelial tight junctions, which are the main structural correlates of the BBB. Nevertheless, as a general pattern, larger blood vessels displayed much more pronounced and/or extensive vascular leaks than smaller vessels and the most prominent vascular leaks in the cerebral cortex were typically associated with small arterioles, the largest vessels in the cerebral cortex, particularly in the PT-Aβ42-treated group (Figs. 3a-d, Fig. 4a). The predominance of arterioles in displaying the most extensive leaks (i.e., in terms of the quantity of the fluid exudates) is most likely related to their increased hydrostatic pressure, which more heavily taxes the structural and functional integrity of the tight junctions that mediate the BBB.

Consistent with this variability, although all brain regions showed some degree of leak, with IgG-positive vascular leaks observed in all regions examined, the specific regional location and extent of any one leak appeared to be sporadic or unpredictable. For

example, Figs 2a-b show IgG leaks from arterioles and capillaries, respectively, in the cerebral cortex of a PT-saline-treated mouse, while another section through the cerebral cortex of the same animal shows no evidence of BBB leak from local arterioles or capillaries (Fig. 2c). Fig. 2d shows a small focal leak occurring at a specific point along the length of a capillary in the hippocampus, while Fig. 2e shows comparable IgG-positive capillaries with no evidence of BBB leak in the cerebellum. However, despite evidence of BBB leak among blood vessels from all of these brain regions, the brainstem and deep cerebellar nuclei generally exhibited a greater degree of BBB breach and vascular leak than either the hippocampus or cerebral cortex across all treatment groups, with less frequent vascular leaks displayed in the cerebral and cerebellar cortices. Although the reasons for this apparent disparity in the stringency of the BBB and regional tolerance for leak is unknown, a similar pattern of vascular leaks has been observed in comparable regions of the human brain. While the underlying bases for the observed variations in the region-specific stringency are not entirely clear, the conservation of this pattern across species underscores its likely importance in the maintenance of strict homeostasis in the more stringent regions, such as the cerebral cortex.

While BBB compromise was demonstrated in both PT-Aβ42- and PT-treated mice, vascular leaks were found to be more prevalent in the brains of mice dually treated with PT and Aβ42 than in corresponding brain regions of animals exposed solely to PT (compare Fig. 3 with Figs. 1 and 2), demonstrating greater evidence of increased permeability in the former. Specifically, both the number of cortex vessels with detectable leaks and the extent of the leak within individual vessels was considerably

greater in PT-Aβ42 treated mice than those treated exclusively with PT. Substantial leakage was primarily limited in this treatment group to the brainstem region, an area normally characterized by diminished BBB stringency in healthy brains. The enhanced BBB penetrability in PT-Aβ42 treated mice may indicate an additive effect of PT and Aβ42 on vessel permeability, possibly due to lipophilic qualities of the latter which may interact with the plasma membrane and contribute to an overall weakening of the tight junctional links between adjacent endothelial cells which comprise the BBB. In contrast to PT-Saline- and PT-Aβ42-treated animals, control animals exhibited an intact BBB within the cortex across Saline-Saline and Saline-Aβ42 groups (Fig. 5), with vascular leaks restricted to a single incident in one mouse from each group, most likely reflecting aging-related anomalies (i.e., since these mice were at ~12 months of age at the time of sacrifice).

Blood-borne Igs traverse the BBB and bind to neurons following efflux from local blood vessels into the brain interstitum

Igs were found to bind selectively to neurons located in the vicinity of leaks, especially neurons positioned within the margins of perivascular leak clouds (Figs. 6-8). For example, Figures 7a-c show increasingly magnified views of a single arteriole in the cerebral cortex emptying into a capillary plexus that is leaking IgG, with several local neurons that have been rendered IgG-immunopositive. Figure 6a is a low magnification view of the cerebral cortex with arrows pointing to a cluster of IgG-positive neurons that are adjacent to a cluster of similar neurons that are IgG-immunonegative on the lower left of the image. This is shown even more dramatically in figures 6b and 6c, in the latter of which a dashed line delineates the border between a brain region infiltrated with

interstitial IgG and a region nearly devoid of interstitial IgG.

In general, neurons within the vicinity of vascular leaks tended to be the most Ig-positive (Fig. 6f), with the intensity of neuronal Ig immunoreactivity decreasing progressively with increasing distance from the vessel leak site or the margin of the leak cloud. This pattern of gradual reduction in intensity with increasing distance from the leak site is consistent with the likelihood that neuron-bound IgG originates from the blood vessels, chronically leaking and diffusing into the surrounding interstitial space and thus providing a vehicle for the continuous supply of brain-reactive autoantibodies to neurons in AD brains. Importantly, intra-neuronal localization of IgG revealed that in addition to neuronal surfaces, to which IgG was typically bound, IgG was also regularly found in the perinuclear cytoplasm, but did not appear to enter the cell nucleus, as evidenced by higher magnification (Figs. 6d-f). This pattern of IgG leak and deposition (i.e., with respect to both the neuronal distribution and within the neuron) mirrors the distribution of IgG-positive neurons seen in AD brains (Nagele et al., 2010).

Neuronal Ig binding was observed in control groups (i.e., PT-saline, Aβ42-saline,Saline-saline) in a diminished manner that corresponded to the degree of BBB breakdown and associated leakage detected, with little to no Ig binding observed in the Aβ42-saline and Saline-saline groups. In particular, as illustrated by Fig.32, PT- Aβ42 treated animals and PT-saline treated animals showed an increase in cortical density of IgG-positive neurons relative to untreated animals, $t(24.06) = 8.25$, $p<.0001$, and $t(24.94) = 6.85$, $p <.0001$, respectively, while there was no significant difference between their respective densities of IgG-positive neurons, $t(37.74) = 1.48$, *ns.* This pattern of results is reflected in $F(2,57)= 32.13$, $p<.001$

IgG that enters the brain interstitium binds selectively to certain subtypes of neurons

In further correspondence to observations in AD brains, the vast majority of IgG was found to preferentially localize to the same neuronal subtype (i.e., pyramidal neurons) (Figs 6-8) that have been demonstrated to accumulate surface-bound Ig in AD brains (Nagele et al., 2010; Levin et al., 2010). This selective manner of localization, whereby intensely IgG-immunopositive and immunonegative neurons (i.e., characterized as distinct neuronal subtypes) coexisted in close proximity, suggests that the observed Ig immunoreactivity may reflect the presence of specific targets on the surfaces of IgG-immunoreactive neuronal subtypes for which at least some antibodies have affinity.

Importantly, these same neuronal subsets are also those shown to internalize and accrue deposits of Aβ42 in AD brains, in yet another resemblance to characteristic features observed in this disease. The presence of Aβ42 in the same neurons that are also IgG-positive suggests that IgG binding to neurons may be mechanistically linked to the intraneuronal accumulation of A□42 peptides, as has been demonstrated recently by Nagele et al. 2010. In addition, the frequent observation of an interface between IgG-positive and IgG-negative brain regions (Figs. 6c, 8e-f) again emphasizes the fact that BBB compromise is not uniform in the brain, but rather occurs sporadically. This observation also reflects what is seen in AD brains and provides a reasonable explanation for the unpredictable pattern of symptoms seen early in the course of the disease, of course depending on the net effect of brain regions that are involved in the BBB leaks as well as the extent of these leaks.

BBB compromise allows injected, blood-derived Aβ42 to bind to and enter neurons following efflux from local blood vessels

Detection of fluorescence was used to identify and track the intra-parenchymal fate of injected exogenous Aβ42 (i.e., for those peptides that were conjugated to fluorescein isothiocyanate; FITC-labeled Aβ42), in concert with immunohistochemical detection of Aβ42 (i.e., to confirm the fate of FITC-labeled Aβ42 with unlabeled Aβ42 peptides). Results obtained by injecting unlabeled Aβ42 peptide were nearly identical to those obtained using the FITC-labeled peptide, with the exception of PT-saline and saline-treated animals (see Figs. 9-10 vs. Figs. 11-14). In the former, the absence of injections containing FITC-labeled Aβ42 precluded detection of this peptide (Figs. 11-13) but did not likewise prevent intraparenchymal appearance of unlabeled Aβ42 peptide, where inherent mouse reserves of this peptide accounted for its detection (Fig. 9). By contrast, appearance of both forms of this peptide were completely blocked in all cases by an intact BBB in saline-injected controls (see Fig. 14 for FITC-labeled Aβ42, see Fig. 10 for unlabeled Aβ42).

In regions of vascular leak, Aβ42 was observed emanating from the walls of blood vessels into the brain interstitial space (see Figs 15-18 for FITC-labeled Aβ42; see Figs. 19f, 20d, 21b for unlabeled Aβ42). In addition, neurons found within or in the adjoining vicinity of these perivascular leak clouds exhibited intense or high levels of Aβ42 (i.e., fluorescence or staining), indicating the presence of surface-adherent Aβ42, clearly derived from the blood vessels via chronic leaks (see Figs. 15b-d, 16e-f, 17b-c, 18b-f for FITC- Aβ42; see Figs. 19f, 20d, 21b for unlabeled Aβ42). In particular,

Figures 15C, 16a-b and 17b show several intensely fluorescent neurons adjacent to a local blood vessel that is leaking FITC-positive Aβ42 into the brain interstitium. This is further supported by the gradual diminution in neuronal fluorescence and/or staining intensity with increasing distance from the source vessel (Fig. 15c-d, 16a), in a parallel pattern to neuronal binding of IgG. Likewise, similar to neuronal IgG binding, an intensity gradient was observed in which the cellular fluorescence and/or staining of Aβ42 greatly exceeded that of its immediate surroundings, indicating an affinity of Aβ42 for neuronal surfaces(Figs. 15b-c, 16e-f, 17b, 18b-d). In addition to neuronal surfaces, Aβ42 was also found deposited in neurons within intracellular stores, indicating intra-neuronal internalization Figs. 16e-f, 17b-c, 18b-f).

In PT-treated animals, a similar pattern of overall Aβ42 deposition within the brain relative to PT-Aβ42 treated animals was detected by targeting total levels of unlabeled Aβ42 peptides (i.e., using brightfield microscopy), but on a far diminished scale as expected, given that the presence of Aβ42 in brains of PT-treated mice likely originated solely from their natural reserves circulating in blood vessels rather than the augmented supply of injected Aβ42 seen in PT- Aβ42-treated mice. In particular, while animals dually treated with PT and Aβ42 exhibited increases in total cortical Aβ42 load relative to both PT-treated and untreated animals ($t(31.22)=5.29$, $p<.0001$, and $t(20.14)=10.42$, $p<.0001$,respectively), animals treated with PT alone demonstrated a tendency toward greater total Aβ42 load in the cortex than untreated animals that failed to reach significance, $t(22.11)= 7.01$, $p = .081$ (see Fig.33) ; these difference are reflected in $F(2,57)= 60.758$, $p<.0001$. As expected, the latter difference was not visible when

targeting FITC-labeled peptides (i.e., using darkfield microscopy), as this technique is restricted to detection of this form of Aβ42, which is not naturally found in mice; however, mice treated with PT and FITC-labeled Aβ42 displayed corresponding increases in total cortical Aβ42 load with respect to both PT-treated ($t(22.47)= 6.39$, $P<.0001$) and saline-treated animals ($t(22.09)= 7.14$, $p<..0001$) as did their counterparts dually treated with PT and the unlabeled form of Aβ42 (see Fig. 34).

Furthermore, this pattern of increased Aβ42 levels in PT-saline treated animals (as in PT- Aβ42 treated animals) was paralleled somewhat with neuronal binding and intracellular demonstration of Aβ42 in particular, albeit with much fewer neurons displaying intracellular Aβ42 (Fig. 9a-b), as intra-neuronal Aβ42 in these mice likely was exclusively derived from their natural serum reserves rather than additional, injected Aβ42 shown in the PT-Aβ42-treated mice. Specifically, as assayed by the density of Aβ42-positive neurons in the cortex under conditions detecting unlabeled Aβ42 peptides (i.e., including both neurons containing surface-bound Aβ42 as well as those containing intracellular Aβ42), animals treated with PT alone exhibited increased cortical density of Aβ42-positive neurons relative to untreated animals ($t(26.28)= 3.53$, $p<.05$), as did mice dually treated with PT and Aβ42 in comparison to both untreated and PT-treated mice ($t(27.09)= 3.37$, $p<.0001$; $t(20.69)= 5.44$, $p<.05$, respectively); these differences are evident in $F(2,57)= 18.99$, $p<.0001$ (see Fig. 35). As noted above, detection of Aβ42 was altogether precluded when targeting FITC-labeled peptides in mice treated with PT and saline (Figs. 11-13; see also Fig. 36); any apparent elevation in fluorescence (i.e., potentially interpreted as the presence of FITC-labeled Aβ42) was likely due to detection of fluorescence associated with lipofuscin, which exhibits autofluorescent properties in

granule-like intracellular regions. Nevertheless, mice exposed to PT and FITC-labeled Aβ42 exhibited an increase in density of Aβ42-positive neurons within the cortex relative to PT- and saline-treated mice, ($t(20.69)= 4.77, p<.0001$, $t(19.80)= 5.34$, $p<.0001$, respectively). As compared to PT-Aβ42 and PT-saline treated animals, both intraparenchymal and neuron-bound Aβ42 was rarely in evidence in brains of the Aβ42-saline and Saline-treated control groups (Fig. 14, Fig. 10a-f; see also Figs. 33-36).

Injected, blood-derived Aβ42 internalizes and accumulates selectively in certain subtypes of mouse neurons, intraneuronal sites, and brain regions in a distribution characteristic of the human AD brain

Injected Aβ42 generally showed a pattern of deposition at the same intraneuronal sites that neurons in human AD brains accumulate amyloid. In particular, FITC-labeled Aβ42 was generally found concentrated in a number of prominent, brightly fluorescent granules of fairly uniform size commonly localized in an aggregated fashion to the perinuclear region of the perikaryal cytoplasm (i.e., likely representing parts of the lysosomal system see Fig. 15c, 16e-f, 17c); in a subset of neurons, these spots were dispersed to a greater extent throughout the span of the cytoplasm (i.e., including peripheral cytoplasmic regions bordering the cell surface), suggesting temporally distinct stages in the sequential pathway comprised of endocytic internalization and intracellular trafficking of vesicles to the perinuclear lysosomal compartment. Unlabeled Aβ42 was typically observed in a relatively similar intracellular distribution, albeit often with somewhat more diffuse immunostaining concentrated within the perikaryon and in select cases proximal segment of the main dendrite trunk, but not the nucleus (Figs. 22a-f, 19a-b, 20); this subtle discrepancy in intracellular distribution of Aβ42 between unlabeled and

FITC-labeled Aβ42 may reflect additional detection of excess, inherent mouse reserves of blood-borne Aβ42 peptide in the former and ensuing alterations in distributional appearance, or alternatively the more regular manifestation of later stages in the endocytic pathway within the latter, or merely nuances in appearance associated with different techniques. In general, smaller neurons tended to have tightly compressed aggregates of several dots (i.e., often appearing as a single spot) whereas larger neurons tended to have more, well-defined spots that might not be tightly aggregated. This may reflect the need of the neuron to sequester the aggregated Aβ away from the entrance to neurites to prevent their blockage and axonal transport failure, as shown in figure 17c, where some neurons with substantial deposits of fluorescent Aβ42-positive material managed to sequester this accumulated material away from the entrances into dendrite trunks and axons.

In addition to intracellular loci of deposition, neuronal internalization of Aβ42 conformed to a distribution resembling human AD with respect to brain region and neuron subtype as well. Specifically, the localization of FITC-labeled Aβ42 was clearly selective for certain types of neurons, principally among them pyramidal cells (Fig. 15c, 16e-f, 17c), with most pronounced labeling of larger pyramidal neurons that populate cerebral cortex layers 4-6. This pattern of findings was paralleled by neuronal distribution of unlabeled Aβ42 peptides: within the cerebral cortex, the larger pyramidal neurons in layers 4-6 were the most prominently Aβ42-positive cells ((Figs. 22a-f, 19a-b, 20), with less dramatic labeling of the smaller cortical pyramidal neurons in cortical layers 2-3, while large mossy neurons in the hilar region and Purkinje cells in the cerebellum showed considerable labeling as well. Disparities in the degree of neuronal

Aβ42 distribution may reflect the relative concentration of alpha 7 nicotinic acetylcholine receptor expression for each respective population of neurons. Interestingly, great variations in the relative content of intracellular Aβ42 were observed among neurons (compare Figs. 19e-f), but neurons within a give brain region tended to contain similar amounts of internalized and accumulated Aβ42 (Figs. 16e-f), which is expected in view of the fact that each of these local neurons within that region is probably serviced by the same feeder vessel in that quadrant of the brain. For example, some regions of the cerebral cortex exhibited rather intense Aβ42-positive immunostaining among many neurons, while other regions were apparently completely devoid of detectable Aβ42 immunostaining (Fig. 19e). In some cases, intensely Aβ42 fluorescent neurons appeared to follow the course of blood vessels through the brain, and these were sometimes apparent in favorable sections that appeared to parallel the course of the vessel (Figs. 15c, 16a, 17a-b).

Together, these results suggest that exogenous, intravascular, Aβ42 is able to penetrate a PT-permeabilized BBB, enter into and diffuse through the brain tissue, bind selectively to certain subsets of brain neurons, and accumulate in the perinuclear cytoplasm of vulnerable neurons. Further, they provide converging evidence for a selective distribution of Aβ42 in mice exposed to Aβ42 and PT that corresponds to that seen in human AD brains, in terms of both targeted brain regions and neuronal subtypes, as well as intra-neuronal loci. In demonstration of this selectivity, positive neurons of the same type were often observed in the same vicinity as negative neurons of a different cell type, whereas some neuronal subtypes in the same tissue sections (e.g., smaller interneurons) were never observed to be Aβ42-positive. While illustrating that neuronal

Aβ42 internalization is clearly neuron cell type-selective, this also internally confirms the specificity and reliability of the Aβ42 staining and reaction. Importantly, neurons with Aβ42 were frequently clustered together, suggesting that neurons in the same locale (i.e., presumably exposed to similar environmental conditions and interstitial Aβ42 levels) were all characterized by the same stage of pathology in an observation that parallels human AD brains, where pyramidal neurons in the same vicinity are typically found to have similar intracellular Aβ42 loads .The fact that the neuronal distribution of Aβ42 parallels that seen in AD, including the same subtypes of neurons accumulating Aβ42 in the present mouse model, suggests that the mechanistic steps are comparable in both systems and highlight the validity of this model.

In contrast to this relatively broad distribution of intracellular Aβ42 under conditions of PT-Aβ42 treatment, intraneuronal deposits of Aβ42 were typically minimal to mild (Fig. 9a-b),, and restricted mainly to large pyramidal and brainstem neurons in PT-saline treated animals, with little detectable Aβ42 in midline and lateral cortex. Occasionally, focal clusters of cortical neurons showed some substantial deposits (Figs. 9a-b), but this was relatively rare. Again, intraneuronal Aβ42 was largely not observed in the Aβ42-saline and Saline-saline control groups (Fig. 10a-f).

Injected, blood-derived Aβ42 may bind to synaptic region in a similar pattern to human AD

Notably, the overall pattern of granular background observed in PT-Aβ42 treated mice suggests higher levels of FITC-labeled Aβ42 binding to synaptic regions, and may indicate that exogenous Aβ42 has some affinity for synapses and synaptic fields (Figs. 22a-f, 19a-d, 19f, 20a-d). This background staining was localized at high

magnification to very tiny granules in the interneuronal space that likely reflect synapses, suggesting the possibility of synaptic binding of Aβ42. This pattern suggestive of synaptic accumulation of Aβ42 was exhibited most prominently in synapses of pyramidal neurons located in cortical regions, and consistent with additional detection of Aβ42 in the molecular layer of the cerebellar cortex, a region dominated by the extensive dendrite trees and synapses of Purkinje neurons (Fig. 21c), where staining appeared more grainy without accompanying labeling of cell bodies. Importantly, the similar size, morphology and distribution of granules seen here compared to those in human AD brains suggests their correspondence to synaptic boutons and previous findings indicating a fairly high affinity of Aβ42 for synaptic boutons in the human brain and in the AD brain in particular. The latter phenomenon is corroborated by select findings in several animals showing labeling of synapses in limited brain regions despite weak or no labeling of cell bodies in the same regions, thus highlighting the possibility of favored affinity of Aβ42 for synaptic boutons.

Some of these trends were paralleled in PT-saline treated animals, where synaptic distribution of Aβ42 was comparatively more prevalent than intraneuronal distribution. In this group, Aβ42-positive immunostaining was apparent in synaptic regions in the cerebral cortex, hippocampus, brainstem, and the molecular layer of the cerebellar cortex. Additional staining was evident within the latter in mossy fibers in the cerebellar granular layer and the dendrite trees belonging to Purkinje cells. Coupled with the above findings demonstrating preferential binding to synapses over cell bodies in several brain regions within select Aβ42-PT treated mice, the relative absence of neuronal cytoplasmic Aβ42 staining as compared to synaptic or surface Aβ42 staining in PT-saline treated animals

provides further support for the possibility that Aβ42 detected in association with synapses is in fact derived from blood-borne stores permitted to leak via BBB breach (i.e., and subsequently diffuse to synaptic regions), rather than intraneuronal stores of Aβ42. In contrast to these findings, Aβ42-saline and Saline-saline controls displayed minimal Aβ42 immunostaining in synaptic regions (Fig. 14; Fig. 10).

Activation of glial fibrillary acidic protein (GFAP) in response to treatment with Pertussis toxin and Aβ42

Immunohistochemical detection of GFAP was used to detect activation of astrocytes, while immunohistochemical detection of Aβ42 in these cells was used to detect the possibility of astrocytic phagocytosis of synaptic and neuronal debris, coupled \with immunohistochemical detection of F480 to detect microglia activation. The latter actions have been demonstrated previously to occur in response to degeneration of Aβ42-containing synapses and neurons in AD brains (i.e., thus resulting in the presence of Aβ42 within astrocytes) by Nagele et al (2003, 2004), as part of an inflammatory response that coincides with greater disease progression, whereas the former has been shown to be occur early, in response to more subtle pathological changes like loss of individual synapses or degradation of dendrites.

In contrast to neurons, immunostaining and fluorescence revealed that astrocytes were consistently Aβ42-negative across groups treated by FITC- and nonfluorescent-Aβ42, demonstrating that they did not directly bind or internalize Aβ42. This suggests that Aβ42 has no particular affinity for astrocyte surfaces, in line with the possibility that a particular receptor present on and specific to neuronal surfaces is the critical determining factor accounting for their selective vulnerability to Aβ42. In addition, this

finding implies that synaptic and neuronal degradation associated with PT-Aβ42 treatment did not progress sufficiently to spur significant astrocytic phagocytosis of synaptic and neuronal debris, in the event of which internalization of this material by astrocytes would have yielded Aβ42-positive astrocytes.

Despite the absence of direct Aβ42 binding or internalization in astrocytes, these cells appeared to play a key role in the local response to Aβ42 accumulation in neighboring neurons. As detected by immunostaining directed at GFAP, clear elevations in GFAP expression were evident in PT- Aβ42 treated mice; this was particularly apparent in brain regions that also showed BBB breakdown and neuronal Aβ42 accumulation, indicating enhanced astrocyte activation precisely in the same regions that exhibit substantial GFAP activation in human AD brains. Activated astrocytes were numerous and tended to be intensely GFAP-immunopositive, especially in the hippocampal hilar region (Figs. 23c-d, 24-25). Aside from the hippocampus, where the consistently elevated intensity of GFAP immunostaining of activated astrocytes suggests that this region is particularly vulnerable to insults imposed by PT-Aβ42 treatment, the cerebral cortex was also substantially affected. In this region, GFAP expression was mostly concentrated in the overlying molecular layer, the layer closest to the surface of the brain that contains primarily the fine dendritic branches and synapses of neurons in the underlying pyramidal cell layers (Fig. 26). Given the favored status of the latter neurons in findings of intraneuronal Aβ42 accumulation, this location is the expected site for evidence of initial neuronal compromise following PT- Aβ42 treatment and activation of cells in this specific region of the cortex is likely a response to synaptic loss. GFAP expression was also evident to a lesser extent in the cerebellar region, where it appeared

in the fibers of the Bergman glia radiating from the Purkinje cell layer up into the cortex. As noted above, astrocytes are the first inflammatory cells to be activated under conditions of damage and thus among the most sensitive biomarkers for local neuropathology, responding perceptibly to early and subtle stages of synaptic loss in AD brains that are not yet detectable with other markers of synaptic density. In light of this temporally specific function, and their frequent colocalization with regions of BBB compromise, Aβ42 deposition, and associated events, their activation in brain regions of PT-Aβ42-treated mice suggests that these regions are responding to emergent damage triggered by sequela of PT-Aβ42 treatment. Thus, these results therefore provide further support for the role of PT-Aβ42 treatment and resulting intraneuronal Aβ42 accumulation in contributing to the dendrite collapse and synaptic loss that are known to elicit astrocyte activation.

Interestingly, GFAP expression was not uniformly distributed within these regions across PT-Aβ42-treated mice. Most frequently, activated astrocytes were found individually (Fig. 26b) or in small clusters that likely reflect BBB leak sites which have compromised the function of local neurons (Figs. 26c-d,f). As shown for both IgG and Aβ42 leaking through a defective BBB, some regions of the cortex of treated animals appeared to be completely unaffected by the treatment and, in this case, showed a complete lack of astrocyte activation (Fig. 26e, 23a-b). As in the cerebral cortex, focal sites of rather intense astrocyte activation (Figs. 25a-b, f) were often observed to be adjacent to regions that lack such astrocytes (Figs, 25c-d) in the hippocampus, again most likely reflecting the effects of local plasma leaks from blood vessels. In particular, unilateral and at times focal astrocyte activation was seen within the hippocampus,

suggesting that the two contralateral sides and/or specific sections of the hippocampus were coping with different levels of pathology, consistent with observations of variable location and extent of BBB breach and its putative role in PT-Aβ42-induced damage. Thus, throughout affected mouse brains, the levels of astrocyte activation varied widely, providing further evidence that sporadic disruption in the integrity of the BBB may be responsible; an example of moderate astrocyte activation is shown in figure 25e.
Very subtle elevations in astrocytic GFAP expression were apparent in some cases in PT-saline treated animals, albeit in a markedly diminished manner relative to PT- Aβ42 treated animals, with minimal to no GFAP labeling detected in the Aβ42-saline and Saline-saline groups. However, these elevations were not consistently detected relative to untreated animals, whereas PT-Aβ42 treated animals displayed clear elevations in levels of GFAP expression in hippocampal astrocytes with respect to both PT-treated and untreated animals, $t(57)= 2.18$, $p<.05$, $t(57)= 2.49$, $p<.05$, respectively (see Fig. 37). Expression of GFAP in Aβ42- and saline-treated animals, wherever present, likely represents a very mild degree of early natural aging-associated changes and thus does not reflect any pathological processes.

In contrast to evidence of astrocyte activation, immunostaining failed to detect F480-positive cells in any of the treatment groups (see Fig. 27), indicating that the inflammatory response associated with PT-Aβ42 treatment was insufficient to induce activation of phagocytic microglia or the immigration of macrophages from the blood into the brain, cellular events that occur in the context of death of local neurons, with the function of removing dead cell debris.

These findings suggest that the neural insult triggered by chronic administration

of PT and Aβ42 yielded a degree of neuropathology characteristic of regions exhibiting mild or emergent damage in the human AD brain and corresponding to a first stage of inflammation rather than a more advanced level involving phagocytosis and microglia, more typically associated with cell death and corresponding to a second stage of inflammation.

Effects of chronic PT-induced BBB permeability and Aβ42 peptide exposure on the structure and functional integrity of neurons

In order to determine the effects of chronic BBB permeability and exposure of Aβ42 peptide on the structural and functional integrity of neurons, morphological examination of neurons was used to detect signs of neuronal degeneration and death potentially associated with PT-Aβ42 treatment. These effects are readily visible as changes in the shape of the neuronal cell body, corkscrewing or twisting of promimal dendrite segments, and cell necrosis. In addition, immunhistochemical detection of MAP2, synaptophysin, and neurofilament proteins, were used to more directly assess potential effects of PT-Aβ42 on the structural integrity of dendrites, synapses, and axons, respectively. None of the former morphological effects were detected in any of the treatment groups as can be confirmed simply by examining the cells presented in essentially all of the previously described figures. This suggests that the pathological consequences described above are insufficient to bring cells to the point of cell degeneration and death. This possibility is supported by the general lack of microglial activation, which is known to occur only in instances of local cell death. In addition, the presence of more mild pathological changes, such as those described above, is supported by the activation of local astrocytes and the observed increased expression of GFAP in

these cells.

Immunohistochemical detection of microtubule-associated protein-2 (MAP2) (Figs. 28-29), a protein localized primarily to neuronal dendrites and associated with the walls of supporting dendritic microtubules, was used to assess the presence of dendrite compromise, as it is typically upregulated along with other cytoskeletal proteins such as neurofilament proteins under conditions of dendrite compromise, in a neuronal effort to further stabilize the cytoskeletal supporting structure of the dendrite and the synaptic tree. Results for the PT- Aβ42 group revealed a slightly increased expression of MAP2 protein in the focal regions of the cerebral and cerebellar cortices (Figs. 28a-c), and a more generally increased MAP2 expression in the hilar region of the hippocampus (Figs. 28e-f). Importantly, these findings, particularly the latter, are regionally distributed in a manner that corresponds with localization of IgG and Aβ42 binding and accumulation in neurons as well as increased local GFAP expression as described above. As for results obtained with IgG and Aβ42, there was considerable regional variation in the level of MAP2 upregulation, with some regions showing much less effect (Fig. 29).

Assessment of synaptic integrity and density using immunostaining directed against synaptophysin (SYN) did not reveal a consistent pattern of alterations in expression associated reliably with treatment across mice and groups (Fig. 30). Wide, sporadic, variation was evident in efficacy and/or intensity of SYN staining across and even within brains of individual mice belonging to the same treatment group. Nevertheless, a number of PT-Aβ42 treated mice exhibited the expected distribution of staining in some regions, including substantial increases in SYN expression in the molecular layer synapses from the cortical pyramidal neurons, and in the hippocampal

synapses, particularly the synapses associated with the giant hilar neurons. Although it is possible that these changes in expression represent local responses to damage, it is difficult to determine that definitively based on these results, limiting the utility of these markers in this study.

Antibodies to neurofilament proteins were used to assess effects of treatment on the structural integrity of axons. Again, as in the case of synaptophysin described above, there was a clear and more general increase in the intensity of NF-specific staining along axonal tracts (Fig. 31), presumably reflecting an increase in the expression of this protein, over corresponding controls (Fig. 10f). However, precise quantification of this effect was hampered by the variable and highly localized distributions of white matter fiber tracts that appear in sections taken through the brain, rendering these findings of limited utility.

PT-saline treated animals showed a very slight increase in expression of MAP2 protein (Fig. 9c-d), which was diminished relative to other PT-Aβ42 treated animals; no other evidence of structural damage was apparent. Aβ42-saline and saline-saline treated groups showed no indications of damage.

Cognitive and Behavioral Function Results:

Cognitive Performance:

Across measures of cognitive ability, mice treated with PT-Aβ42 evidenced a pattern of subtle to moderate deficits on a number of tasks in comparison to corresponding control groups (i.e., mice treated with PT solely, Aβ42 solely, or saline), and demonstrated comparable performance on the remaining tasks; thus, these mice consistently failed to outperform all other groups on every task. In contrast, mice treated solely with PT generally did not exhibit a decrement in performance compared to other

control groups, with similar performance to Aβ42-treated or untreated mice observed across cognitive tasks, excepting a subtle decrement on a single test.

Acquisition:

On tasks assessing acquisition abilities, mice treated with PT- Aβ42 demonstrated a variable pattern of performance, exhibiting subtle but clear deficits on select measures, and largely intact performance on others, relative to other control groups. PT-treated mice consistently evidenced comparable acquisition to other control groups, including untreated and Aβ42-treated mice.

Odor Discrimination. Despite no significant differences observed in overall performance on the odor discrimination task between groups, ($F(3,39)= 1.69$, *ns*), inspection of the acquisition curves suggests that rate of acquisition was in fact slower in the PT-Aβ42 treated group with respect to other groups, an effect that became increasingly apparent as trials progressed (see Fig. 38). This pattern was reflected in a significantly greater number of errors than each other group on the final two trials (e.g., $t(14.56)=-3.03$, $p<.05$, $t(15.33)= -2.18$, $p<.05$, $t(12.23)=-2.76$, $p <.05$, for PT-, Aβ42-, and saline-treated animals, respectively, on trial 4).

*Passive Avoidance***.** Similarly, PT- Aβ42-treated mice tended to exhibit inferior performance on the passive avoidance task, although this difference did not reach significance across all groups, $F(3,39)=1.97$, $p=.13$. In particular, their performance was significantly worse than animals administered saline ($t(39)=2.37$, $p <.05$), but not PT or Aβ42, $t(39)=1.62$, $p=.11$, and $t(39)=1.06$, ns, respectively (Fig. 39).

Lashley maze. In the Lashley III maze, PT-Aβ42 treated mice learned how to navigate the maze in a manner comparable to mice in other groups, $F(9.59, 35)= .26$, *ns.*

Nevertheless, although overall rates of acquisition were largely similar in this task, there was a significant effect between groups across trials, in large part due to initial differences in performance that first manifested on the earliest trial (see Fig. 40), on which PT-Aβ42-injected mice tended to make more errors than other groups (e.g., $t(19.38)= -1.98$, $p=.06$, $t(17.74)= -1.49$, $p=.16$, as compared to PT- and Aβ42-treated mice, correspondingly). Although inferior performance on this trial influenced performance across subsequent trials, these differences did not reflect subjects' ability to learn, as they originated on the first trial, prior to any learning having occurred.

*Water Maze***.** In the water maze, all groups exhibited equivalent performance across trials, as indicated by $F(3, 39)=1.03$, *ns.* In particular, no deficits were observed in PT-Aβ42-treated animals' ability to learn the platform location (Fig. 41).

Retention:

In contrast to their varying pattern of performance on tasks assessing acquisition abilities, mice treated with PT-Aβ42 exhibited consistent impairment on measures of retention abilities. This is particularly marked given that these deficits were expressed on tasks for which initial acquisition had been intact. PT-treated mice demonstrated a qualitatively similar but attenuated deficit on one measure.

Long Term Memory: Water Maze. PT-Aβ42 treated mice demonstrated a mild deficiency in retention relative to other groups in the water maze, although this difference was not significant across all groups, $F(3, 39)=2.43$, $p=.08$ (Fig. 42). Specifically, a significant decrement in performance was observed in relation to PT-treated animals ($t(39)=2.60$, $p<.01$) whereas this pattern did not reach significance with respect to Aβ42- and saline-administered animals, ($t(39)= 1.77$, $p=.09$, $t(39)=1.64$, $p =.11$, respectively).

This pattern was particularly notable given intact acquisition observed on this task in PT-Aβ42-treated animals, with all groups demonstrating nearly identical latencies to reach the platform by the final trial of training (see Fig. 41).

Long Term Memory: Lashley Maze. Animals treated with both PT and Aβ42 showed a reduction in retention compared to all other groups in the Lashley III Maze, as did animals treated solely with PT in relation to some other groups; this pattern of results is reflected in $F(3, 39)=3.55$, $p<.05$ (Fig. 43). The former decrement reached significance with respect to untreated ($t(21.82)=-2.36$, $p<.05$) and Aβ42-treated ($t(14.08)=3.13$, $p<.01$ but not PT-treated animals ($t(18.46)=-1.42$, $p=.17$). Again, this decline in retention was especially notable, as it occurred in the context of and despite comparable acquisition rates during initial training on this task. Although it is noted that animals in this group completed training trials with nominally slightly inferior performance but statistically comparable (i.e., due to the above noted mild elevation in errors observed at the outset of training), the magnitude of their retention deficit markedly exceeded the anticipated degree of impairment based solely on this potential minor disadvantage (see Fig. 44). In addition, while a performance decrement was also observed in PT-treated mice relative to remaining control groups (i.e., saline- and Aβ42-treated mice), here this decline reached significance only with respect to animals treated by Aβ42, ($t(19.34)=-1.35$, $p=.19$, $t(15.70)=-2.23$, $p<.05$, respectively).

Selective Attention:

On a task assessing selective attention, a measure of cognitive ability appreciably dissociated from both acquisition and retention, the pattern of results was similar to that reported across retention and select acquisition tasks, with a deficit evidenced by PT-

Aβ42-treated mice, which manifested preferentially on later trials, as indicated by $F(3,37)=12.45$, $p<.001$. This deficiency appeared to be related to an interference effect that likely accumulated across successive trials given selective expression on latter trials (see Fig. 45), demonstrated by significant increases in errors relative to each other group on trials 5-7 (e.g., $t(37)=-3.07$, $p<.01$ for PT -treated mice, $t(37)= -2.57$, $p<.05$ for Aβ42-treated mice, $t(37)=-2.94$, $p <.01$ for saline-treated mice, for trial 5.)

Sensory/Motor Function/Skills and Unlearned Behaviors:

In general, mice treated jointly with PT and Aβ42 displayed a relatively distinct pattern of functioning across measures of unlearned behaviors and sensory and motor skills. While altered behavioral responses were observed in some but not all measures, alterations were frequently associated with behaviors related to emotionality or anxiety, with a tendency to manifest heightened responses; motor skills were generally intact. Overall, in contrast to prior similarities to other control groups evidenced on cognitive measures, here animals treated with PT tended to exhibit a corresponding pattern of skills or behavior to PT- Aβ42 treated mice, albeit often with less consistent or appreciable effects.

Measures of Exploration Behavior:

On tasks assessing the propensity for exploration, mice treated with PT-Aβ42 exhibited mildly variable behavioral responses, with reductions shown in some measures but not others. Overall, PT-treated mice displayed qualitatively similar behavior but with a more consistent attenuation of exploratory tendencies.

Dark-Light Preference. Animals treated with both PT and Aβ42 showed a reduction in percentage of time spent in the light compartment on the dark-light

preference test, as did PT-treated animals; this pattern of results is reflected in $F(3, 39)=3.55$, $p<.05$ (Fig. 46). In particular, while PT-Aβ42 and PT-treated mice did not differ from each other in percentage of time in the light compartment, $t(38)=.53$, *ns*, both groups displayed a significantly attenuated propensity for exploration on this task or tendencies in this pattern with respect to Aβ42- and saline-treated mice (e.g., $t(38)= 2.14$, $p<.05$; $t(38)=1.74$, $p=.09$; $t(38)=-2.58$, $p<.01$; $t(38)= 2.23$, $p<.05$, for PT-Aβ42-treated mice and PT-treated mice, in relation to Aβ42- and saline-treated mice, respectively).

Open Field. In the open field task, mice treated by PT tended to exhibit diminished exploratory tendencies, as reflected in $F(3,39)=1.74$, $p=.17$. Specifically, this reduction in the percentage of open quadrant entries reached significance in relation to saline-treated mice, $t(39)= 2.21$, $p<.05$ (Fig. 47).

***Measures of Anxiety-Stress and Pain Reactivity*:**

On tasks assessing measures of anxiety, stress and pain reactivity, mice treated with PT-Aβ42 exhibited a pattern of altered expression of behavioral responses associated with emotionality. This tendency was likewise manifested in PT-treated animals.

Shock Freeze. PT-Aβ42-treated animals tended to show a moderated stress response; this trend, paralleled in mice treated with PT, was collectively reflected in $F(3, 39)= 1.93$, $p= .14$. In particular, both the PT-Aβ42 and the PT-treated groups displayed a diminished shock reaction relative to the saline-treated mice, with reduced latencies to movement following a shock (Fig. 48), although this did not reach significance in either case, $t(12.51)=1.71$, $p=.10$, $t(11.84)= 2.07$, $p=.06$, respectively. This decrease in fear-related immobilization freezing occurred independently of and despite an increase in pain

sensitivity, as suggested by shorter latencies to lick a hind paw when confined to the hot plate (see below).

Hot Plate. Animals treated with both PT and Aβ42 showed shorter latencies to lick hind paw during placement on a hot surface, as did PT-treated animals; this pattern of results is reflected in $F(3,39)=19.391$, $p<.001$. This reduction in latency was demonstrated significantly in each group with respect to both Aβ42-treated and non-treated groups ($t(39)= 5.67$, $p<.001$, $t(39)=4.89$, $p<.001$, $t(39)=-5.85$, $p<.001$, $t(39)= 5.10$, $p<.001$, for PT-Aβ42-treated mice and PT-treated mice, in relation to Aβ42- and saline-treated mice, respectively), whereas PT-Aβ42- and PT-treated groups displayed a comparable degree of pain sensitivity to each other, $t(39)=.32$, *ns* (Fig. 49).

Measures of General Locomotor Activity and Motor Strength-Coordination:

On measures of general locomotion, motor coordination, balance, and grip strength, PT- Aβ42-treated animals demonstrated a clear and consistent pattern of intact functioning; this trend was evident in PT-treated animals as well, suggesting no significant impact on motor activity or strength resulting from administration of PT or Aβ42 or a combination thereof.

Open Field. There was no significant difference between groups in general locomotor activity, as assessed by the total number of quadrant entries, $F(3,39)=1.47$, *ns* (Fig. 50). This suggests that animals' overall level of locomotor activity was not impacted by treatment or pharmacological manipulation.

Balance Beam. Similarly, joint treatment with PT and Aβ42 or either agent in isolation failed to affect animals' motor coordination, as evidenced by their latencies to fall from a balance beam, a measure on which performance was comparable across

groups, $F(3,39)=.63$, *ns* (Fig. 51).

Rod Suspension. The above pattern (i.e., of comparable motor coordination) was corroborated by animals' performance on this measure, as assessed through their latency to fall from a suspended rod. There was no significant differences between groups on this measure of grip strength and motor coordination, $F(3, 39)=.28$, *ns* (Fig. 52).

GENERAL DISCUSSION:

Mounting evidence suggests that cerebrovascular damage may play a key contributory role in disease progression; in particular, several studies have demonstrated that AD brains consistently exhibit morphological evidence of BBB dysfunction (Deane and Zlokovic, 2007; Kalaria, 1999; Mooradian, 1988). Furthermore, a number of findings have provided increasing support for the critical contribution of intraneuronal accumulation of Aβ peptide to AD pathology. However, in spite of numerous attempts to elucidate the factors that govern the initiation and/or progression of this disease, the source of this peptide and the mechanisms by which it interacts with neuronal surfaces and accumulates within neurons remain elusive. Of particular importance to understanding the pathological mechanisms that underlie the deposition and accumulation of β-amyloid within the brain parenchyma of Alzheimer's disease patients is determining the source of these peptides. Given the elevated levels of Aβ42 within the intracerebral vasculature relative to that in the brain interstitium, in the context of documented prevalence of BBB defects, a natural source of the Aβ peptides that deposit within the brain may be the blood. While several studies have indicated preliminary evidence that the blood may indeed contribute Aβ peptides to the brain (Nagele et al., 2007, 2010), this source has not yet been widely recognized as a major contributor to the amyloid that eventually deposits in the brain of AD patients. Despite recently emerging empirical support pointing to this likelihood, the possibility that the blood may serve as a major chronic source of the amyloid that deposits in the AD brain has thus far not been directly and systematically tested.

In order to address this, it is important to demonstrate explicitly that plasma Aβ

peptides can penetrate a defective BBB and accumulate selectively within specific types of neurons in a distribution resembling AD. To that end, we tested experimentally whether or not disruption of BBB integrity can unleash a chain of critical pathogenic events and thereby trigger the appearance of a cluster of pathological features simulating AD, including extravasation of plasma Aβ42, entry into the brain parenchyma, and ultimately intraneuronal deposition in the characteristic pattern of AD. To achieve this, an experimental mouse model was developed to replicate these key initial pathogenic factors using pertussis toxin (PT) to induce chronic BBB breakdown coupled with introduction of soluble Aβ42 into the venous blood. Indeed, comparison between mice subjected to both manipulations (i.e., PT- Aβ42-treated mice) and other treatment control groups provided confirmation that disruption of the BBB in mice was required for entry of Aβ peptides into the brain, since mice injected with saline instead of pertussis toxin failed to show Aβ peptide outside of blood vessels in the brain parenchyma, whereas mice treated solely with PT exhibited some, albeit significantly less pronounced intraparenchymal and, particularly strikingly, less intraneuronal accumulation of Aβ42.

Vascular leak was observed in all mice treated by PT, thus permitting the efflux of blood-borne components that include IgG from local blood vessels into the brain interstitium, and thereby providing direct evidence for BBB breakdown induced by chronic PT treatment. While leakages tended to be more prominent in arterioles rather than venules or capillaries, and in subcortical structures and hippocampus as compared to cerebral cortex, they were generally sporadic in location and extent and not limited to specific brain regions or vessel types, demonstrating that BBB compromise was not uniform. This observation mirrors what is seen in AD brains, particularly in early stages,

and likely accounts in part for the unpredictable pattern of symptoms seen early in the course of the disease. Nevertheless, in general, mice exposed solely to PT demonstrated considerably less evidence of BBB breakdown as well as markedly less prominent and fewer associated sequelae (i.e., limited in this group to findings pertaining to Aβ42 and IgG described below) than mice treated dually with both PT and Aβ42.

Neurons situated within or in adjoining regions to these vascular leaks were intensely Aβ42- positive, with an intensity gradient observed relative to their surroundings, indicating an affinity of Aβ42 for neuronal surfaces. In general, in a similar pattern to AD, neurons within the immediate vicinity of vascular leaks tended to be the most Aβ42-positive, with the intensity of neuronal Ig decreasing progressively with increasing distance from the vessel leak site, suggesting that neuron-bound IgG originates from the local blood vessels via chronic leak and extravasation. Regional deposition and intracellular internalization of Aβ42 conformed to a distribution analogous to human AD with respect to implicated neuron subtypes as well as their respective brain regions, with consistent, selective binding to the surfaces of and accumulation within specific subsets of hippocampal and cortical pyramidal neurons. Although Aβ42-positive neurons were found in the cerebral cortex, hippocampus, cerebellum, and brainstem, variations in neuronal distribution of Aβ42 within these regions were characterized by clustering of neurons with accumulated Aβ42 and comparable degrees of Aβ42 accumulation observed in neurons within a given locale. This pattern suggested that neurons in the same area were all characterized by the same stage of pathology, as evidenced in AD, and likely reflected in part sporadic disparity in causally related regional BBB perturbation. Similar to regional distribution, intracellular Aβ42 showed a

pattern of deposition at the same intraneuronal sites evidenced in human AD, with predominant manifestation in prominent granules within the cytoplasm suggestive of compartments in the lysosomal system , but with a subset of larger neurons exhibiting additional granules sequestered away from the entrances into dendrite trunks, axons, and perinuclear cytoplasm. Synaptic binding of Aβ42 was also observed, most prominently in synapses of pyramidal neurons located in cortical regions. In a corresponding pattern to AD, the favored affinity of Aβ42 for synaptic boutons was apparent from the presence of synaptic staining in select brain regions despite weak or no labeling of cell bodies in the same regions; these findings also provide further evidence that Aβ42 detected in association with synapses is more likely derived from blood-borne (i.e., extraneuronal) stores permitted to leak into interstitial space via BBB disruption, rather than intraneuronal stores of Aβ42.

In a parallel pattern to neuronal binding of Aβ42, IgG was also found to bind preferentially to neurons located in the vicinity of leaks, especially those situated within the margins of the surrounding perivascular leak cloud. A gradual reduction in intensity of neuron-bound IgG immunoreactivity was observed as distance increased from the source vessel, confirming that the local blood vessels are the source of the neuron-bound, IgG. In addition, the fact that neurons within the leak cloud consistently showed greater intensity than the leak cloud itself corroborates the tendency of IgG to accumulate on neuronal surfaces. This pattern of IgG deposition mirrors the distribution of Ig-positive neurons seen in AD brains. Importantly, within these leak regions, IgG was selectively localized to the same neuronal subtypes (i.e., predominantly pyramidal neurons) that accumulated surface-bound and intracellular Aβ42, a finding that further corresponds to

observations in AD brains (Nagele et al., 2010; Levin et al., 2010). This selective pattern of localization suggests that the observed Ig binding likely reflects the presence of specific targets on the surfaces of certain neuronal subtypes for which at least some antibodies have affinity and furthermore that IgG binding may be mechanistically linked to the internalization of exogenous Aβ42 and ultimately intraneuronal accumulation of these peptides within these cells. In contrast to neurons, astrocytes were consistently Aβ42-negative, again suggesting that soluble, exogenous Aβ peptides in the interstitial space of the brain are able to recognize and bind to as yet unidentified factors on neuronal surfaces which are apparently lacking on the surfaces of glial cells. However, these cells showed evidence of activation in mice treated dually with both PT and Aβ42 in what appeared to be a key role in the local response to Aβ42 accumulation in neighboring neurons, representing a first stage inflammatory response. Increased activation was preferentially exhibited in PT- Aβ42 treated mice in brain regions that also showed BBB breakdown and neuronal Aβ42 accumulation, consistent with the distribution of activation in human AD brains. In particular, astrocytic activation was more prevalent in the cerebral cortex and particularly the hippocampus, where the consistent activation of astrocytes suggests that this region is particularly vulnerable to neurological insult precipitated by PT- Aβ42 treatment. Interestingly, astrocyte activation was not uniformly distributed within these regions across PT- Aβ42-treated mice, consistent with observations of variable location an extent of BBB breach in the context of the latter's putative contributory role to pathology. These findings provide further support for the role of BBB disruption and ensuing intraneuronal Aβ42 accumulation in contributing to the dendritic collapse and synaptic damage that are associated with astrocyte activation.

More direct but subtle evidence of dendritic repair was also apparent in PT- Aβ42-treated mice, concentrated in the very large neurons in the hilar region of the hippocampus adjacent to the dentate gyrus, which are particularly vulnerable to excessive Aβ42 accumulation in AD brains. In a number of mice, a corresponding and co-localized increase in activation of local astrocytes confirmed the likelihood of compromised dendrite and synaptic integrity in this region. In contrast, results showed no evidence of axonal repair, and no consistent direct evidence of synaptic loss.

Taken together, these results provide compelling evidence for a selective distribution of Aβ42 in mice exposed to Aβ42 and PT that corresponds to that seen in human AD brains, in terms of both targeted brain regions and neuronal subtypes, as well as intra-neuronal loci. In a demonstration of this selectivity, positive neurons of the same type were often observed in the same vicinity as negative neurons of a different cell type. While factors regulating the observed cell type specificity of these Aβ peptides remain to be determined, this selectivity may be partly linked to the relative degree of alpha 7 nicotinic acetylcholine receptor expression on neuronal surfaces, a possibility supported by the profile of neuron subtypes favored. Furthermore, these results strongly suggest a pattern of distribution of IgG within the parenchyma as well as neuron-bound that is characteristic of human AD; this trend is further evident in consistent patterns of subtle dendrite degradation, and astrocytic activation as part of a first stage inflammatory response.

Collectively, these results indicate that plasma-derived Aβ peptides and anti-neuronal autoantibodies can penetrate a defective BBB, binding selectively to the surfaces of certain types of neurons and accumulating within them in the characteristic

pattern of AD. The importance of this observation lies in the demonstration that disruption of the BBB and the resulting influx of exogenous Aβ42 and anti-neuronal autoantibodies from the blood can, by itself, mimic the events seen in neurons of AD brains, and thus simultaneously provides compelling evidence implicating the blood as a likely primary source of amyloid that deposits in AD brains and anti-neuronal autoantibody-induced endocytosis as a likely means of entry into neurons. In view of the widespread breakdown of the BBB in AD brains (Deane and Zlokovic, 2007; Kalaria, 1999), these findings suggest that not only does the blood serve as a chronic source of Aβ peptides that gain access to the brain tissue through a compromised BBB, but also that the influx of soluble, exogenous Aβ42 into the brain may be the origin of the intracellular Aβ42 that accumulates within neurons. Furthermore, these conclusions support the possibility that the chronic and simultaneous influx of blood-borne, Aβ42 peptides and brain-reactive autoantibodies into the brain interstitium across a defective BBB and their selective binding to neurons contributes critically to initiation and/or progression of AD pathology by driving the intracellular accumulation of Aβ42 in these cells.

Importantly, the events induced and simulated by these manipulations reproduce and conform most closely to an earlier stage in the disease process, analogous to a prodromal phase of dementia (i.e., commonly known as MCI, at times referred to as amnestic MCI in the context of AD). In general, early AD-mediated events include compromised integrity of the blood-brain barrier and associated influx of plama components into brain parenchyma, intraneuronal accumulation of Aβ42 peptide, dendrite collapse, synaptic loss, and resulting activation of astrocytes in a first stage local inflammatory response, whereas appearance of amyloid plaques and neurofibrillary

tangles, axonal damage, local neuronal degeneration and loss, and accompanying second stage inflammation including influx of immigrant macrophages and microglia activation, emerge only during later stages in the progression of disease. In this case, the appearance of blood-brain barrier perturbation and influx of plasma components, associated neuronal binding of IgG, fairly extensive neuronal and to some extent synaptic binding, considerable intracellular accumulation of Aβ42, substantial astrocytic activation, and subtle evidence of dendritic or synaptic collapse, all point to the presence of experimentally-induced pathology distinctive to and in accordance with an early disease stage. In particular, astrocytes are the first inflammatory cells to be activated under conditions of damage, and thus are among the earliest and most sensitive biomarkers for local neuropathology, responding perceptibly to early and subtle stages of synaptic loss in AD brains that are not yet detectable with other markers of synaptic density. In light of this temporally specific function, their activation generally signifies an inflammatory response specific to early disease processes and, in brain regions of PT- Aβ42-treated mice, suggests that these regions are responding to emergent damage triggered by sequelae of PT- Aβ42 treatment. In contrast to evidence of astrocyte activation, the extent of the inflammatory response associated with PT- Aβ42 treatment was insufficient to induce activation of phagocytic microglia or the immigration of macrophages from the blood into the brain. These findings provide further support that the neural insult triggered by chronic administration of PT and Aβ42 yielded a degree of neuropathology characteristic of regions exhibiting mild or emergent damage in the human AD brain and corresponding to a first stage of inflammation rather than a more advanced level involving phagocytosis and microglia, more typically associated with cell death and

corresponding to a second stage of inflammation. This temporal assignment is also in particular concordance with observations indicating subtle evidence of dendritic collapse in the present study.

Moreover, the absence of amyloid plaques, neurofibrillary tangles, axonal degradation, and neuronal degeneration and loss, and axonal degradation in this study is consistent with an earlier, more mild level of PT- Aβ42-induced damage rather than a more advanced stage of neuropathology in these brains, given that appearance of these pathological features is generally restricted to brains with more advanced disease states. In addition, the absence of direct and consistent indications of synaptic loss and less subtle indications of dendritic degradation in this study corroborates this possibility. Converging with this, the additional absence of Aβ42-positive astrocytes suggests that synaptic and neuronal degradation associated with PT- Aβ42 treatment did not progress sufficiently to spur significant astrocytic phagocytosis of synaptic and neuronal debris here, in the event of which internalization of this material by astrocytes would have yielded Aβ42-positive astrocytes, as has been demonstrated in human AD brain (Nagele et al., 2003). Collectively, these findings point to a neuropathological profile consistent with an early stage in the course of AD, demonstrating that events set in motion by chronic disruption of the BBB here, including intracellular accumulation of Aβ42, did not burden or stress neurons sufficiently and/or in an adequately sustained fashion to provoke significant synaptic, dendritic, axonal, and ultimately neuronal degeneration; this suggests that the brain naturally engages in clearance of Aβ42 peptides and compensatory mechanisms to combat associated structural and metabolic challenges and furthermore has the capacity to ward off or at least delay adverse consequences of the latter until it

may reach a critical point or threshold at which it is no longer capable of keeping up with disease burden or pathological load. This is consistent with neuroadaptive processes that have been postulated to underlie the theoretical construct of cognitive reserve and partly account for its modulation of function (Jankowsky et al, 2005).

This profile of observed neuropathological features and the stage of pathology they represent complements and coincides with the cognitive and behavioral expression of disturbance associated with PT- Aβ42- induced BBB defects and related events Taken together, neuropathological sequelae of this disturbance converge with those manifested in the cognitive and behavioral domains, in reflecting a common, emergent, phase of pathology, particularly with respect to pattern and extent of deficits in the latter domains. In particular, animals subjected to experimental manipulation of BBB integrity and plasma Aβ42 levels demonstrated a somewhat subtle yet clear trend of disruption of certain aspects of cognitive as well as behavioral functions. With respect to cognitive functioning, they displayed a pattern of variable down-regulation of acquisition abilities, with a more consistent and preferential deficit apparent in the capacity for long-term retention; the specificity of the latter effect was particularly salient in light of intact acquisition on corresponding measures. Selective attention evidenced a pattern of performance consistent with increased susceptibility to interference, manifested in specific impairment on latter test trials, a segment most sensitive to accrual of interference. Animals exposed to PT- Aβ42 treatment also exhibited an aggregate tendency to attenuated exploratory behavior; in addition to up-regulation of emotionality and/or anxiety in these animals, this effect may also be interpreted to reflect a diminished drive for novelty-seeking, which is more consistent with observations of diminished

stress reactivity.

The aggregate pattern of variable effects demonstrated with respect to specific aspects of cognitive as well as behavioral functioning suggest the possibility that the experimental manipulation used here impacted individual domains differentially due to associated regional variation in pathology load (i.e., preferential impact on long-term retention reflecting greater hippocampal pathology); however, this possibility was not supported by the observed pattern of neuropathological distribution, nor was it corroborated by the collective pattern of performance across tasks (i.e., hippocampal-dependent tasks were not consistently impaired). This suggests that variability in functional effects may be due to a more subtle combination or complex interaction of regional presence and load of pathology with performance demands, task-specific parameters and/or constraints, or differential susceptibility to neural insult (e.g., due to factors such as resource demands, degree of automaticity, etc.) specific to distinct domains or tasks that rely on the integrity of a given region. This possibility is broadly in line with research on the construct of cognitive reserve, which suggests that specific domains of function may vary in their ability to withstand pathological changes in their respective underlying brain regions, and be more or less resilient or impervious to disease burden due to disparate demands in allocation of neural resources for distinct functions or divergent thresholds of damage in region-related functional capacity for different domains ((Mori et al., 1997; Ando et al., 2001; Richards & Sacker, 2003; Tucker-Drob et al., 2009; Stern et al., 1999).

In animals subjected to experimental manipulation of BBB integrity but not accompanying augmentation of plasma Aβ42 (i.e., resulting in neuropathological

sequelae which partly reproduced that seen in animals exposed to both, but with vastly diminished scope and magnitude; PT-treated animals), a complex and multifaceted response ensued to manipulation within behavior and cognitive domains. Consistent with the status and extent of their neuropathological disturbance, these animals exhibited a divergent profile of functional alteration, with behavioral expression resembling animals treated with PT and Aβ42 to some extent, and cognitive expression replicating other control groups (i.e., associated with no neurological or functional changes) more closely. This suggests that specific systems that subserve different functional domains may be differentially sensitive to neurological changes or disturbance. Each domain may possess a distinct threshold for manifestation of functional disturbance or expression of response to neurological damage that affects its respective function independently of other functions. Accordingly, while the degree of neuropathological alterations may have been insufficient to reach the critical threshold necessary for inducing functional changes in cognitive abilities, this degree of pathology may have been adequate to produce changes in behaviors like exploration. This possibility is consistent with above described evidence from research on cognitive reserve suggesting differential susceptibility to disease burden in distinct domains of function. Alternatively, distinctions in functional expression of neurological disturbance may be associated with or reflect disparate effects of experimental manipulation on underlying regions in the brain; however, this possibility is not likely in the context of sporadic distribution of changes in the brain evident in this group, with no clear or consistent pattern of regional alteration across animals. Yet another possibility concerns the temporal structure of functional assessment in the present study: in view of the position of cognitive tests towards the beginning of the assessment

battery and the predominant position of behavioral measures towards the end, it is possible that different patterns of expression in these two domains may simply reflect their distinct points in the time course of pathology progression, as continued and prolonged manipulation may have only generated sufficient disease burden to affect function later in the time course, a pattern which would yield effects preferentially on unlearned rather than cognitive behaviors (i.e., given that the bulk of testing for the former took place towards the end of the test battery, whereas the converse was true for the latter). Nevertheless, marked effects observed on exploration in the open field in this group mitigate against this possibility, as this measure was assessed at the onset of testing, prior to all other tasks. Moreover, the pattern of performance on measures of long-term retention and selective attention further suggest that differences between these groups are not merely a function of temporal factors, since these measures yielded a clear dissociation in cognitive function between both group (i.e., with deficits demonstrated by PT- Aβ42 treated animals but not PT-treated animals), despite their placement within in latter portions of the battery of cognitive tests.

It is important to note that the combined effects of pathological manipulation across cognitive and behavioral domains occurred in the absence of a significant impact on general locomotor activity or ataxic effects on motor coordination and strength. In particular, the observation of heightened pain sensitivity does not correspond to a demonstrated reduction in stress response and as such cannot be argued to account for the latter; the concurrent attenuation of exploration may therefore reflect a decreased drive for novelty-seeking, consistent with a reduced rate of habituation to novelty associated with mildly deficienct information acquisition, rather than an increase in anxiety or stress

reactivity. With respect to cognitive functions, this effect on pain sensitivity is not likely to have significantly impacted learning or attentional performance, given that the pattern of effects across tasks was not characteristic of the anticipated pattern were heightened pain sensitivity to have played a considerable mediating role, as the cognitive task most sensitive to pain in the current battery yielded *impairment* in these animals rather than enhancement of acquisition (i.e., passive avoidance).

The aggregate pattern of functional repercussions of experimental manipulation of BBB integrity and plasma Aβ42 levels is particularly illuminating in view of implications for AD pathogenesis. Taken together, this profile is most consistent with a prodromal or emergent phase of AD (i.e., MCI), both with respect to absolute degree and distribution of impairment across domains of cognition or behavior. As evidenced by its name, this stage in disease progression of AD is generally characterized by a subtle or mild degree of impairment. In particular, individuals suffering from the amnestic variant of MCI, or the form of MCI generally considered a transitional state for AD, typically display a specific profile that includes preferential deficits in long-term retention as compared to initial acquisition, coupled with variability in other domains of cognitive functioning; behavioral disturbance is also common, including mild to moderate neuropsychiatric problems and mood changes such as anxiety, irritability, and apathy (Libon et al, 2008; Hwang et al., 2004; Peterson et al., 1999). In contrast, significant disturbance of sensorimotor function is rarely seen in patients with MCI and typically only emerges in more advanced stages of dementia (Machulda et al., 2003; Thompson et al, 2007). Many features of this collective pattern of amnestic MCI symptomology are mirrored in the functional expression of neuropathology observed in the present experimental model,

where behavioral and cognitive effects observed tended to be subtle to modest, with limited manifestation of more dramatic deficits. Furthermore, the variable pattern of cognitive and behavioral deficits demonstrated here mirrors the unpredictable behavioral presentation and lack of consistent characterization of cognitive impairment associated with MCI. However, the most compelling parallels concern the specific profile of cognitive and behavioral impairment exhibited by animals treated with PT and Aβ42, most prominently including a preferential deficit in long-term retention with respect to acquisition capacity, in addition to mild changes in selective attention, emotionality, and stress reactivity.

In the context of the neuropathological alterations that were found to characterize these animals, this pattern of behavioral and cognitive results is especially intriguing. The former were dominated by intracellular accumulation of Aβ42, which has been linked to cognitive effects more generally and in particular, to deficits in long-term retention (Gold & Janus, 2005). This pattern of associations is consistent with findings in humans, where amnestic MCI (i.e., the above noted prodromal phase of AD) is characterized both by predominant intracellular Aβ42 accumulation and preferential impairment in retention. Aβ42 deposition within neurons is a relatively early event in human AD that seems to coincide temporally and spatially with loss of synapses, (D'Andrea et al., 2001; Oddo et al., 2003; Wang et al., 2002) a crucial predictor of functional alterations. This has led some to postulate that the gradual growth of Aβ42 deposits may progressively impair the ability of neurons to support their extensive dendritic arbors, thereby contributing to early synaptic loss that ultimately manifests in functional impairment (Lacor et al., 2004; Nimmrich and Ebert, 2009). In fact,

remarkably, the pattern of results in the present model dovetails very closely with the staging observed in longitudinal studies assessing the progression of pathology in the 3xTg-AD model, the solitary model which definitively surpasses the present model in progression of pathology (Billings et al., 2005, Gold & Janus, 2005). In this case, studies have demonstrated that the emergence of a specific and preferential deficit in long-term retention (i.e., with respect to acquisition as well as other cognitive functions) coincides temporally with the initial appearance of intracellular accumulation of Aβ42 and that both can be traced to the initial phases of pathology progression, corresponding to emergent or early disease stages (i.e., MCI). These changes both occur first in the cascade of significant pathological features with respect to neuronanatomy as well as behavior and cognition, prior to the emergence of any other major pathological alterations in both respects. Crucially, clearance of intracellular Aβ42 with anti- Aβ42 antibodies was linked to amelioration of cognitive deficits, suggesting a causal role for the former in the latter. These findings converge with above noted research indicating temporal and spatial association of Aβ42 deposition within neurons with synapse loss, an important factor in functional decline (D'Andrea et al., 2001; Oddo et al., 2003; Wang et al., 2002), as well as the results of the present study. In addition to reduced capacity to support dendritic arbors and associated synapse loss, others have posited various mechanisms for adverse functional consequences of intracellular Aβ42 accumulation and related events in early disease progression. For instance, several studies have shown that Aβ42 found within multivesicular bodies of neurons can cause disruption of the sorting capacity of these organelles, ultimately causing disruption of the Ubiquitin-Proteasome pathway (Almeida et al, 2007). Others have documented the ability of Aβ peptides to accumulate within

mitochondria and increase the production of cytotoxic reactive oxygen species. Furthermore, associated IgG-induced endocytosis of Aβ42 may have dire consequences to the functional integrity of neurons, as a result of receptor loss compromising neuronal function, and considerable cellular stress ensuing from recovery efforts.

In addition to providing supportive evidence for the putative role of a defective BBB compromise and associated access to plasma Aβ42 and neuron-binding autoantibodies in AD pathogenesis, these findings also support the validity and utility of this experimental approach as a physiologically relevant model for AD pathogenesis and thus a potential platform with which to investigate different aspects of pathogenesis and further elucidate its mechanisms. More generally, converging with the previously described growing body of evidence implicating the alpha7 nicotinic acetylcholine receptor in neuronal binding of Aβ42 peptides and in turn the neuronal binding of IgG in internalization of this peptide (Nagele et al., 2007, 20010; D'Andrea & Nagele, 2003), the present set of results provides evidence corroborating the broader mechanistic theories on which the current experimental model is based regarding pathogenesis of AD. Thus, based on these findings, a working model for the proposed mechanism and sequence of events is presented in figure 53. In this model, local BBB breakdown permits chronic access of blood-borne brain-reactive autoantibodies and Aβ42 peptide to the brain tissue in proportion to the extent of the vascular leak. Soluble Aβ42 preferentially accumulates on the surfaces of certain subtypes of neurons beginning in the vicinity of the leak, especially those expressing the alpha7 nicotinic acetylcholine receptor (a7nAChR), for which Aβ42 has been shown to have strong binding affinity (Clifford et al., 2008; Wang et al., 2000a; Wang et al., 2009b). We suggest that the

concurrent and selective binding of autoantibodies to cell surfaces of the same neuron subtypes that bind Aβ42 sets into motion a mechanism to clear the bound antibody that also facilitates the chronic internalization and accumulation of cell surface-associated Aβ42 via antibody-induced endocytosis. It has been demonstrated that antibody-mediated crosslinking of antigen targets on cell surfaces can induce endocytosis (Abulrob et al., 2005; Salisbury et al., 1980; Wehland et al., 1982). Thus, under conditions of chronic antibody binding to the cell surface, it might be expected that the autoantibody and its antigen target would be continually stripped from the cell surface and internalized, with the resulting endocytic vesicles eventually fusing with the lysosomal compartment for degradation (Mellman, 1982; Rosenthal et al., 1973; Schwartz et al., 1986; Zhang et al., 2009). Intraneuronal Aβ42 accumulations would increase gradually over time due to the fact that Aβ42 is largely nondegradeable within the lysosomal compartment as a result of its tendency to self assemble into insoluble fibrils under the pH conditions found in this environment (Cataldo and Nixon, 1990; Cataldo et al., 1997; Grbovic et al., 2003). In turn, continuous intracellular accumulation of Aβ42 would eventually lead to one or more of the above noted host of potential cytotoxic effects on the neuron, including progressive impairment of its ability to support its dendritic arbors, which, coupled with chronic receptor stripping and associated stress on the cell ensuing from continuous receptor replacement, would ultimately disrupt the anatomical and functional integrity of the cell.

In order to evaluate the efficacy and predictive strength of the present experimental model, it is important to examine extant models of AD pathology, as juxtaposition of their relative merits and limitations may inform an understanding of this

model's recapitulative power. Prompted by discovery of genetic mechanisms underlying a rare heritable form of AD, a series of transgenic mouse models have been designed in recent years to investigate potential mechanisms of AD pathogenesis (Duff and Suleman, 2004). While these models are widely used in current research on AD, specific pathological features that arise in these models vary considerably among the different transgenic models. Although none of these models show the same degree of neuronal loss and amyloid deposition seen in advanced AD brains, most display some degree of synaptic loss and Aβ42 deposition (Dong et al., 2007; Irizarry et al., 1997). Nevertheless, extracellular accumulation of the latter is generally the defining feature of most models, with Aβ42 deposition typically manifested in extraneuronal loci, whereas prominent intracellular accumulation of Aβ42 is largely restricted to several select models (Gold and Janus, 2005), despite growing recognition as a key and distinguishing feature of AD pathology. Furthermore, the appearance of characteristic neurofibrillary tangles and neuritic plaques, and significant synaptic, axonal, and neuronal degradation is limited to one model, 3xTg-AD (Gold and Janus, 2005), which incidentally displays marked intracellular accumulation as well. In many respects, the level of pathology achieved in the preponderance of AD transgenic mouse models appears to be generally commensurate with that commonly observed in brains of patients showing mild cognitive impairment (Gold and Janus, 2005). In the domain of behavior, this pattern of relative pathology is largely mirrored in many respects, with a number of parallels manifested in cognitive performance. In particular, these models predominantly demonstrate select deficits in isolated tasks; this is in qualitative accord with the overall pattern of cognitive and behavioral expression observed in the present model, characterized by distinct effects

on various learned and unlearned behaviors. Thus, with the exception of the 3xTg-AD model, the present experimental model is broadly consistent with the overall level of pathology observed in previous transgenic models; in particular, this model appears to generate a degree of neuropathological and behavioral or cognitive alterations that appears to approximate or in certain key respects modestly surpass the extent of pathology observed in these transgenic models in reproducing conditions of AD, with the latter effects predominantly in regard to select pivotal features of neuropathology (i.e., a relative increase in intracellular Aβ42 accumulation).

However, together with the aforementioned modest differences in pathology, several other key distinctions can be said to critically differentiate between the experimental model developed here and a number of previous transgenic models. Among them, whereas some models have been associated with more dramatic impairment on isolated tasks, the present model arguably yields a more wide-ranging collection of deficits, arguably resulting in a relatively more pervasive trend of behavioral disturbance than a number of transgenic models. Further, taken together, the distinct profile of individual deficits that jointly contribute to this latter feature bears a marked resemblance to the aggregate pattern of deficits that is specific to amnestic MCI, as documented previously. In fact, as noted above, neuropathological and cognitive features of this model coincide with documented characterization of pathogenic progression in the 3xTg-AD model revealing a close temporal association between emergence of significant intracellular Aβ42 accumulation and a preferential deficit in retention rather than acquisition (Billings et al, 2005). Most importantly, in addition to these disparities in appearance of pathology, one crucial divergence between this model and all other models

which confers a unique advantage to the present model is that it recapitulates the underlying mechanisms of pathogenesis in a physiologically relevant context, rather than generating an artificial schema with a set of conditions that are consequently inherently limited in replicating the disease process. Given that the majority of cases of dementia have no clearly defined direct genetic origin, and that longitudinal studies in humans tend to indicate a complex interplay between a multiplicity of factors contributing to pathogenesis in the sporadic variants of AD (i.e., non-hereditary spontaneous forms), these genetic models are poorly suited for elucidating mechanisms of AD pathogenesis for the scantily understood sporadic variant. Related to this, a further major shortcoming of transgenic mice with mutations causing abnormalities in Aβ42 protein expression that the present model attempted to circumvent is that mutations are introduced into otherwise young and healthy transgenic mice that are consequently lacking in a core component of physiological relevance.

Despite a number of apparent strengths of the present experimental model over many existing transgenic models in certain respects, this model is constrained by several limitations. It is important to note that some of these limitations also inherently apply to the present set of neuropathological and behavioral results, hampering their predictive capacity. One such flaw concerns the age of the mice; notably, although the present model explicitly selected mice in emerging stages of senescence, the maturity of these mice may not have been adequately developed to capture all critical aging-related elements (i.e., as it was likely most analogous to advanced stages of middle age in humans rather than full-blown elderly). Given the consistent and robust link between advanced age and development of AD (i.e., in sporadic, non-hereditary variants of

Alzheimer's), this is a core feature of AD that is likely to be important in attempts to replicate pathology and determine causal mechanisms. While the age of the mice used in the present model is sufficiently advanced to allow activation of processes associated with senescence, their relative youth may have attenuated key mechanisms implicated in AD pathogenesis and thus curbed emergence of more dramatic pathology. In addition, while the dynamic nature of the present model (i.e., continuous manipulation of putative pathogenic conditions) affords the benefit of replicating integral elements of the temporal course of AD (i.e., characterized as insidious and gradually progressive over a lengthy period of time) and thereby optimizes the physiological relevance of this model, it also presents a potential confound for purposes of studying behavior and cognitive functioning, particularly when using a lengthy battery as was performed here. Of particular relevance in the present model, attempts to identify pathological factors influencing or specific to a particular domain or system of cognition and/or behavior would be optimally supported by demonstration of consistent effects on all tasks relying on the domain or system in question; however, such efforts may be precluded or hindered by significant alterations in pathology in a continuously shifting disease course that may take place during the intervening time between two chronological points at which distinct tasks subserved by a common system are administered.

More generally, a number of intrinsic and unavoidable challenges arise when attempting to use animal models to simulate a human disease, as a result of distinct species-specific characteristics that inevitably impact potential disease mechanisms, which likewise pertain to the present model. Such flaws are endemic to all mouse models that attempt to translate from rodent to human pathology. In this case, of particular

consequence, these include the general absence of atherosclerosis in the rodent and their short lifespan, which significantly moderates the potential degree of cerebrovascular pathology an animal might sustain, a critical factor in development and progression of the disease process within the present theoretical framework for AD pathogenesis. In particular, these animals lack the larger arteries found in humans, blood vessels that are most associated with susceptibility to blood brain barrier dysfunction and ensuing vascular leak given their increased hydrostatic pressure. Several other limitations concern the broader underpinning theories of pathogenesis which this model is designed to test directly. In particular, some evidence suggests that intracellular accumulation of Aβ42 may occur in response to stress and thus might reflect rather than drive pathological processes including alterations in cognition; nevertheless, the preponderance of data mitigates against this possibility, such as the temporal sequencing of its appearance in relation to other neuropathological alterations (Golde & Janis, 2005). Similar questions might arise with respect to the putative status of BBB disturbance as well as neuronal binding of autoantibodies as initiating or contributing pathological factors or secondary consequences of ongoing disease pathology, although here again temporal association of these events with early disease stages, prior to emergence of several key neuropathological alterations, points to the former possibility. Nevertheless, despite these potential critiques, this model is comparable or superior to most extant animals models in reproduction of pathological and behavioral alterations associated with AD, with the above-noted critical advantage of a sound basis for its propelling pathogenic mechanisms. Furthermore, the postulated mechanistic theories on which it is based hold striking and robust explanatory value, accounting for a number of phenomena and

defining features that characterize AD symptomology, its course, and patterns of incidence.

In particular, as noted above, the mechanistic scenario presented here sheds light on a number of previously unexplained features of AD that have until now defied explanatory attempts and escaped elucidation. Most prominently, this model accounts for the robust link between aging and development of AD (i.e., sporadic variants), as preferential expression of this disease would be expected to occur in the elderly who are clearly more vulnerable to microvascular pathology and associated BBB compromise. Equally compelling, this scenario readily lends itself to a lucid explanation of the consistent association between vascular risk factors and incidence of AD, as it provides a platform for a key role of vascular pathology in implicated disease processes. Relatedly, this pathogenic theory of AD also elucidates the factors behind its delayed onset in active and healthy individuals (i.e., individuals presumably with good microvascular health and an intact BBB) and its potent affiliation with trauma in the brain (e.g., such as stroke or head impact injuries), which is known to induce BBB compromise. It also affords a plausible explanation for the fact that elderly individuals with autoimmune diseases such as SLE often undergo a pronounced, AD-like decline in cognitive functioning. Importantly, and in direct concordance with results of the present study, this scenario accounts for observations of local regional covariation in neuropathological features with sporadic distribution of BBB compromise throughout the brain in earlier or emerging stages of AD, lending a reasonable explanation for the relatively unpredictable pattern of cognitive symptoms seen early in the course of the disease. In addition to these important epidemiological features, this model also provides an explanation for numerous

pathological characteristics of AD, such as the well-known selectivity of AD for cholinergic and cholinoceptive neurons, which is likely in part attributable to the selective binding of Aβ42 with alpha7 nicotinic acetylcholine receptors found on their surfaces.

The results of the present study, in confirmation of broader implications of this mechanistic scenario, highlight the potentially important role of autoimmunity and brain-reactive autoantibodies in the pathogenesis of AD. These findings hold more sweeping significance and lend valuable insight to our understanding of autoimmune diseases in general, and potentially other neurodegenerative disorders. The contributory role that autoimmunity plays in human pathology has been well documented. Autoantibodies, components of the immune system with specificity to self-antigens, are found in sera and are partly responsible for initiation and progression of pathogenic events in numerous diseases. However, more recently, mounting evidence has shown support for the specific coupling of autoimmunity to neuropsychiatric disorders. In fact, a number of studies have implicated serum autoantibodies in a wide range of neurological and/or psychiatric diseases and syndromes. For instance, schizophrenia has been linked to the presence of a number of different serum autoantibodies, including several directed against different types of neuronal surface receptors (Graus et al., 2009). Neuron-binding autoantibodies have also been detected in sera following streptococcal infections, especially in individuals that subsequently develop any of a number of conditions, including obsessive compulsive disorder, Sydenham's chorea, Tourette syndrome, pediatric autoimmune neuropsychiatric disorders associated with streptococcal infection (PANDAS), and Hashimoto's encephalopathy (Gordon, 2009; Hoekstra and Minderaa, 2005). They are

also found in sera from elderly patients with systemic lupus erythematosus (SLE) that undergo a marked decline in cognitive functioning (Diamond et al., 2006), which may be causally linked to specific brain-reactive autoantibodies detected in a subset of SLE patients that are directed against DNA but crossreact with the NR2a and NR2b subunits of the N-methyl-D-aspartate receptor (NMDAR) (DeGiorgio et al., 2001; Diamond et al., 2006). Among neurodegenerative diseases, a high incidence of specific autoantibodies has been identified in patients with Parkinson's disease, amyotrophic lateral sclerosis, vascular dementia, and Alzheimer's disease (AD) (Diamond et al., 2009; Mecocci et al., 1993; Terryberry et al., 1998). In the case of AD, several studies have documented the presence of high titers of autoantibodies directed against both brain-associated and non-brain targets, including neuron-binding autoantibodies (Loeffler et al., 1997;Singh, 1997).

In light of the present results, certain trends observed among this body of findings may be illuminated and more readily understood. One explanation for the occurrence of brain-reactive autoantibodies is that the brain is an immunoprivileged region of the body, where neither immune components nor antigens can freely pass (Zlokovic, 2008). This is due to the presence of the BBB, which, under normal conditions of integrity, serves the function of excluding the relatively large, potentially self-reactive antibodies, from the brain parenchyma. As a result, the immune system has little mechanistic opportunity to establish tolerance to brain antigens and thereby to prevent generation of antibodies targeting these antigens. As underscored by the present findings and their supporting mechanistic scenario, this property of the immune system and the resulting incidence of neuron-binding autoantibodies renders it increasingly likely that an antibody-centered immune response might ensue in the context of BBB breakdown. Conversely, it is also

reasonable to speculate that healthy individuals are currently free of pathology because they possess an intact BBB that prevents access of their blood-borne, brain-reactive autoantibodies to neurons in the brain. Recognition of this possibility critically suggests that disease mechanisms with an autoimmune basis may be far more wide-ranging than previously thought. Furthermore, it also affords crucial insight into factors potentially regulating the causal mechanisms and course of progression for diseases that possess an autoimmune component. For instance, in many neuropsychiatric disorders characterized by higher levels of anti-neuronal antibodies, the waxing and waning nature of symptoms suggest that autoantibodies may only periodically gain access to their brain parenchyma targets. In neurodegenerative diseases, which are typically accompanied by inflammation, the latter may secondarily affect the integrity of the BBB (Weisman et al., 2006), and thus a compromised BBB and/or the presence of brain-reactive autoantibodies may play a vital and hitherto generally unacknowledged role in the progression of many brain neurodegenerative disease. Indeed, vascular pathologies within the brain would be expected to have a negative influence on BBB integrity (Bailey et al., 2004; Clifford et al., 2008) and as such may trigger neuronal dysfunction due to initiation of or increases in exposure to neuron-binding autoantibodies. Importantly, based on the present as well as previously demonstrated findings, specific predictions would be associated with the presence of specific types of brain-reactive autoantibodies (e.g., those that robustly bind AD- implicated neuron subtypes), which in the sera of individuals with BBB compromise, such as elderly individuals with relatively poor vascular health, might suggest predisposition of these individuals to neurological complications exacerbated by the chronic binding of autoantibodies to neuronal targets in the brain.

Thus, the clinical significance of the present results partly derives from the identification of autoimmunity as an important causative factor in the initiation and progression of AD and the accompanying recognition that certain autoantibodies or individual autoantibody profiles are likely to present a greater disease risk than others with regard to their potential to contribute to disease initiation and/or progression. Conceivably, autoantibodies targeting exposed neuronal cell surface proteins may be effective in mediating the internalization and accumulation of exogenous, cell surface-associated Aβ42 in these neurons. If this supposition is substantiated, then the rate at which this occurs in the brain of the afflicted patient would be expected to depend in part on the titer of brain reactive autoantibody(s) in their blood, the specificity of their particular autoantibody profile for implicated neurons, and the relative abundance of corresponding target protein(s) on the surfaces of vulnerable neurons to which the autoantibodies are able to gain access. Furthermore, in joint regulation of the latter variable, these findings crucially pinpoint disruption or compromise of the BBB as the critical complementary factor, without which the potential contribution of autoimmunity is rendered inconsequential, as no access is granted to the autoantibodies in question. From a clinical standpoint, if brain-reactive autoantibodies as well as Aβ peptides chronically gain entry into the brain through a defective BBB, then the exact brain location of the BBB compromise, the magnitude of the breach, whether it is focal or global, and the rate of its progression, will further influence the rate of progression in individual cases of AD. Moreover, given that these variables continue to change as the patient ages and the disease evolves, it is plausible that some combination thereof contributes to the observed heterogeneity in the nature and severity of the dementia from

one individual to the next, including the age of disease onset, the specific site(s) of its developing pathology, the rate of disease progression and the varying pattern of cognitive and/or behavioral symptoms that appear during the course of this disease. As evidenced in the present set of results, this effect is illustrated by the factors that govern cognitive and behavioral expression of the disease in emerging stages, where the unpredictable pattern of symptoms seen early in the course of the disease is likely in part attributable to the sporadic nature of regional BBB breach that is particularly marked during this stage of disease. Based on this understanding of contributory factors in initiation and progression of AD, a number of implications for diagnosis, evaluation and treatment implications become apparent. While the binding targets of antineuronal auto-antibodies found in AD patients as well as the general population have yet to be fully determined, elucidation of these targets and individual differences in auto-antibody profiles may yield valuable tools to facilitate assessment of diagnosis, prognosis, and staging of AD progression. Ultimately, in the search for effective treatment and/or prevention strategies, they may prove to be vital targets to prevent or at least delay the onset and progression of AD pathogenesis. In addition, the potential merits of therapeutic approaches aimed at lowering reducing plasma levels of Aβ peptides and preventing their transit across the BBB are clear.

Given their potential utility in aiding diagnostic and prognostic evaluation of AD, one potential central aim of future research is self-evident; developing such tools is critically contingent on proper identification and full characterization of individual differences in autoantibody profiles and/or titers, with particular emphasis on those associated with development or progression of AD or normal functioning. Such specific

elucidation would also lend a great advantage to the experimental model developed in the present study, as it would permit an additional manipulation aimed at implicated autoantibody profiles, in a more direct and fully developed test of the pathogenic theories presented here. Furthermore, with respect to this experimental model, several other specific limitations can be readily addressed with modification of associated manipulations or at least minimized with adjustment thereof. Most significantly, future applications of this model would be greatly enhanced by the use of aged animals better corresponding to elderly humans, as well as a prolonged period of pharmacological manipulation, particularly prior to onset of behavioral and cognitive testing, to facilitate closer approximation of AD-associated pathological alterations both in general and for purposes of evaluating potential behavior correlates. In addition, the latter objective would also be well-served by cross-sectional as well as longitudinal studies to allow for tracking dynamic changes in neuropathological as well as cognitive and behavioral alterations during disease progression, which may potentially inform our understanding of the role the former plays in the latter as the disease evolves.

In conclusion, these results indicate that plasma-derived Aβ peptides and anti-neuronal autoantibodies can penetrate a chronically defective BBB, binding selectively to the surfaces of certain types of neurons and accumulating within them in the characteristic pattern of AD. Crucially, these findings demonstrate that chronic BBB compromise and the ensuing influx of exogenous Aβ42 and anti-neuronal autoantibodies from the blood over time can set off a cascade of neurological events and associated cognitive and behavioral changes that resemble those apparent in emerging AD. Taken in the context of research indicating widespread BBB deficiency in AD brains (Deane

and Zlokovic, 2007; Kalaria, 1999), these findings provide compelling evidence that the blood may serve as a chronic source of Aβ42 peptides as well as neuron-binding autoantibodies in AD as they gain access to the brain tissue through a compromised BBB, and that the influx of soluble, exogenous Aβ42 into the brain may be the origin of the intracellular Aβ42 that accumulates within neurons in AD. Thus, based on the present study, it appears likely that chronic BBB dysfunction plays a key role in pathogenesis of AD, by permitting entry of blood-borne, Aβ42 peptides and brain-reactive autoantibodies into the brain interstitium and thereby driving the intraneuronal accumulation of Aβ42.

BIBLIOGRAPHY:

Abulrob, A., Sprong, H., Van Bergen en Henegouwen, P., & Stanimirovic, D. (2005). The blood brain barrier transmigrating single domain antibody: mechanisms of transport and antigenic epitopes in human brain endothelial cells. *Journal of Neurochemistry, 95***,** 1201-14.

Andreasen, N. & Blennow, K. (2002). B-amyloid (Aβ) protein in cerebrospinal fluid as a biomarker for Alzheimer's disease. *Peptides, 23,* 1205-14.

Ando J, Ono Y, Wright MJ (2001). Genetic structure of spatial and verbal working memory. *Behavioral Genetics,* 31, 615-24.

Bahr, B.A., Hoffman, K.B., Yang, A.J., Hess, U.S., Glabe, & C.G., Lynch, G. (1998). Amyloid β protein is internalized selectively by hippocampal field CA1 and causes neurons to accumulate amyloidogenic carboxyterminal fragments of the amyloid precursor protein. *Journal of Comparative Neurology, 397***,** 139-47.

Bailey, T.L., C.B. Rivara, A.B. Rocher, and P.R. Hof, (2004). The nature and effects of cortical microvascular pathology in aging and Alzheimer's disease. *Neurology Research, 26*(5), 573-8.

Braak, H., Braak, E., (1991). Demonstration of amyloid deposits and neurofibrillary changes in whole brain sections. *Brain Pathology, 1,* 213–216.

Breteler, M.M., (2000). Vascular risk factors for Alzheimer's disease: an epidemiologic perspective. *Neurobiology of Aging, 21*(2), 153-60.

Breteler, M.M., (2000). Vascular involvement in cognitive decline and dementia. Epidemiologic evidence from the Rotterdam Study and the Rotterdam Scan Study. *Annals of N Y Academy of Sciences, 903,* 457-65.

Buee, L., Hof, P.R., & Delacourte, A. (1997). Brain microvascular changes in Alzheimer's disease and other dementias. *Annals of N Y Academy of Sciences, 826,* 7-24.

Cataldo, A.M., Nixon, R.A., (1990). Enzymatically active lysosomal proteases are associated with amyloid deposits in Alzheimer brain. *Proceedings of National Academy of Sciences USA, 87***,** 3861-5.

Cataldo, A.M., Barnett, J.L., Pieroni, C., Nixon, R.A., (1997). Increased neuronal endocytosis and protease delivery to early endosomes in sporadic Alzheimer's disease: neuropathologic evidence for a mechanism of increased β-amyloidogenesis. *Journal of Neuroscience, 17***,** 6142-51.

Chengappa, K.N., Carpenter, A.B., Keshavan, M.S., Yang, Z.W., Kelly, R.H., Rabin, B.S., & Ganguli, R., (1991). Elevated IGG and IGM anticardiolipin antibodies in a subgroup ofmedicated and unmedicated schizophrenic patients. *Biological*

Psychiatry, 30, 731-5.

Chui, D.H., Tanahashi, H., Ozawa, K., Ikeda, S., Checler, F., Ueda, O., Suzuki, H., Araki, W., Inoue, H., (1999).Transgenic mice with Alzheimer presenilin 1 mutations show accelerated neurodegeneration without amyloid plaque formation. *Nature Medicine, 5*(5), 560-564.

Citron, M., Vigo-Pelfrey, C., Teplow, D.B., Miller, C., Schenk, D., Johnston, J., Winblad, B., Venizelos, N., Lannfelt, L., & Selkoe, D.J. (1994). Excessive production of amyloid β-protein by peripheral cells of symptomatic and presymptomatic patients carrying the Swedish familial Alzheimer disease mutation. *Proceedings of National Academy of Sciences USA, 91*(25), 11993-7.

Citron, M., Westaway, D., Xia, W., Carlson, G., Diehl, T., Levesque, G., Johnson-Wood, K., Lee, M., Seubert, P., Davis, A., Kholodenko, D., Motter, R., Sherrington, R., Perry, B., Yao, H., Strome, R., Lieberburg, I., Rommens, J., Kim, S., Schenk, D., Fraser, P., St. George Hyslop, P., Selkoe, D.J. (1997). Mutant presenilins of Alzheimer's disease increase production of 42-residue amyloid β-protein in both transfected cells and transgenic mice. *Nature Medicine 3*, 67-72.

Clifford, P.M., Zarrabi, S., Siu, G., Kinsler, K.J., Kosciuk, M.C., Venkataraman, V., D'Andrea, M.R., Dinsmore, S., & Nagele, R.G. (2007). Aβ peptides can enter the brain through a defective blood-brain barrier and bind selectively to neurons. *Brain Research, 1142,* 223-36.

D'Andrea, M.R., Nagele, R.G., Wang, H.Y., Peterson, P.A., & Lee, D.H., (2001). Evidence that neurons accumulating amyloid can undergo lysis to form amyloid plaques in Alzheimer's disease. *Histopathology, 38*(2), 120-34.

D'Andrea, M.R., (2003). Evidence linking neuronal cell death to autoimmunity in Alzheimer's disease. *Brain Research., 982***,** 19-30.

D'Andrea, M.R. & Nagele, R.G. (2006). Targeting the alpha 7 nicotinic acetylcholine receptor to reduce amyloid accumulation in Alzheimer's disease pyramidal neurons. *Current Pharmaceutical Design, 12*(6), 677-84.

Deane, R., Wu, Z. & Zlokovic, B.V. (2004). RAGE (yin) versus LRP (yang) balance regulates alzheimer amyloid β-peptide clearance through transport across the blood-brain barrier. *Stroke, 35*(11 Suppl 1), 2628-31.

Deane, R., & Zlokovic, B.V., (2007). Role of the blood-brain barrier in the pathogenesis of Alzheimer's disease. *Current Alzheimer Research 4***,** 191-7.

DeGiorgio, L.A., Konstantinov, K.N., Lee, S.C., Hardin, J.A., Volpe, B.T., & Diamond, B., (2001). A subset of lupus anti-DNA antibodies cross-reacts with the NR2 glutamate receptor in systemic lupus erythematosus. *Nature Medicine 7***,** 1189-93.

de la Torre, J.C. (2004). Is Alzheimer's disease a neurodegenerative or a vascular

disorder? Data, dogma, and dialectics. *Lancet Neurology 3*(3)184-90.

de la Torre, J.C., (2004). Alzheimer's disease is a vasocognopathy: a new term to describe its nature. *Neurology Research 26*, 517–524.

Diamond, B., Kowal, C., Huerta, P.T., Aranow, C., Mackay, M., DeGiorgio, L.A., Lee, J., Triantafyllopoulou, A., Cohen-Solal, J., & Volpe, B.T., (2006). Immunity and acquired alterations in cognition and emotion: lessons from SLE. *Advances in Immunology, 89,* 289-320.

Diamond, B., Huerta, P.T., Mina-Osorio, P., Kowal, C., & Volpe, B.T., (2009). Losing your nerves? Maybe it's the antibodies. *Nature Reviews Immunology. 9,* 449-56.

Dong, H., Martin, M.V., Chambers, S., & Csernansky, J.G., (2007). Spatial relationship between synapse loss and β-amyloid deposition in Tg2576 mice. *Journal of Comparative Neurology 500*, 311–321.

Duff, K., & Suleman, F., (2004). Transgenic mouse models of Alzheimer's disease: how useful have they been for therapeutic development? *Brief Funcional Genomic Proteomic 3,* 47–59.

Dziewczapolski, G., Glogowski, C.M., Masliah, E., & Heinemann, S.F., (2009). Deletion of the alpha 7 nicotinic acetylcholine receptor gene improves cognitive deficits and synaptic pathology in a mouse model of Alzheimer's disease. *Journal of Neuroscience 29,* 8805-15.

Farkas, E. & P.G. Luiten, (2001).Cerebral microvascular pathology in aging and Alzheimer's disease. *Progress in Neurobiology, 64* (6), 575-611.

Felician, O. & Sandson, T.A., (1999). The neurobiology and pharmacotherapy of Alzheimer's disease. *Journal of Neuropsychiatry & Clinical Neuroscience. 11*, 19–31.

Ferreira, A., Lu, Q., Orecchio, L, & Kosik, K.S., (1997).Selective phosphorylation of adult tau isoforms in mature hippocampal neurons exposed to Fibrillar Aβ. *Molecular and Cellular Neuroscience 9*(3), 220-234.

Firer, M., Sirota, P., Schild, K., Elizur, A., & Slor, H., (1994). Anticardiolipin antibodies are elevated in drug-free, multiply affected families with schizophrenia. *Journal of Clinical Immunology 14,* 73-8.

Games, D., Adams, D., Alessandrini, R., Barbour, R., Borthelette, P., Blackwell, C., Carr, T., Clemens, J., Donaldson, T., Gillespie, F., Guido, T., Hagopian, S., Johnson-Wood, K., Khan, K., Lee M., Leibowitz, P., Lieberburg, I., Little, S., Masliah, E., McConlogue, L., Montoya-Zavala, M., Mucke, L., Paganini, L., Penniman, E., Power M., Schenk, D., Seubert, P., Snyder, B., Soriano, F., Tan, H., Vitale, J., Wadsworth, S., Wolozin, B., Zhao, J., (1995).Alzheimer-type neuropathology in transgenic mice overexpressing V717F β-amyloid precursor protein. *Nature 373,*

523-527

Ganguli, R., Rabin, B.S., Brar, & J.S., (1992). Antinuclear and gastric parietal cell autoantibodies in schizophrenic patients. *Biological Psychiatry, 32***,** 735-8.

Ghiso, J., Calero, M., Matsubara, E., Governale, S., Chuba, J., Beavis, R., Wisniewski, T. & Frangione, B. (1997). Alzheimer's soluble amyloid β is a normal component of human urine. *FEBS Letters 408*(1) 105-8.

Golde, T.E., & Janus, C., (2005).Homing in on intracellular Aβ. *Neuron 45*(5), 639-642.

Gordon, N., (2009). Sydenham's chorea, and its complications affecting the nervous system. *Brain Development 31***,** 11-4.

Gouras, G.K., Tsai, J., Naslund, J., Vincent, B., Edgar, M., Checler, F., Greenfield, J.P., Haroutunian, V., Buxbaum, J.D., Xu, H., Greengard, P., & Relkin, N.R., (2000). Intraneuronal Aβ42 accumulation in human brain. *American Journal of Pathology 156***,** 15-20.

Graus, F., Saiz, A., & Dalmau, J., (2009). Antibodies and neuronal autoimmune disorders of the CNS. *Journal of Neurology* 257 (4), 509-517.

Grbovic, O.M., Mathews, P.M., Jiang, Y., Schmidt, S.D., Dinakar, R., Summers-Terio, N.B., Ceresa, B.P., Nixon, R.A., & Cataldo, A.M. (2003). Rab5-stimulated up-regulation of the endocytic pathway increases intracellular β-cleaved amyloid precursor protein carboxyl-terminal fragment levels and Aβ production. *Journal of Biological Chemistry 278***,** 31261-8.

Grossman, H.C., Hale, G., Light, K., Kolata, S., Townsend, D.A., Goldfarb, Y., Kusnecov, A., Matzel, L.D., (2007).Pharmacological modulation of stress reactivity dissociates general learning ability from the propensity for exploration. *Behavioral Neuroscience 121*(5), 949-96.

Hardy, J., (1992). An 'anatomical cascade hypothesis' for Alzheimer's disease. *Trends in Neurosciences 15*(6), 200-201.

Hardy, J., & Selkoe, D.J., (2002).The amyloid hypothesis of Alzheimer's disease: progress and problems on the road to therapeutics. *Science 297,* 353-356.

Hartley, D.M., Walsh, D.M., Ye, C.P., Diehl, T., Vasquez, S., Vassilev, P.M., Teplow, D.B., Selkoe, D.J., (1999). Protofibrillar intermediates of amyloid β-protein induce acute electrophysiological changes and progressive neurotoxicity in cortical neurons. *The Journal of Neuroscience 19*(20), 8876-8884.

He, Y., Janssen, W.G.M., Vissavajjhala, P., Morris, J.H., (1998).Synaptic distribution of GluR2 in hippocampal GABAergic interneurons and pyramidal cells: a double-label immunogold analysis. *Experimental Neurology 150*(1), 1-13.

Hebert, L.E., Scherr, P.A., Bienias, J.L., Bennett, D.A., & Evans, D.A. (2003). Alzheimer disease in the US population: prevalence estimates using the 2000 census. *Archives of Neurology, 60*(8), 1119-22.

Heston, L.L. (1977). Alzheimer's disease, trisomy 21, and myeloproliferative disorders: associations suggesting a genetic diathesis. *Science,* 196(4287), 322-3.

Hoekstra, P.J. & Minderaa, R.B . (2005). Tic disorders and obsessive-compulsive disorder: is autoimmunity involved? *International Review of Psychiatry, 17*(6), 497-502.

Hsiao, K., Chapman, P., Nilsen, S., Eckman, C., Harigaya, Y., Younkin, S., Yang, F., & Cole, G., (1996). Correlative memory deficits, Aβ elevation, and amyloid plaques in transgenic mice. *Science 274*, 99–102.

Hwang, T.J., Masterman, D.L., Ortiz, F., Fairbanks, L.A., Cummings, J.L. (2004) Mild Cognitive impairment is associated with characteristic neuropsychiatric symptoms. *Alzheimer Disease & Associated Disorders 18*, 17-21

Irani, S., & Lang, B., (2008). Autoantibody-mediated disorders of the central nervous system. *Autoimmunity. 41***,** 55-65.

Irizarry, M.C., McNamara, M., Fedorchak, K., Hsiao, K., & Hyman, B.T. (1997). APPSw transgenic mice develop age–related A β deposits and neuropil abnormalities, but no neuronal loss in CA1. *Journal of Neuropathology and Experimental Neurology 56*, 965–973.

Jankowsky, J.L., Melnikova, T., Fadale, D.J., Xu, G.M., Slunt, H.H., Gonzales, V., Younkin L.H., Younkin, S.G., Borchelt, D.R., Savonenko, A.V., (2005).Environmental enrichment mitigates cognitive deficits in a mouse model of Alzheimer's disease. *The Journal of Neuroscience 25*(21), 5217-5224.

Johnson-Wood, K., Lee, M., Motter, R., Hu, K., Gordon, G., Barbour, R., Khan, K., Gordon, M., Tan, H., Games, D., Lieberburg, I., Schenk, D., Seubert, P., & McConlogue, L., (1997).Amyloid precursor protein processing and Aβ42 deposition in a transgenic mouse model of Alzheimer disease. *Proceedings of National Academy of Sciences USA 94*(4), 1550-1555.

Kalaria, R.N., et al., (1996). Production and increased detection of amyloid β protein and amyloidogenic fragments in brain microvessels, meningeal vessels and choroid plexus in Alzheimer's disease. *Molecular Brain Research 35*, 58–68.

Kalaria, R.N., (1999). The blood-brain barrier and cerebrovascular pathology in Alzheimer's disease. *Annals of NY Academy of Sciences 893***,** 113-25.

Kandimalla, K.K., et al., (2005). Pharmacokinetic analysis of the blood–brain barrier transport of 125I-amyloid β protein 40 in wild-type and Alzheimer's disease transgenic mice (APP,PS1) and its implications for amyloid plaque formation.

Journal of Pharmacology & Experimental Therapeutics 313, 1370–1378.

Kirvan, C.A., Swedo, S.E., Kurahara, D., & Cunningham, M.W. (2006). Streptococcal mimicry and antibody-mediated cell signaling in the pathogenesis of Sydenham's chorea. *Autoimmunity. 39***,** 21-9.

Kolata, S., Light, K., Grossman, H.C., Hale, G., Matzel, L.D., (2007). Selective attention is a primary determinant of the relationship between working memory and general learning ability in outbred mice. *Learning & Memory 14*(1), 22-28.

Kolata, S., Light, K., Townsend, D.A., Hale, G., Grossman, H.C., Matzel, L.D. (2005). Variations in working memory capacity predict individual differences in general learning abilities among genetically diverse mice. *Neurobiology of Learning & Memory 84*(3), 241-246.

Koo, E.H. & Squazzo, S.L., (1994). Evidence that production and release of amyloid β-protein involves the endocytic pathway. *Journal of Biological Chemistry 269*, 17386–17389.

Kowal, C., DeGiorgio, L.A., Nakaoka, T., Hetherington, H., Huerta, P.T., Diamond, B., & Volpe, B.T. (2004). Cognition and immunity; antibody impairs memory. *Immunity, 21*(2), 179-88.

LaFerla, F.M., Green, K.N., & Oddo, S. (2007). Intracellular amyloid-β in Alzheimer's disease. *Nature Review of Neuroscience, 8*(7) 499-509.

Levin, E.C., Acharya, N.K., Han, M., Zavareh, S., Sedeyn, J.C., Venkataraman, V., & Nagele, R.G. (2010). Brain-reactive autoantibodies are nearly ubiquitous in human sera and may be linked to pathology in the context of blood-brain barrier breakdown. Manuscript submitted for publication, University of Medicine and Dentistry of New Jersey

Loeffler, D.A., Juneau, P.L., Nguyen, H.U., Najman, D., Pomara, N., & LeWitt, P.A. (1997). Immunocytochemical detection of anti-hippocampal antibodies in Alzheimer's disease and normal cerebrospinal fluid. *Neurochemistry Research 22***,** 209-14.

Lue, L.F., Kuo, Y.M., Roher, A.E., Brachova, L., Shen, Y., Sue, L., Beach, T., Kurth, J.H., Rydel, R.E., Rogers, J., (1999).Soluble amyloid β peptide concentration as a predictor of synaptic change in Alzheimer's disease. *American Journal of Pathology 155*, 853-862.

Machulda, M.M., Ward, H.A., Borowski, B., Gunter, J.L. (2003). Comparison of memory fMRI response among normal, MCI, and Alzheimer's patients. *Neurology 61*,500-506.

Matzel LD, Han YR, Grossman H, Karnik MS, Patel D, Scott N, Specht SM, Gandhi CC. (2003). Individual differences in the expression of a "general" learning ability in

mice. *Journal of Neuroscience 23*(16), 6423-6433.

Matzel, L.D., Townsend, D.A., Grossman, H., Han, Y.R., Hale, G., Zappulla, M., Light, K., Kolata, S., (2006).Exploration in outbred mice covaries with general learning abilities irrespective of stress reactivity, emotionality, and physical attributes. *Neurobiology of Learning & Memory 86*(2), 228-240.

Mayeux, R., Honig, L.S., Tang, M.X., Manly, J., Stern, Y., Schupf, N., & Mehta, P.D. (2003). Plasma A[β]40 and A[β]42 and Alzheimer's disease: relation to age, mortality, and risk. *Neurology, 61*(9), 1185-90.

Mecocci, P., Ekman, R., Parnetti, L., & Senin, U. (1993). Antihistone and anti-dsDNA autoantibodies in Alzheimer's disease and vascular dementia. *Biological Psychiatry. 34***,** 380-5.

Mellman, I.S. (1982). Endocytosis, membrane recycling and Fc receptor function. *Ciba Found Symp*. 35-58.

Mocellin, R., Walterfang, M., & Velakoulis, D. (2007). Hashimoto's encephalopathy: epidemiology, pathogenesis and management. *CNS Drugs. 21***,** 799-811.

Moechars, D., Lorent, K., & Van Leuv, F., (1999). Premature death in transgenic mice that overexpress a mutant amyloid precursor protein is preceded by severe neurodegeneration and apoptosis. *Neuroscience 91*(3), 819-830

Monestier, M., & Kotzin, B.L. (1992). Antibodies to histones in systemic lupus erythematosus and drug-induced lupus syndromes. *Rheumatology Disorders Clinic North America, 18***,** 415-36.

Mooradian, A.D. (1988). Effect of aging on the blood-brain barrier. *Neurobiology of Aging 9***,** 31-9.

Mori E, Hirono N, Yamashita H, Imamura T, Ikejiri Y, Ikeda M, Kitagaki H, Shimomura T, Yoneda Y (1997). Premorbid brain size as a determinant of reserve capacity against intellectual decline in Alzheimer's disease. *American Journal of Psychiatry* 154, 18-24.

Mori C, Spooner ET, Wisniewsk KE, Wisniewski TM, Yamaguch H, Saido TC. (2002).. Intraneuronal Abeta42 accumulation in Down syndrome brain. *Amyloid* 9,88-102.

Morris, R.G.M. (1974).Pavlovian conditioned inhibition of fear during shuttlebox avoidance behavior. *Learning Motivation 5*, 424-447.

Morris, R.G.M. (1981). Spatial localization does not require the presence of local cues. *Learning Motivation 12*, 239–260.

Nagele, R.G., D'Andrea, M.R., Anderson, W.J., & Wang, H.Y. (2002). Intracellular accumulation of β-amyloid(1-42) in neurons is facilitated by the alpha 7 nicotinic

acetylcholine receptor in Alzheimer's disease. *Neuroscience, 110(*2), 199-211.

Nagele, R.G., D'Andrea, M.R., Lee, H., Venkataraman, V., & Wang, H.Y. (2003). Astrocytes accumulate Aβ42 and give rise to astrocytic amyloid plaques in Alzheimer disease brains. *Brain Research, 971*(2), 197-209.

Nagele, R.G., Wegiel, J., Venkataraman, V., Imaki, H., & Wang, K.C. (2004). Contribution of glial cells to the development of amyloid plaques in Alzheimer's disease. *Neurobiology of Aging 25***,** 663-74.

Nagele, R.G., Clifford, P.M., Siu, G., Levin, E.C., Acharya, N.K., Han, M., Kosciuk, M.C., Venkataraman, V., Zarrabi, S., Kinsler, K., Patel, N., & Levitas, A. (2010). Brain-reactive autoantibodies in human serum can drive amyloid β 1-42 (Aβ42) deposition in neurons: implications for Alzheimer's disease. Manuscript submitted for publication, University of Medicine and Dentistry of New Jersey

Nalbantoglu, J., Tirado-Santagio, G., Lahsaini, A., Poirier, J., Goncalves, O., Verge, G., Momoli, F., Welner, S.A., Massicotte, G., Julien, J.P., & Shapiro, M.L., (1997). Impaired learning and LTP in mice expressing the carboxy terminus of the Alzheimer amyloid precursor protein. *Nature 387*, 500-505.

Noseworthy, M.D., & Bray, T.M., (2000). Zinc deficiency exacerbates loss in blood-brain barrier integrity induced by hyperoxia measured by dynamic MRI. *Proceedings of the Society for Experimental Biology and Medicine 223*(2), 175-182.

Oddo, S., Caccamo, A., Kitazawa, M., Tseng, B.P., & LaFerla, F.M. (2003). Amyloid deposition precedes tangle formation in a triple transgenic model of Alzheimer's disease. *Neurobiology of Aging 24***,** 1063-70.

Oddo, S., Caccamo, A., Tran, L., Lambert, M.P., Glabe, C.G., Klein, W.L., & LaFerla, F.M., (2006).Temporal profile of amyloid-β (Aβ) oligomerization in an *in vivo* model of Alzheimer disease: a link between Aβ and tau pathology. *The Journal of Biological Chemistry 281,* 1599-1604.

Oddo, S. & LaFerla, F.M., (2006). The role of nicotinic acetylcholine receptors in Alzheimer's disease. *Journal of Physiology-Paris 99,* 172-179.

Petersen, R.C., Smith, G.E., Waring, S.C., Ivnik, R.J., Tangalos, E.G., Kokmen, E. (1999) Mild Cognitive Impairment: Clinical characterization and outcome. *Archives of Neurology* 56, 303-308.

Poduslo, J.F., et al., (1999). Receptor-mediated transport of human amyloid β-protein 1–40 and 1–42 at the blood–brain barrier. *Neurobiology of Disease 6*, 190–199.

Price, J.L., Rubin, E.H., & Morris, J.C., (2000).Revisiting Alzheimer's disease from a new prospective: can "risk factors" play a key role? *Journal of Alzheimer's Disease 2*(2), 113-114.

Rank, K.B., Pauley, A.M., Bhattacharya, K., Wang, Z., Evans, D.B., Fleck, T.J., Johnston, J.A., & Sharma, S.K., (2002).Direct interaction of soluble human recombinant tau protein with Aβ42 1-42 results in tau aggregation and hyperphosphorylation by tau protein kinase II. *FEBS Letters 514*(2-3), 263-268.

Richards M, Sacker A (2003). Lifetime antecedents of cognitive reserve. *Journal of Clinical and Experimental Neuropsychology* 25, 614-24

Rosenthal, A.S., Davie, J.M., & Rosenstreich, D.L., & Cehrs, K.U., (1973). Antibody-mediated internalization of B lymphocyte surface membrane immunoglobulin. *Experimental Cell Research 81***,** 317-29.

Salisbury, J.L., Condeelis, J.S., & Satir, P., (1980). Role of coated vesicles, microfilaments, and calmodulin in receptor-mediated endocytosis by cultured B lymphoblastoid cells. *Journal of Cell Biology 87***,** 132-41.

Sara S.J., Roullet P., & Przybyslawski J., (2001). Consolidation of memory for odor-reward association: B-adrenergic receptor involvement in the late phase. *Learning & Memory 6*, 88–96.

Schwartz, A.L., Ciechanover, A., Merritt, S., Turkewitz, A., (1986).Antibody-induced receptor loss. Different fates for asialoglycoproteins and the asialoglycoprotein receptor in HepG2 cells. *Journal of Biological Chemistry 261(*32), 15225-15232.

Selkoe, D.J., (1998).The cell biology of beta-amyloid precursor protein and presenilin in Alzheimer's disease. *Trends Cell Biology 8*(11), 447-453.

Seubert, P., et al., (1992). Isolation and quantification of soluble Alzheimer's β-peptide from biological fluids. *Nature 359*, 325–327.

Singh, V.K., (1997). Neuroautoimmunity: pathogenic implications for Alzheimer's disease. *Gerontology*. 43**,** 79-94.

Sirota, P., Firer, M.A., Schild, K., Tanay, A., Elizur, A., Meytes, D., & Slor, H. (1993). Autoantibodies to DNA in multicase families with schizophrenia. *Biological Psychiatry 33***,** 450-5.

Skoog, I., Wallin, A., Fredman, P., Hesse, C., Aevarsson, O., Karlsson, I., Gottfries, C.G., & Blennow, K. (1998). A population study on blood-brain barrier function in 85-year-olds: relation to Alzheimer's disease and vascular dementia. *Neurology, 50*(4), 966-71.

Stern Y, Albert S, Tang MX, Tsai WY. (1999) Rate of memory decline in AD is related to education and occupation: cognitive reserve? *Neurology. 53,* 1942-7.

Terryberry, J.W., Thor, G., Peter, J.B. (1998). Autoantibodies in neurodegenerative diseases: antigen-specific frequencies and intrathecal analysis. *Neurobiology of Aging 19***,** 205-16.

Thompson, P.M., Hayashi, K.M., Dutton, R.A., Chiang, M.C., Leow, A.D., Sowell, E.R., De Zubicaray, G., Becker, J.T., Lopez, O.L., Aizenstein, H.J., Toga, A.W., (2007).Tracking Alzheimer's Disease. *Annals of NY Academy of Sciences 1097*, 183-214.

Tucker-Drob EM, Johnson, KE, Jones, RN (2009). The cognitive reserve hypothesis: A longitudinal examination of age-associated declines in reasoning and processing speed. *Developmental Psychology*. 45, 431-46.

Ujiie, M., Dickstein, D.L., Carlow, D.A., & Jefferies, W.A. (2003). Blood-brain barrier permeability precedes senile plaque formation in an Alzheimer disease model. *Microcirculation, 10*(6), 463-70.

Verdile, G., Gnjec, A., Miklossy, J., Fonte, J., Veurink, G., Bates, K., Kakulas, B., Mehta, P.D., Milward, E.A., Tan, N., Lareu, R., Lim, D., Dharmarajan, A., & Martins, R.N., (2004).Protein markers for Alzheimer disease in the frontal cortex and cerebellum. *Neurology 63*(8), 1385-1392.

Verdile, G., Fuller, S., Atwood, C.S., Laws, S.M., Gandy, S.E., & Martins, R.N., (2004).The role of beta amyloid in Alzheimer's disease: still a cause of everything or the only one who got caught? *Pharmacology Research 50*(4), 397-409.

Verdile, G., Groth, D., Mathews, St, P., Hyslop, G., Fraser, P., Ramabhadran, T.V., Kwok, J., Schofield, P., Carter, T., Gandy, S., & Martins, R. (2004).P4-265. Baculoviral expression of the presenilin mutation lacking exon 9 increase levels of an amyloid beta-like protein in SF9 insect cells. *Neurobiology of Aging 25*, S550-S551.

Wada, H. (1998). Blood-brain barrier permeability of the demented elderly as studied by cerebrospinal fluid-serum albumin ratio. *Internal Medicine, 37*(6), 509-13.

Walsh, D.M., Hartley, D.M., Kusumoto, Y., Fezoui, Y., Condron, M.M., Lomakin, A., Benedek, G.B., Selkoe, D.J., Teplow, D.B., (1999). Amyloid beta-protein fibrillogenesis. Structure and biological activity of protofibrillar intermediates. *Journal of Biological Chemistry 274*(36), 25945-25952.

Wang, H.Y., Lee, D.H., D'Andrea, M.R., Peterson, P.A., Shank, R.P., & Reitz, A.B. (2000). β-Amyloid(1-42) binds to alpha7 nicotinic acetylcholine receptor with high affinity. Implications for Alzheimer's disease pathology. *Journal of Biological Chemistry, 275*(8), 5626-32.

Wang, H.Y., Lee, D.H., Davis, C.B., Shank, R.P., (2000). Amyloid peptide Aβ(1-42) binds selectively and with picomolar affinity to alpha7 nicotinic acetylcholine receptors. *Journal of Neurochemistry 75***,** 1155-61.

Wang, H.Y., D'Andrea, M.R., Nagele, R.G. (2002). Cerebellar diffuse amyloid plaques are derived from dendritic Aβ42 accumulations in Purkinje cells. *Neurobiology of Aging 23***,** 213-23.

Wang, H.Y., Stucky, A., Liu, J., Shen, C., Trocme-Thibierge, C., & Morain, P., (2009). Dissociating beta-amyloid from alpha 7 nicotine acetylcholine receptor by a novel therapeutic agent, S 24795, normalizes alpha 7 nicotinic acetylcholine and NMDA receptor function in Alzheimer's disease brain. *Journal of Neuroscience 29*(35), 10961-10973.

Wehland, J., Willingham, M.C., Gallo, M.G., Rutherford, A.V., Rudick, J., Dickson, R.B., & Pastan, I., (1982). Microinjection of anticlathrin antibodies into cultured fibroblasts: clathrin coated structures in receptor-mediated endocytosis and in exocytosis. *Cold Spring Harb Symp Quant Biology 46 Pt 2***,** 743-53.

Weisman, D., Hakimian, E., & Ho, G.J., (2006). Interleukins, inflammation, and mechanisms of Alzheimer's disease. *Vitamins & Hormones 74***,** 505-30.

Wilson, C.A., et al. (1999). Intracellular APP processing and Aβ production in Alzheimer disease. *Journal of Neuropathology & Experimental Neurology 58*, 787–794.

Younkin, S.G., (1995).Evidence that Aβ42 is the real culprit in Alzheimer's disease. *Annals of Neurology 37*(3), 287-288.

Zhang, M., Chen, L., Wang, S., & Wang, T., (2009). Rab7: roles in membrane trafficking and disease. *Bioscience Reports 29***,** 193-209.

Zlokovic, B.V., et al. (1993). Blood–brain barrier transport of circulating Alzheimer's amyloid β. *Biochemical & Biophysical Research Communications 197*, 1034–1040.

Zlokovic, B.V. (2004). Clearing amyloid through the blood-brain barrier. *Journal of Neurochemistry 89*(4), 807-11.

Zlokovic, B.V. (2005). Neurovascular mechanisms of Alzheimer's neurodegeneration. *Trends Neuroscience 28*(4), 202-8.

Zlokovic, B.V., (2008). The blood-brain barrier in health and chronic neurodegenerative disorders. *Neuron 57***,** 178-201.

FIGURE LEGEND

Fig. 1 Histological sections through the brains of PT-Saline-treated mice immunostained to detect IgG

a-c. Perivascular leak clouds showing IgG-positive material emanating from local arterioles and binding to neurons. d. Dashed line indicates the interface separating IgG-positive and IgG-negative regions of the brain. Neurons in the former are intensely IgG-positive. e-f. Sections through the cerebral cortex and hippocampus at higher magnification showing intensely IgG-positive neurons coexisting with IgG-negative neurons.

Fig. 2. Histological sections through the brains of PT-Saline-treated mice immunostained to detect IgG .

a. Section showing leaky arteriole with IgG-positive material emerging along a good length of the vessel. b. Section of cortex showing small focal BBB leak from local capillaries. c. Cortex showing IgG-positive blood vessels with no significant leak.

d. Section of the hippocampus showing focal leak in the hilar region. e. Cerebellum showing capillaries in the molecular layer, one of which is leaking.

Fig. 3. Histological sections through the brains of PT- Aβ42-treated mice immunostained to detect IgG.

a-b. Sections showing intense focal IgG-positive leaks. Comparable vascular leaks occur also in the subcerebellar brainstem (c) and hippocampus (d). e-f. IgG-positive leak clouds were also occasionally seen in association with venules.

Fig. 4. Histological sections through the brains of PT- Aβ42-treated mice immunostained to detect IgG.

a. Streams of IgG-positive material emerging from an arteriole. b. Portion of cerebral cortex showing a wide expanse of cortical tissue that contains abundant IgG. IgG positive neurons are abundant in this region. c-f. Sections through the cortex showing both focal and more widespread IgG leak from local capillaries.

Fig. 5. Histological sections through the brains of Saline-Saline-treated mice immunostained to detect IgG.

a-b. IgG leaks in the hippocampus (a) and cerebral cortex (b) are rare. IgG is confined to blood vessels.

Fig. 6. Histological sections through the brains of PT- Aβ42-treated mice immunostained to detect IgG showing that IgG binds preferentially to certain subtypes of neurons.

a-b. Sections showing regions with both IgG-positive and IgG-negative neurons. c. The dashed line indicates the rough interface between IgG-positive and –negative brain regions. d-e. IgG is present primarily in the cell body of neurons, but not astrocytes. f. Neurons within or near leak clouds are the most IgG-immunopositive.

Fig. 7. Histological sections through the brains of PT- Aβ42-treated mice immunostained to detect IgG.

a-c. Progressive enlargements of a region of the cortex showing the branching of a small arteriole into a small capillary bed. IgG-positive material is leaking from the capillary bed into the surrounding interstitial space. d. IgG-positive leak cloud from local arteriole. e-f. Sections through the subcerebellar brainstem showing mild IgG leaks from local blood vessels and a few IgG-positive neurons.

Fig. 8. Histological sections through the brains of PT- Aβ42-treated mice immunostained to detect IgG. a-c.

Most neurons in this region of the cerebral cortex are IgG immunopositive. d. Section showing tiny IgG-positive leak cloud emerging from a single capillary. e-f. Sections of the cerebral cortex

showing interface between IgG-positive and –negative regions, with intensely IgG-positive neurons populating the former.

Fig. 9. Histological sections through the brains of PT-Saline-treated mice immunostained to detect Aβ42, MAP2 and synaptophysin.
In all cases, expression of these proteins was reduced when compared to the PT- Aβ42 group.

Fig. 10. Histological sections through the brains of Saline-Saline-treated mice immunostained to detect IgG (a-b), Aβ42 (c-d), GFAP (e) and NF protein (f).
All were dramatically reduced compared to the PT- Aβ42 group.

Fig. 11. Frozen sections through the brains of mice treated with PT-Saline showing a nearly complete lack of FITC- Aβ42 signal.

Fig. 12. Frozen sections through the brains of mice treated with PT-Saline showing lack of FITC-Aβ42 signal.

Fig. 13. Frozen sections through the cerebral cortex of mice treated with PT-Saline showing a general lack of FITC- Aβ42-specific signal, but the presence of variable numbers of lipofuscin foci, usually one per neuron.

Fig. 14. Frozen sections through the brains of mice treated with Saline-Saline showing a lack of FITC-labeled Aβ42-specific signal in the cerebral cortex (a-b) and hippocampus (c-d), with some autofluorescent lipofuscin bodies observable in neurons (b).

Fig. 15. Frozen sections through the brains of mice treated with PT and FITC-labeled Aβ42.
a. Blood vessel with associated Aβ42-positive leak cloud. b-c. Aβ42-positive neurons in vicinity of capillaries (b) and arterioles (c-d). e. Section through cortex generally lacking significant FITC- Aβ42. f. Section through the hippocampus showing blood vessels with little or no leaks.

Fig. 16. Frozen sections through the brains of mice treated with PT and FITC-labeled Aβ42.
a-b. Arterioles with substantial leaks of FITC- Aβ42 in the cerebral cortex. c-d. Sections through the hippocampus showing most FITC- Aβ42 confined to blood vessels. e-f. Higher magnifications of sections through the cerebral cortex showing FITC- Aβ42 within neurons confined to small granules of rather uniform size.

Fig. 17. Frozen sections through the brains of mice treated with PT and FITC-labeled Aβ42.
a-c. Sections through the cerebral cortex showing prominent vascular leaks with FITC- Aβ42 streaming from these leak sites and accumulating within local neurons. In some neurons with particularly abundant intracellular Aβ42, this material is often sequestered away from the entrances into axons and dendrites (c). d. Section through hippocampus showing minimal leak of Aβ42. e-f. Sections showing that neurons containing FITC- Aβ42 granules can be observed in both the presence (e) and absence of a local vessel with a conspicuous BBB leak.

Fig. 18. Frozen sections through the brains of mice treated with PT and FITC-labeled Aβ42 showing prominent arterioles with significant FITC- Aβ42 leaks (a) and numerous neurons with abundant FITC- Aβ42 sequestered in their cytoplasm (b-f).

Fig. 19. Histological sections through the brains of PT- Aβ42-treated mice immunostained to detect Aβ42.
a-d. Sections through the frontal cortex showing rather wide variations in the intensity of Aβ42-positive immunolabeling, with neurons in each region showing comparable immunolabeling intensity. e. Section through region of the cortex that is completely devoid of Aβ42. f. Section showing a small leaky arteriole and a local neurons confined to the leak cloud with elevated intracellular Aβ42.

Fig. 20. Histological sections through the brains of PT-Aβ42-treated mice immunostained to detect Aβ42 showing several neurons in the vicinity of a small capillary leak, with neurons proximal to this leak more intensely Aβ42 immunopositive.

Fig. 21. Histological sections through the brains of PT- Aβ42-treated mice immunostained to detect Aβ42.

a. Section showing widespread or diffuse Aβ42 immunolabeling. b. Section showing Aβ42 concentrated around three leak sites. c. Section of cerebellum showing fairly uniforma and intense Aβ42-positive immunostaining in the molecular layer dendrites belonging to nearby Purkinje neurons. d. Section through cortex showing only weak Aβ42 immunoreactivity in a few neurons and a general lack of Aβ42 reactivity in the "background" synapses.

Fig. 22. Histological sections through the cerebral cortex of PT- Aβ42-treated mice immunostained to detect Aβ42.

Most Aβ42 is localized to a specific subset of neurons, mostly pyramidal neurons, with Aβ42-positive material abundant in the cell body and main dendrite trunk, but not the nucleus.

Fig. 23. Histological sections through the brains of PT-Aβ42-treated mice immunostained to detect GFAP in activated astrocytes.

a. Region of cortex with weak GFAP immunolabeling of astrocytes in the cortical molecular layer. b. Comparable region lacking GFAP immunostaining. c-d. Region near the hippocampus showing a focal point of intense GFAP immunostaining, suggesting a site of astrocyte activation presumably corresponding to a region BBB breakdown and neuronal Aβ42 internalization.

Fig. 24. Histological sections through the hippocampal region of PT- Aβ42-treated mice immunostained to detect GFAP in activated astrocytes.

This region possesses the highest degree of astrocyte activation, with the hilar region of the hippocampus containing the largest and most intensely GFAP-positive astrocytes.

Fig. 25. Histological sections through the hippocampal region of PT- Aβ42-treated mice immunostained to detect GFAP in activated astrocytes.

a-b. Sections showing several foci of astrocyte activation that correspond in size to IgG-positive leaks. c-e. Sections illustrating weak to moderate GFAP immunostaining. f. Section showing several foci of astrocyte activation.

Fig. 26. Histological sections through the brains of PT-Aβ42-treated mice immunostained to detect GFAP in activated astrocytes.

Activated astocytes are GFAP immunopositive and their patchy distribution is reflective of the distribution of small focal leaks in the BBB. e. Section through region of cortex completely lacking GFAP immunolabeling, suggesting that local astrocytes are non-activated or are quiescent. f. Intense activation of astrocytes in the upper portion of the molecular layer of the cerebral cortex.

Fig. 27. Histological sections through the brains of PT- Aβ42-treated mice immunostained to detect F480 in phagocytic cells such as macrophages.

Both the cortex and hippocampus showed no F480 immunoreactivity, except for a few cells restricted to the meninges surrounding the brain tissue.

Fig. 28. Histological sections through the brains of PT- Aβ42-treated mice immunostained to detect MAP2 expression in neuronal dendrites.

a-d. MAP2 is only weakly expressed in cerebral cortex neurons, and not at all in the white matter. e-f. Clearly, the most prominent MAP2 immunostaining is seen in the hilar region of the hippocampus.

Fig. 29. Histological sections through the hippocampal regions of PT- Aβ42-treated mice immunostained to detect MAP2 expression in neuronal dendrites.

Some brains show weak MAP2 immunostaining.

Fig. 30. Histological sections through the hippocampus and cortex of PT- Aβ42-treated mice immunostained to detect synaptophysin.

Synapstophysin was effective in localizing synapses, but the staining results were inconsistent.

Fig. 31. Histological sections through the brains of PT- Aβ42-treated mice immunostained to detect neurofilament protein, primarily in axons.

a-b. Sections through the hippocampus showing relatively weak NF upregulation, especially in the hilar region. c-d. Sections through the basolateral cortex showing weak upregulation of NF expression in cortical dendrites and ascending axons. e. Section showing intensely NF-positive axon tracts. F. Section of cortex showing a nearly complete lack of NF staining, again highlighting the sporadic nature of the damage.

Fig. 32. Cortical Density of IgG-positive Neurons.

Illustrated is the mean number of Ig-G positive neurons in the cortical region of the brain per 20x viewing field for each treatment group. Brackets indicate standard error. Animals treated with PT-Sal and PT- Aβ42 exhibited a significantly greater density of Ig-G positive neurons relative to the Sal-Sal group ($p<..01$)

Fig. 33. Total Cortex AB42 Load: Unlabeled.

The average area of Aβ42 (both intra and extra-neural) of the cortex region relative to the total area of the slide at 20x magnification is shown for each treatment group. Brackets indicate standard error. Animals treated with PT- Aβ42 exhibited a significantly greater relative amount of Aβ42 as compared to the Sal-Sal and PT-Sal groups ($p<.01$)

Fig. 34. Total Cortex Aβ42 Load: FITC-Labeled.

The average area of FITC labeled Aβ42 (both intra and extra-neural) of the cortex region relative to the total area of the slide at 20x magnification is shown for each treatment group. Brackets indicate standard error. Animals treated with PT- Aβ42 exhibited a significantly greater relative amount of Aβ42 as compared to the Sal-Sal and PT-Sal groups ($p<.01$)

Fig. 35. Cortical Density of Aβ42-positive Neurons: Unlabeled.

The mean number of Aβ42 positive neurons in the cortical region of the brain per 20x viewing field is shown for each treatment group. Brackets indicate standard error. Animals treated with PT-Sal and PT- Aβ42 exhibited a significantly greater density of Aβ42 positive neurons as compared to the Sal-Sal group ($p<..01$)

Fig. 36. Cortical Density of Aβ42-positive Neurons: FITC-Labeled.

The mean number of FITC-labeled Aβ42 positive neurons in the cortical region of the brain per 20x viewing field is shown for each treatment group. Brackets indicate standard error. Animals treated with PT-Sal and PT- Aβ42 exhibited a significantly greater density of Ig-G positive neurons relative to the Sal-Sal group ($p<.01$)

Fig. 37. Hippocampal Astrocytic Activation.

Illustrated is the mean number of Ig-G positive neurons per 20x viewing field in the cortical region of the brain for each treatment group. Brackets indicate standard error. Animals treated with PT-Sal and PT- Aβ42 exhibited a significantly greater density of Ig-G positive neurons ($p<.01$)

*Fig. 38. Odor Discrimination Error***.**

Animals were trained to locate food in randomly assorted locations by using an odor cue to guide their behavior. Illustrated are the mean errors to locate the target food cup for animals in each treatment group. Brackets indicate standard error. As indicated by the asterisk, both on Trial 4 and on Trial 5 the PT- Aβ42 group showed significant deficits relative to the Sal- Aβ42, the PT-Sal group, and the Saline-Saline group ($p<.05$).

*Fig. 39. Passive Avoidance: Post/Pre Latency***.**

Upon stepping from a safe platform, animals were exposed to a presentation of a bright light and loud noise. The mean ratio of post-training to pretraining step latencies is illustrated. Brackets indicate standard errors. Animals treated with PT- Aβ42 showed a significantly lower latency than animals treated with PT-Sal ($p<.05$).

Fig. 40. Lashley Maze: Errors to Complete.

Animals were trained to locate food in the Lashley Maze. Mean errors to reach the goal box across trials are depicted for animals in each treatment group. Brackets indicate standard error. On trial 4, PT-Sal-treated mice committed significantly more errors than Sal- Aβ42-treated mice ($p<.05$). On trial 5, PT- Aβ42-treated mice committed significantly more errors than PT-Sal-treated mice, and PT-Sal-treated mice showed significantly more errors than Sal-Sal-treated mice ($p<.05$).

Fig. 41. Water Maze: Latency to Locate Platform.

Animals were trained to locate a hidden platform submerged below the surface in a tank of water. Illustrated is the latency to locate the hidden platform recorded across each of 12 training trials for animals in each treatment group. Brackets indicate standard error.

Fig. 42. Water Maze Retention: Percentage Time in Target Quadrant.

Following a 30-day retention interval, animals were then administered a 60-sec "probe" trial in which the escape platform was removed from the maze and the percent of time spent searching in the target quadrant was recorded. The mean time in the target quadrant is depicted. Brackets indicate standard error.

Fig. 43. Lashley Maze: Errors to Complete: Long-term Retention

Animals were trained to locate food in the Lashley Maze over 6 trials. Following a 30-day retention interval, they were administered two trials of the Lashley Maze (trials 7-8) to test their retention. A measure of retention was computed for each animal by obtaining a difference score between the errors committed on the first post-time lapse trial (i.e., trial 7) and the average of the last two acquisition trials (trials 5-6). Brackets indicate standard error.

Fig. 44. Lashley maze: Errors to Complete: Long-term Retention.

Animals were trained to locate food in the Lashley Maze over 6 trials and re-tested on 2 trials following a 30-day retention interval.

Fig. 45. Selective Attention.

Animals were trained on an odor discrimination task and a visual analogue of this same task in each of two distinct contexts. At the time of testing, the odor and visual cues were simultaneously presented on successive trials in either the context that signaled the odor discrimination-dependent cues or the visual discrimination-dependent cues. This required animals to selectively attend to appropriate cues and simultaneously filter out task-relevant distracter cues in order to perform efficiently. The average number of errors across the eight test trials is plotted as a function of treatment group. On trial 5, 6, and 7, the PT-Aβ42 group committed significantly more errors than each of the other groups, suggesting heightened susceptibility to accrual of interference over time.

Fig. 46. Dark/Light Test: % Time in Light compartment.

In the dark-light preference test, the percentage of time spent in the light compartment was examined as an index of anxiety-dependent exploration behavior. Percentage of time spent in light compartment is depicted for animals in each treatment group. Brackets indicate standard error.

*Fig. 47. Open Field: % Entries into Open Quadrants***.**

In the open field task, the percentage of entries into the open (unwalled) quadrants of the open field reflects exploratory behavior. Percentage of entries compartment is depicted for animals in each treatment group. Brackets indicate standard error.

Fig. 48. Shock-Induced Freeze: Latency to activity.

Latency to activity after an administered shock is depicted for animals in each treatment group. Brackets indicate standard error.

Fig. 49. Pain Sensitivity: Latency to Lick Hind Paw.

Sensitivity to pain was measured by recording the latency time to lick hind paw during placement on a hot plate. Latency to lick hind paw is depicted for animals in each treatment group. Brackets indicate standard error.

Fig. 50. Open Field: Total # of Quadrant Entries.

Animals were placed in an open field, and the total number of quadrant entries into an open field were recorded. This can be treated as a representation of general locomotor activity. Total number of quadrant entries is depicted for animals in each treatment group. Brackets indicate standard error.

Fig. 51. Balance Beam: # of Crossings.

Animals were placed on a narrow, elevated beam. The number of crossings is depicted for animals in each treatment group. Brackets indicate standard error.

Fig. 52. Rod Suspension: Latency to Fall.

Animals were hung by their front paws from an elevated rod. Latency (s) to fall is depicted for animals in each treatment group. Brackets indicate standard error.

*Fig. **53**. A generalized mechanism for AD pathogenesis with two major contributing factors: breakdown of the blood-brain barrier (BBB) and the presence of neuron-binding autoantibodies in the serum.*

In STEP 1, breach of the BBB results in chronic extravasation of plasma components including autoantibodies and soluble Aβ42 peptide. Autoantibodies bind to targets on neuronal surfaces; soluble exogenous Aβ42 has selective affinity for the surfaces of neurons that express the alpha7 nicotinic acetylcholine receptor (a7nAChR). In STEP 2, neurons continually attempt to clear their surfaces of bound antibodies by receptor-mediated endocytosis, which drives internalization of both autoantibodies and Aβ42 and the stripping of other key cell surface membrane proteins. In the lysosomal compartment, autoantibodies, but not Aβ42, are degraded, leading to gradual neuronal Aβ42 accumulation. In STEP 3, excessive intaneuronal Aβ42 accumulations lead to inability of the neuron to support their large dendrite trees, leading to progressive dendrite collapse, synaptic loss and eventual cell death. Local release of intracellular Aβ42 leads to a cloud of Aβ42 residue that forms a spherical amyloid plaque. Bar =100 μm.

Effects of PT-SALINE on BBB integrity
PT causes microvascular leaks
IgG can be used as a barometer of PT-induced BBB leak

Fig. 1 **PT-SALINE**: PT causes BBB compromise,leak of plasma components and selective binding of IgG to local pyramidal neurons

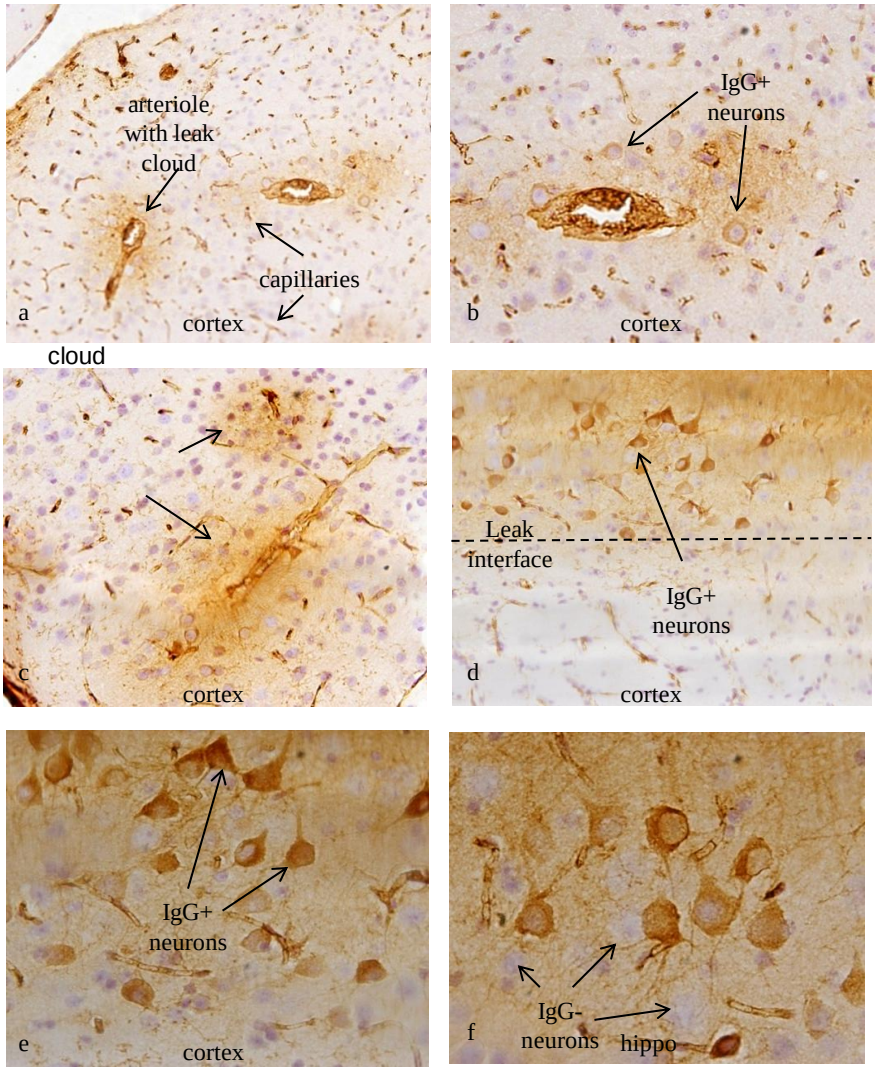

Note: All immunostained to detect IgG

Effects of PT-SALINE on BBB integrity
PT causes microvascular leaks
IgG can be used as a barometer of PT-induced BBB leak

Fig. 2 **PT-SALINE**: PT causes both focal and more extensive vascular leaks

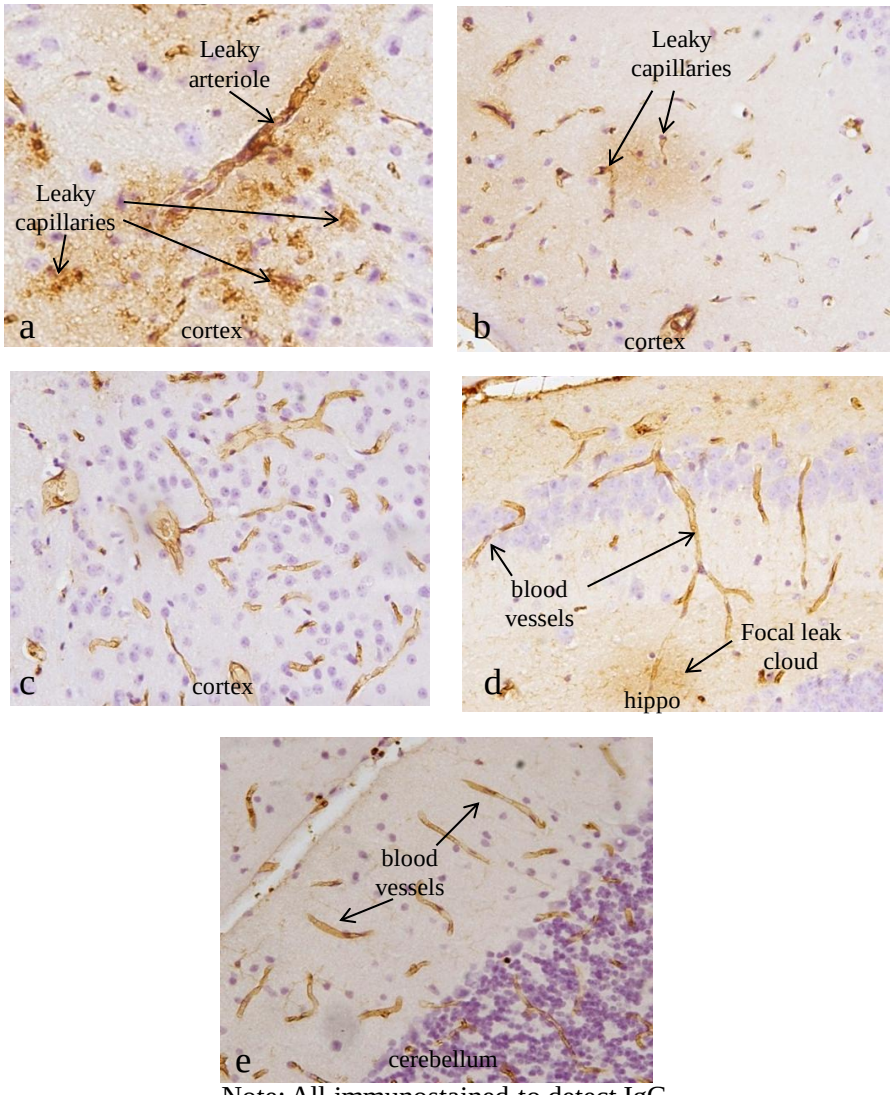

Note: All immunostained to detect IgG

Effects of PT-Aβ42 on BBB integrity
PT-Aβ42 causes microvascular leaks.
IgG can be used as a barometer of PT-induced BBB leak

Fig. 3 **PT-Aβ42**. IgG leak foci from brain arterioles and capillaries

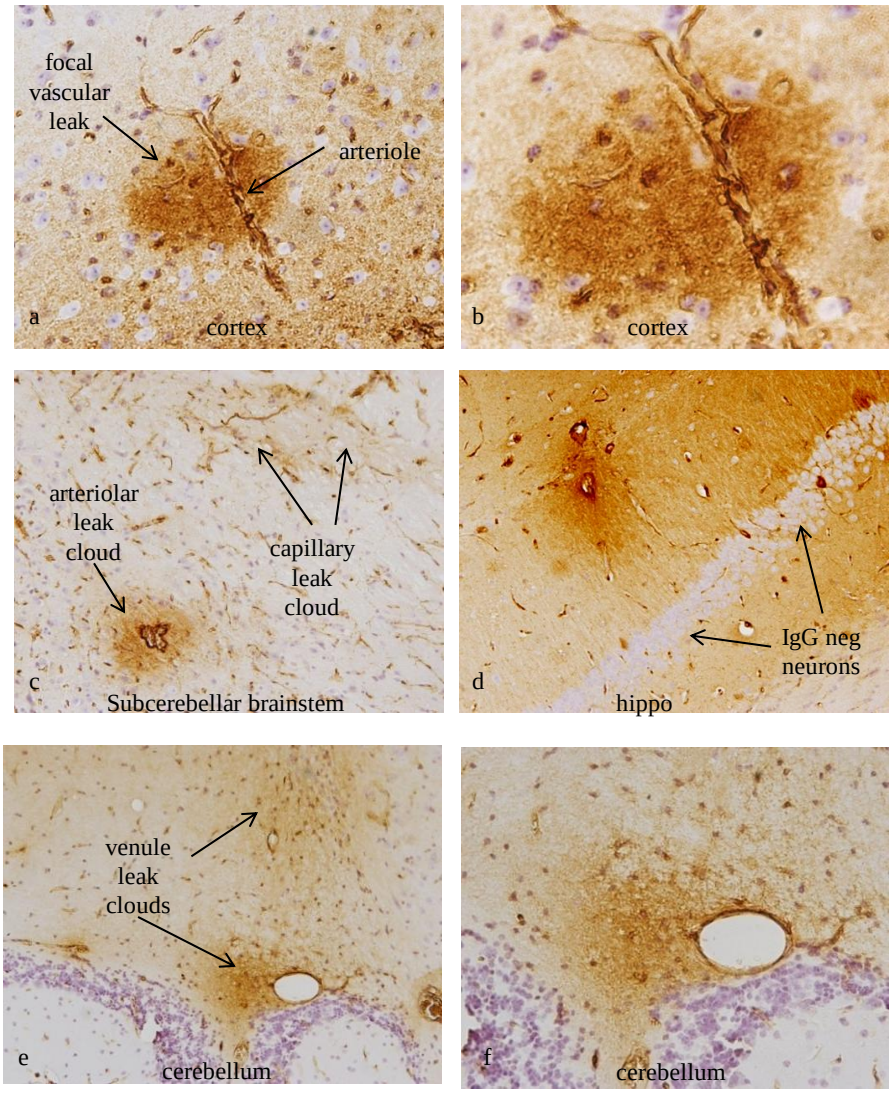

Note: All immunostained to detect IgG

Effects of PT-Aβ42 on BBB integrity
PT-Aβ42 causes microvascular leaks.
IgG can be used as a barometer of PT-induced BBB leak

Fig. 4 **PT-Aβ42**: IgG leaks from the microvasculature, arterioles and capillaries, and can be distributed throughout the brain parenchyma

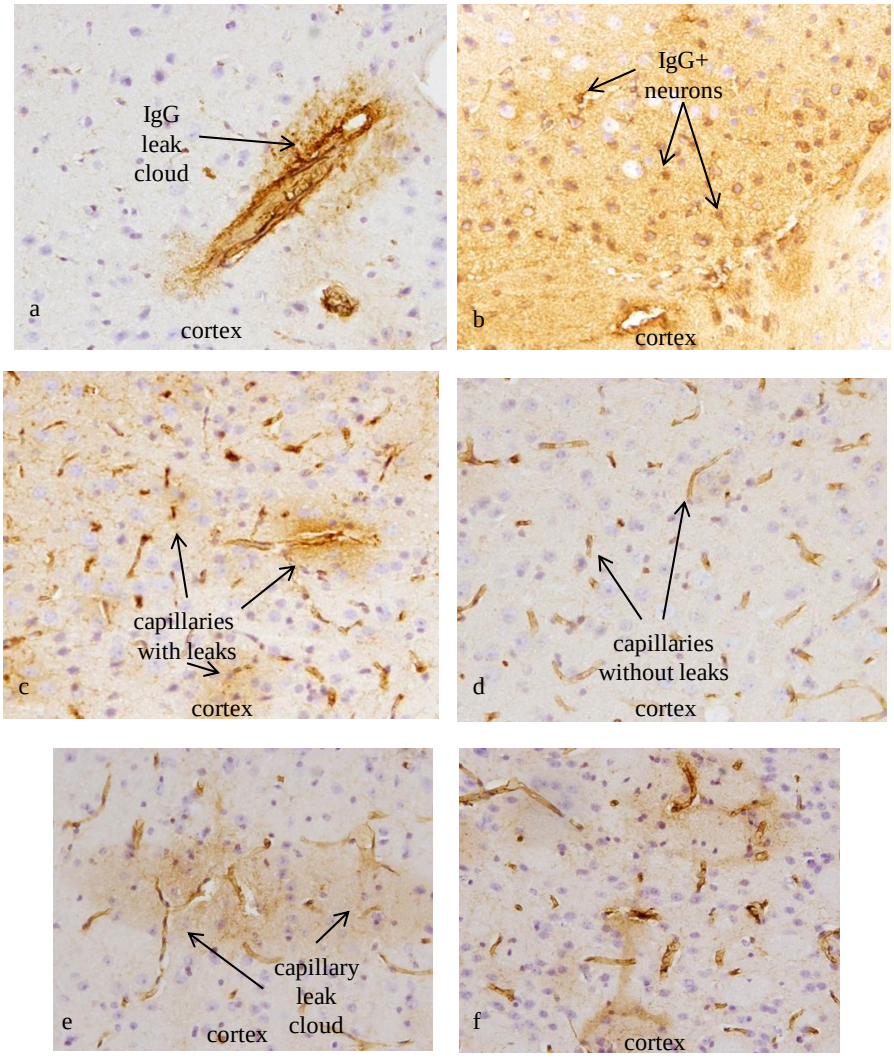

Note: All immunostained to detect IgG

Effects of SALINE-SALINE on BBB integrity
Saline has no effect on BBB.

Fig. 5 **SALINE-SALINE:** No IgG leaks – IgG is confined to the vasculature

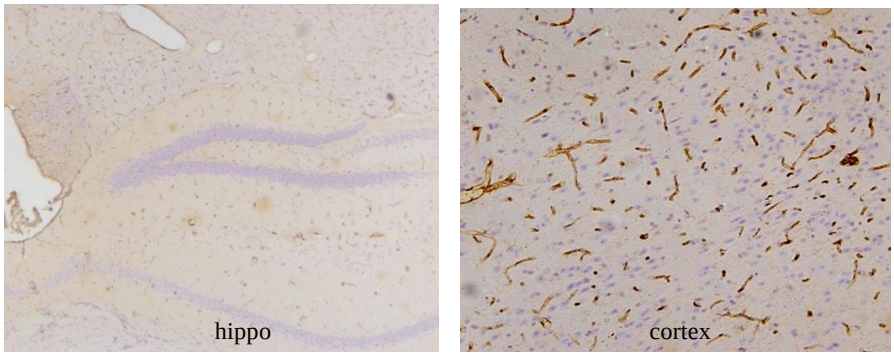

Note: All immunostained to detect IgG

IgG that leaks from blood vessels binds selectively to pyramidal neurons

Fig. 6 **PT-Aβ42**: Leaked IgG binds to neurons in the cerebral cortex

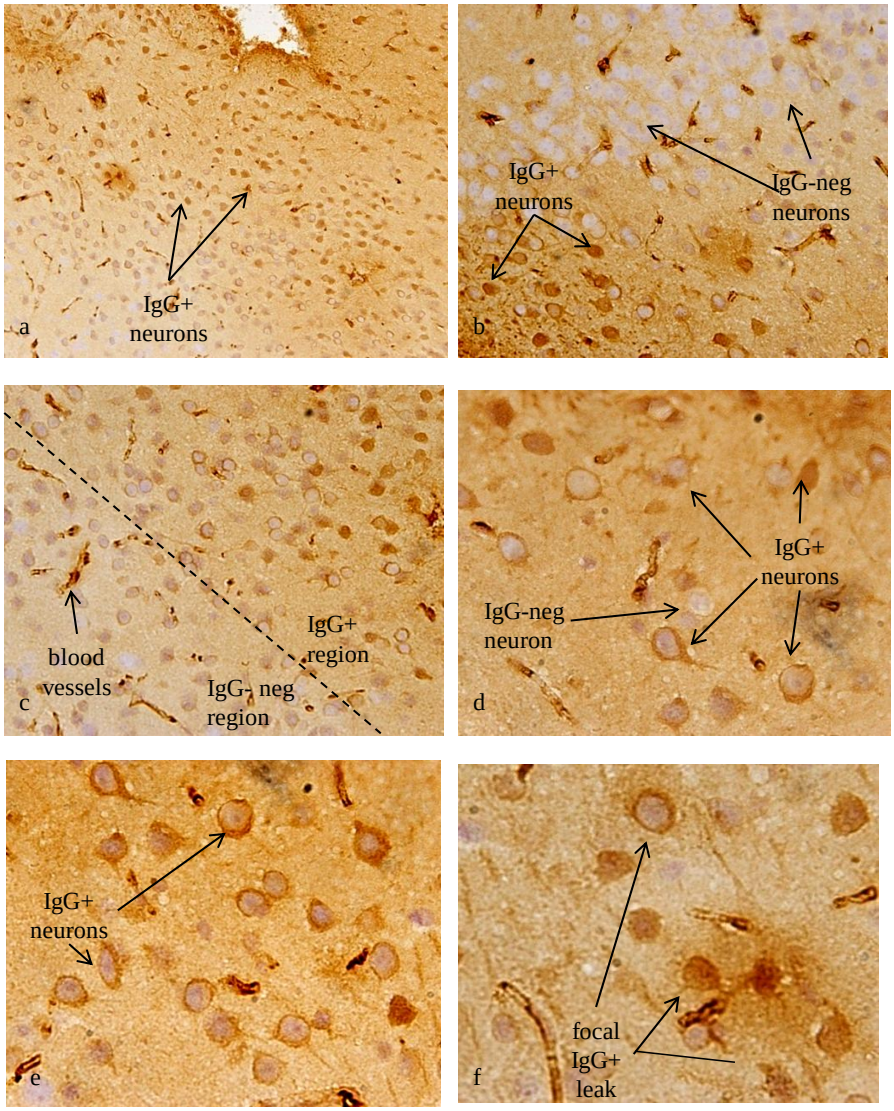

Note: All immunostained to detect IgG

IgG that leaks from blood vessels binds selectively to pyramidal neurons

Fig. 7 **PT-Aβ42**: IgG binds to neurons in the cerebral cortex and brainstem

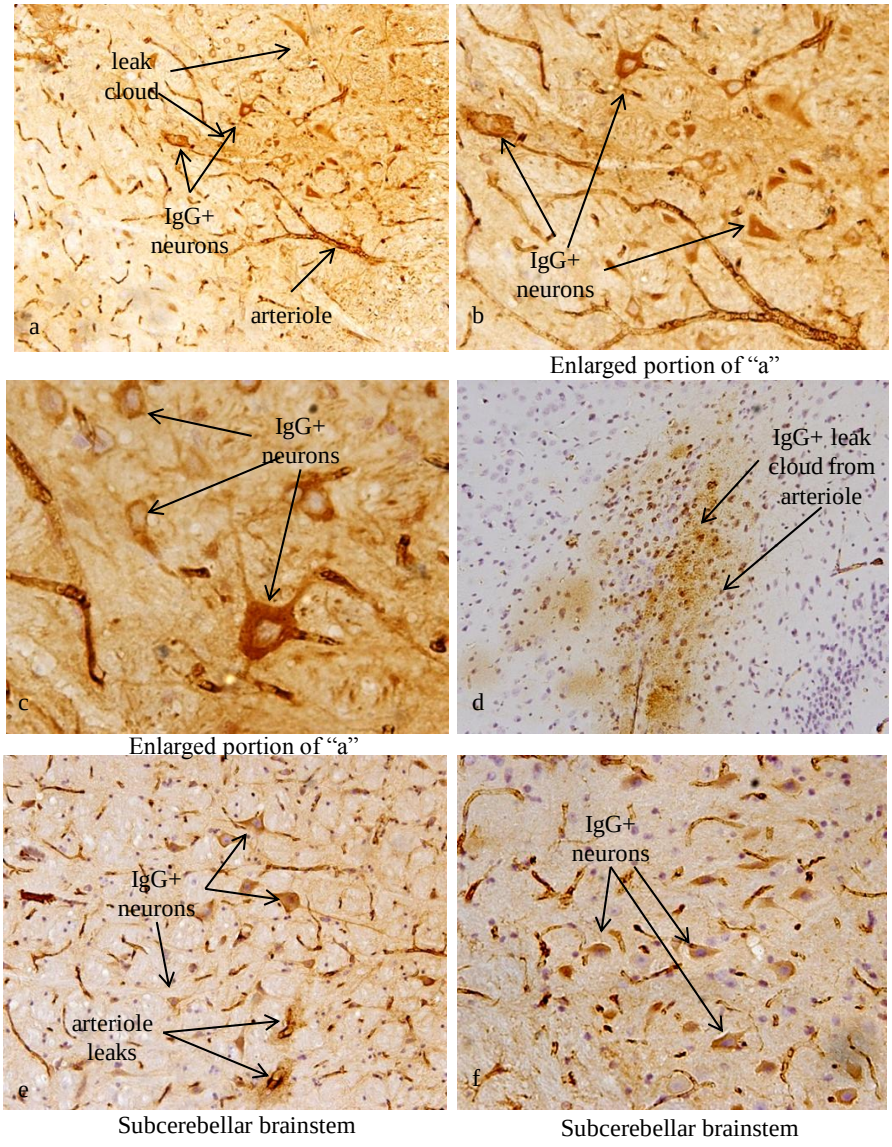

Note: All immunostained to detect IgG

IgG that leaks from blood vessels binds selectively to pyramidal neurons

Fig. 8 **PT-Aβ42**: Leaked IgG binds to and is internalized by neurons in the cerebral cortex

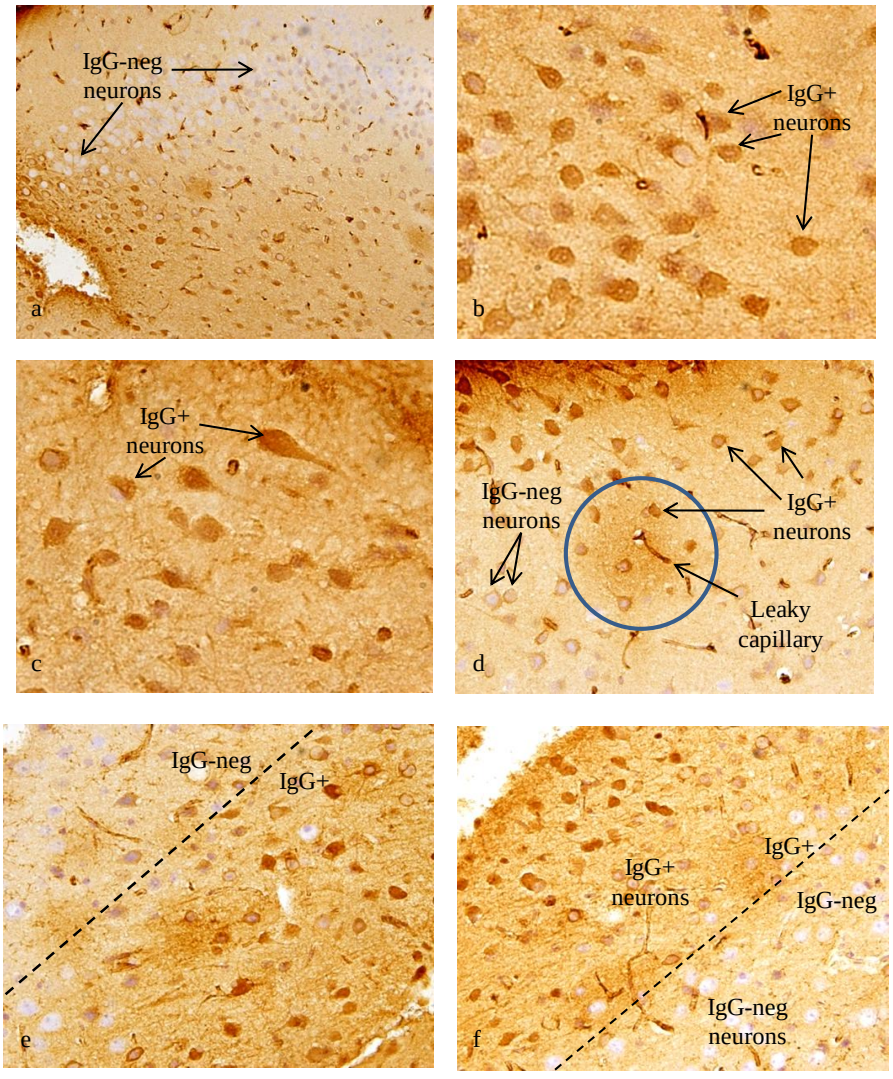

Note: All immunostained to detect IgG

Brightfield confirmation of FITC-Aβ42 data: PT-SALINE

Fig. 9 **PT-SALINE**: Brains show minimal neuronal Aβ42 loading. No detectable changes in MAP2 and synaptophysin expression.

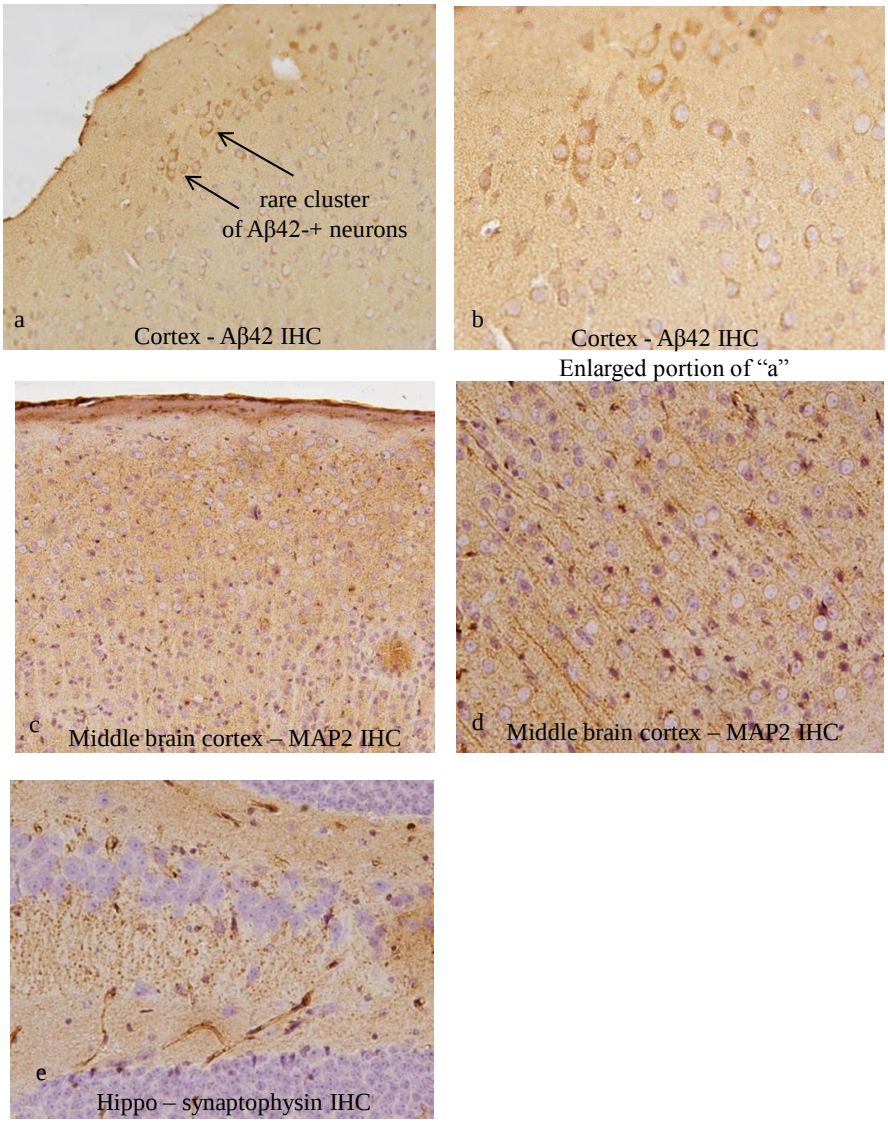

Brightfield confirmation of FITC-Aβ42 data: SALINE-SALINE

Fig. 10 **SALINE-SALINE:** Brains show no detectable IgG leak and neuronal Aβ42 accumulation and minimal GFAP, MAP2, NF and Syn expression

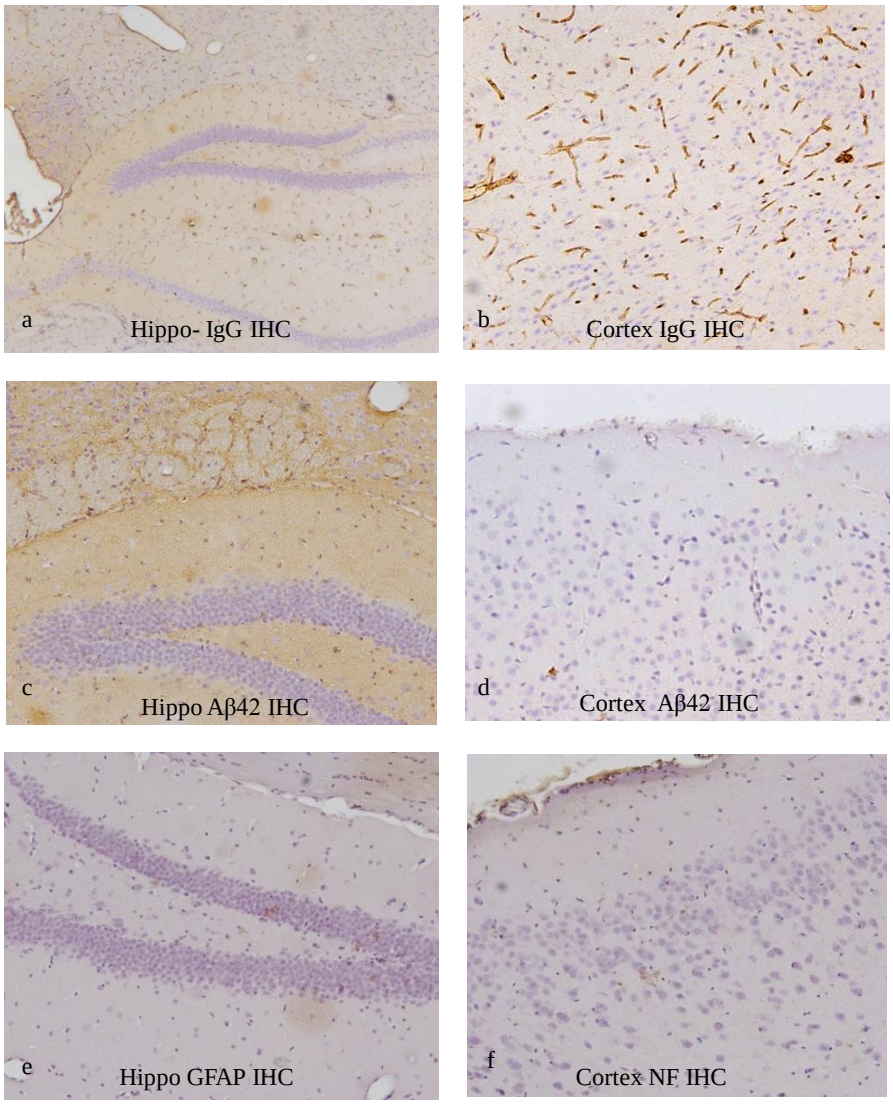

Tracking the fate of injected FITC-labeled Aβ42: PT-SALINE

Fig. 11 **PT-SALINE:** No detection of FITC-labeled Aβ42

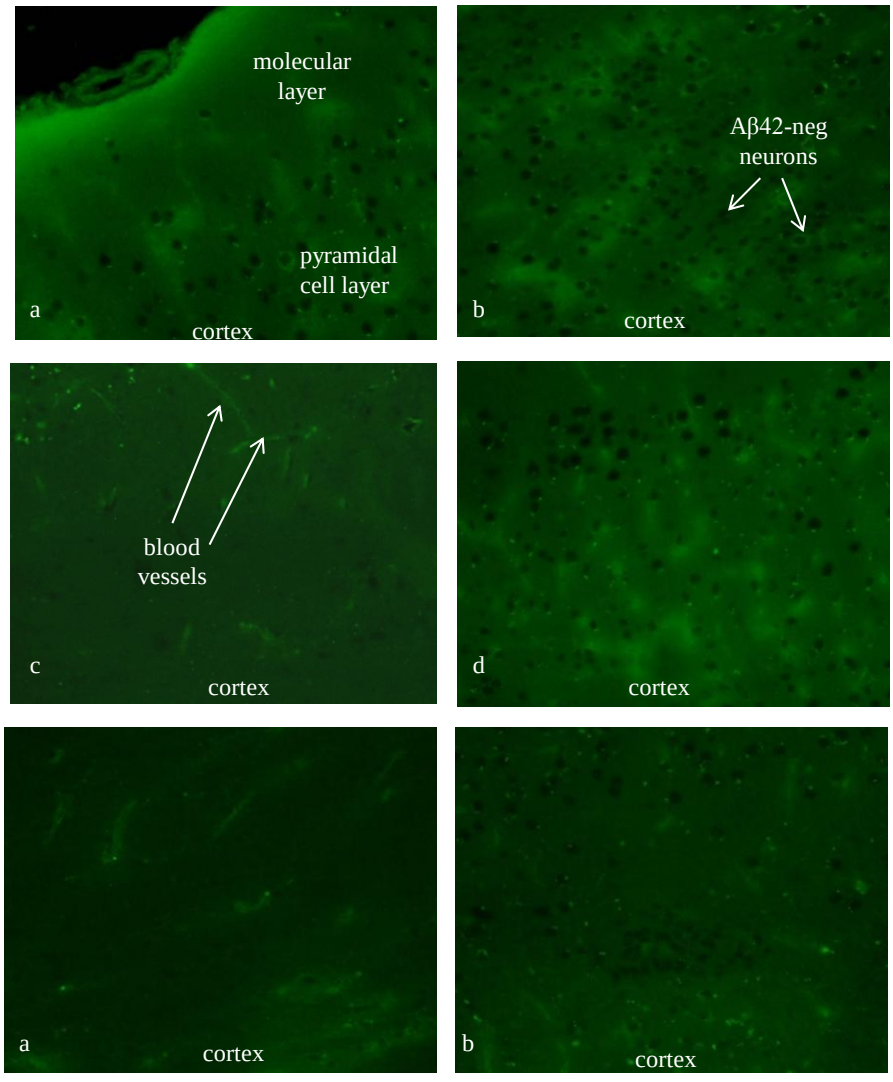

Tracking the fate of injected FITC-labeled Aβ42: PT-FITC Aβ42

Fig. 12 **PT-SALINE:** Only backgound autofluorescence is detected

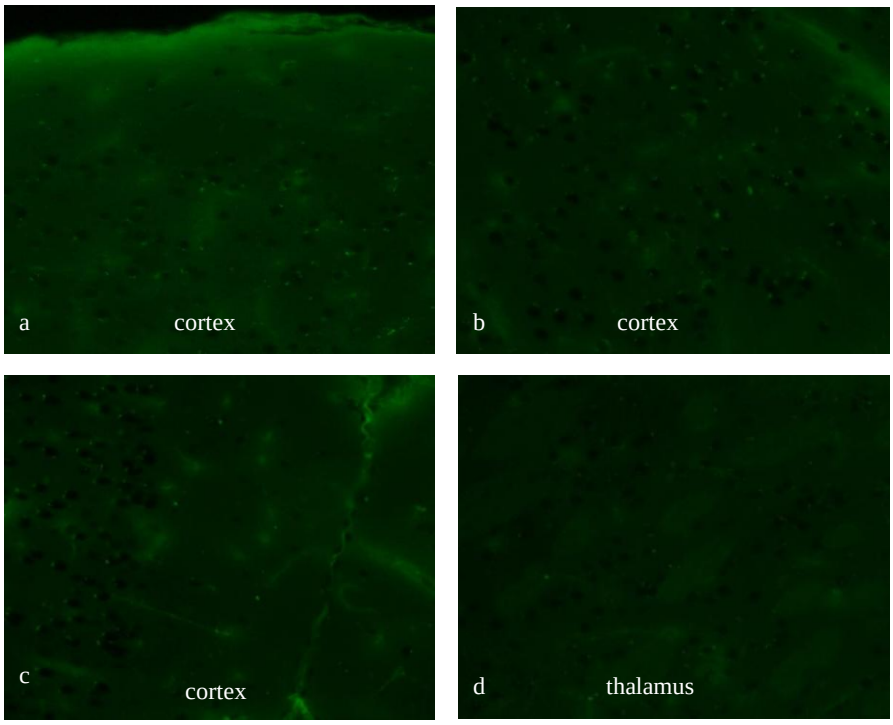

Tracking the fate of injected FITC-labeled Aβ42: PT-SALINE

Fig. 13 **PT-SALINE**: Some brains possess a single autofluorescent lipofuscin granules that are readily distinguishable from the numerous Aβ42-containing fluorescent granules seen in PT-FITC Aβ42 group

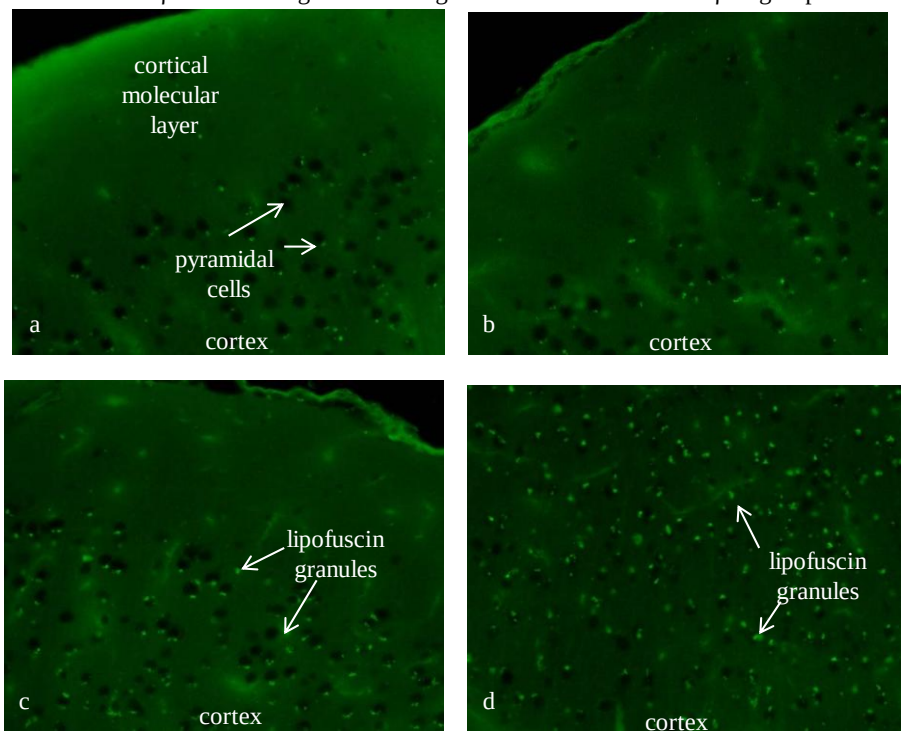

Tracking the fate of injected FITC-labeled Aβ42: SALINE-SALINE

Fig. 14 **SALINE-SALINE:** Detectable fluorescence is associated only with lipofuscin and background autofluorescence of the walls of blood vessels

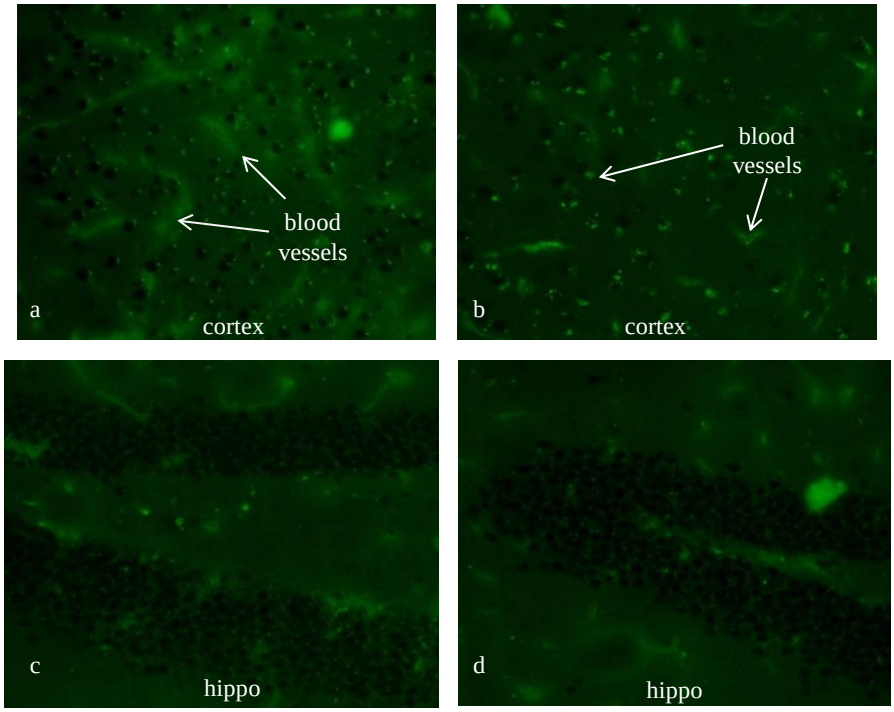

Tracking the fate of injected FITC-labeled Aβ42: PT-FITC Aβ42

Fig. 15 **PT-FITC Aβ42:** FITC-Aβ42 leaks from blood vessels, binds to neurons and is internalized by neurons

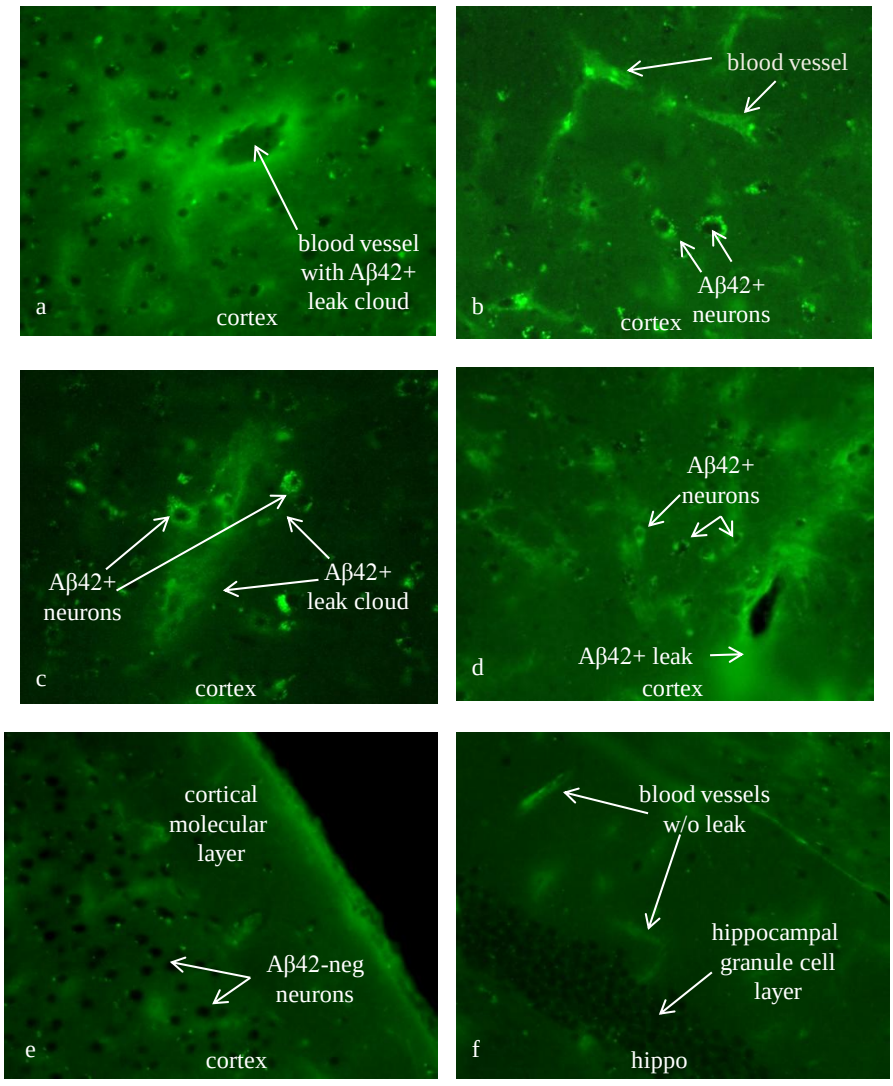

Tracking the fate of injected FITC-labeled Aβ42: PT-FITC Aβ42

Fig. 16 **PT-FITC Aβ42**: Aβ42 leaks from blood vessels and accumulates in neurons in intracellular granules of uniform size

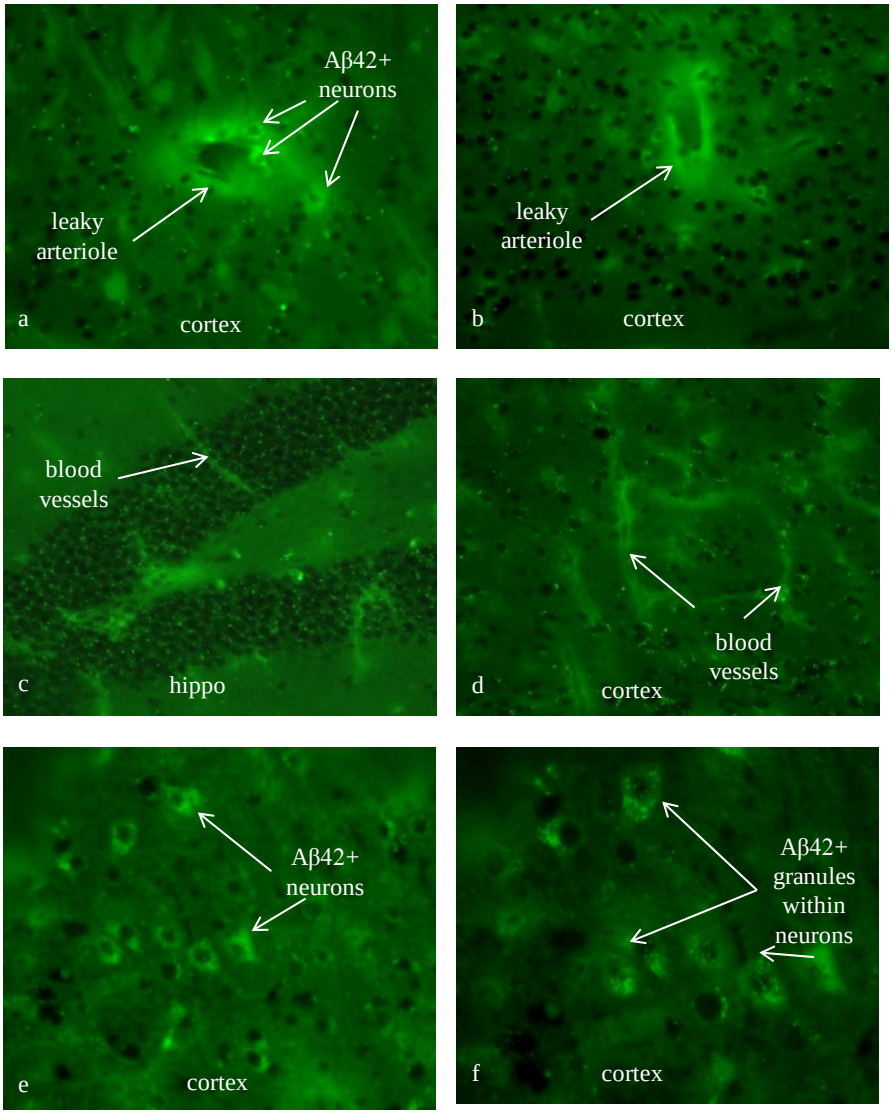

Tracking the fate of injected FITC-labeled Aβ42: PT-FITC Aβ42

Fig. 17 **PT-FITC Aβ42**: Aβ42 leaks from blood and accumulates in neurons

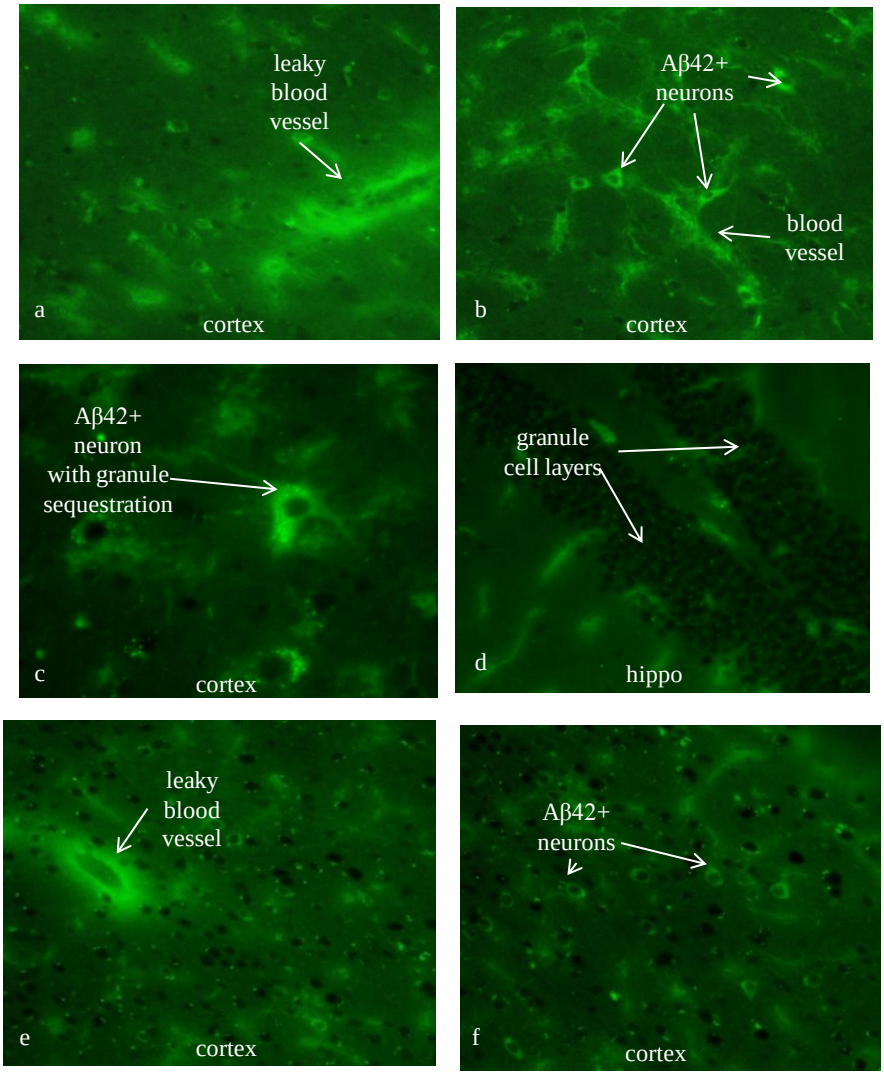

Tracking the fate of injected FITC-labeled Aβ42:
PT-FITC Aβ42

Fig. 18 **PT-FITC Aβ42**: Extensive leaks lead to extensive intraneuronal Aβ42

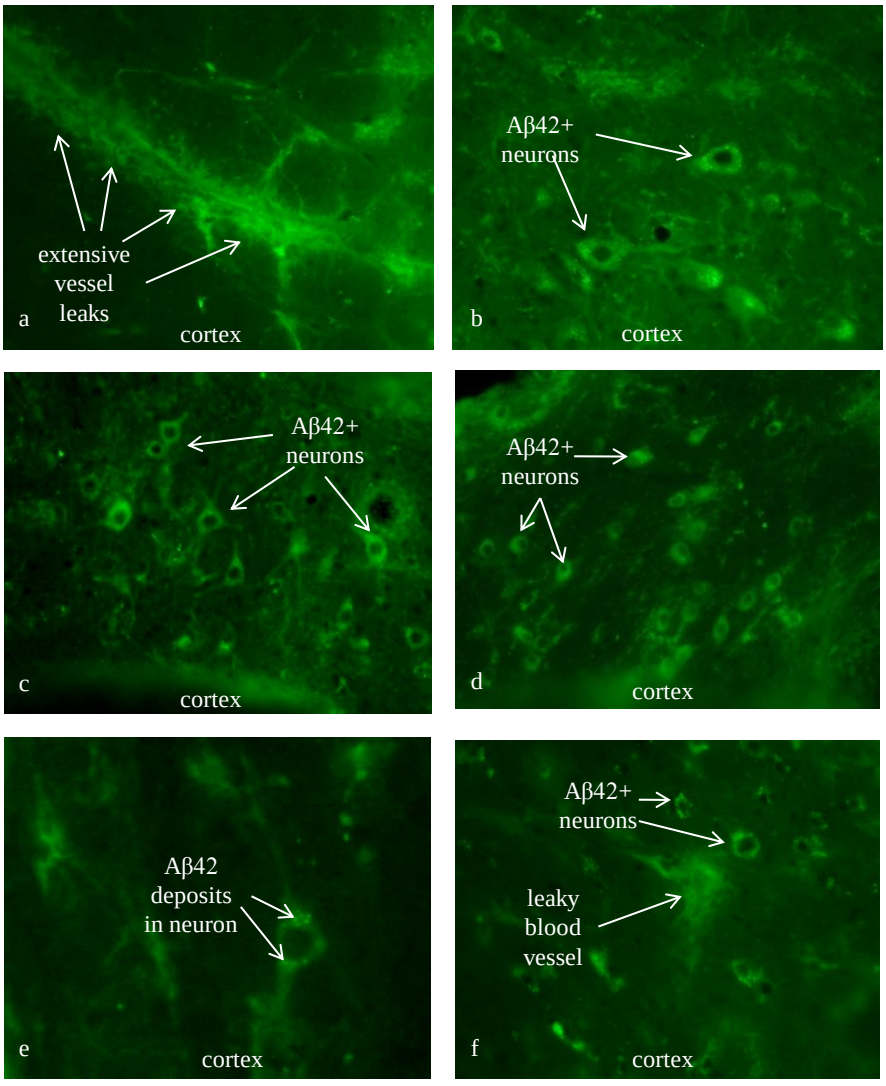

Brightfield confirmation of FITC-Aβ42 data: PT-Aβ42

Fig. 19 **PT-Aβ42:** Aβ42 binds to and accumulates selectively and differentially in the cell bodies of pyramidal cells

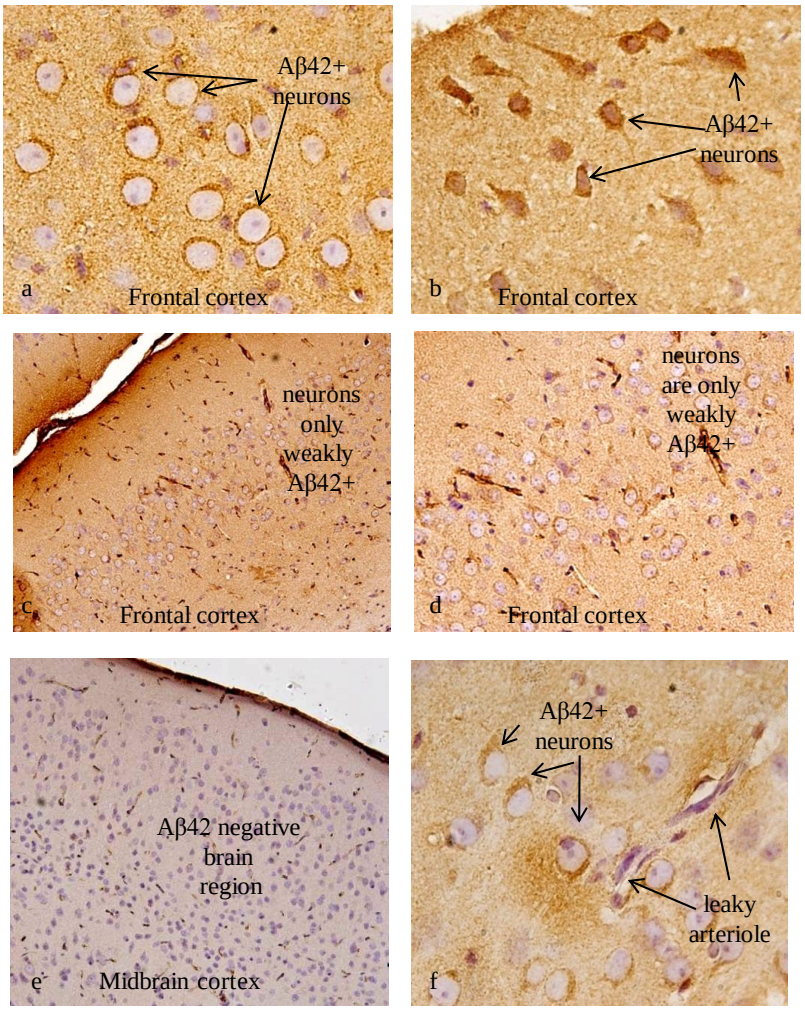

Brightfield confirmation of FITC-Aβ42 data: PT-Aβ42

Fig. 20 **PT-Aβ42:** Aβ42 from focal leaks determine the extent of intracellular Aβ42 accumulation in local pyramidal neurons

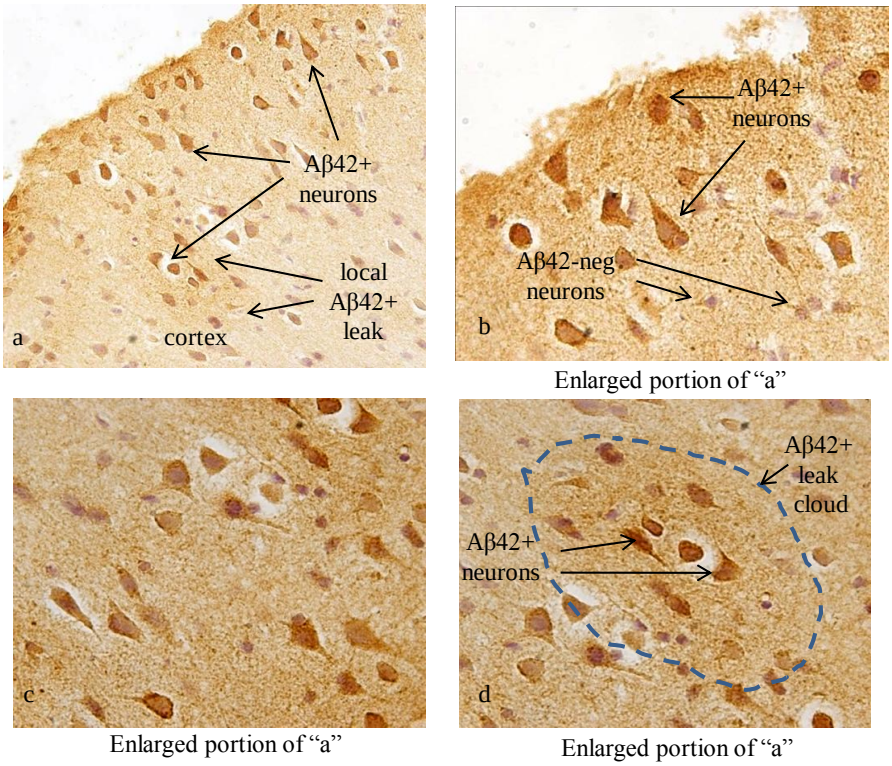

Brightfield confirmation of FITC-Aβ42 data: PT-Aβ42

Fig. 21 **PT-Aβ42:** Both widespread and focal distribution of Aβ42. In the cerebral cortex and cerebellum

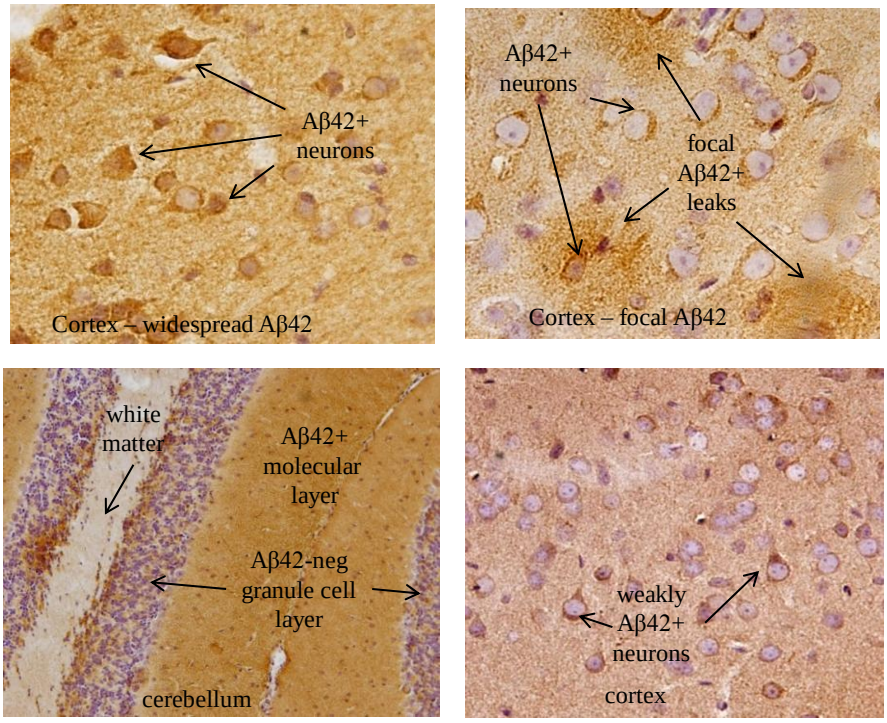

Brightfield confirmation of FITC-Aβ42 data: PT-Aβ42

Fig. 22 **PT-Aβ42:** Aβ42 binds to and accumulates selectively in the cell body of pyramidal neurons

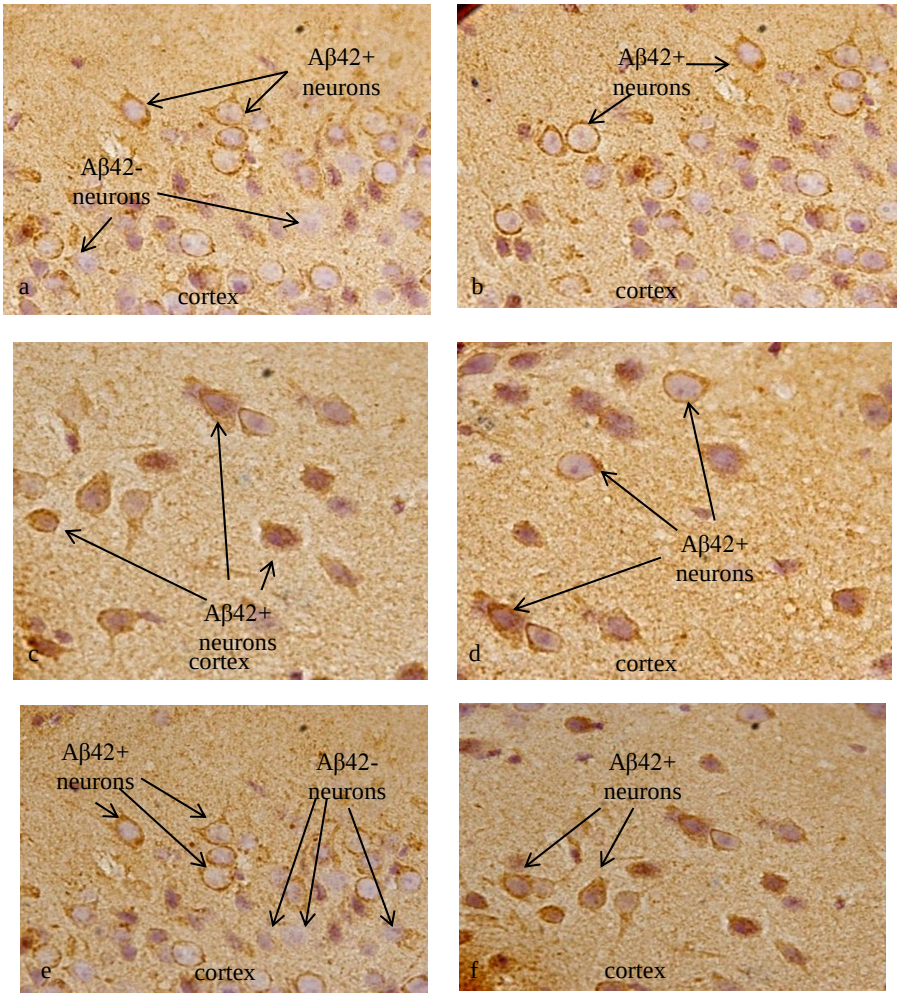

Brightfield confirmation of FITC-Aβ42 data: PT-Aβ42

Fig. 23 **PT-Aβ42**: Site-specific variations in astrocytes activation

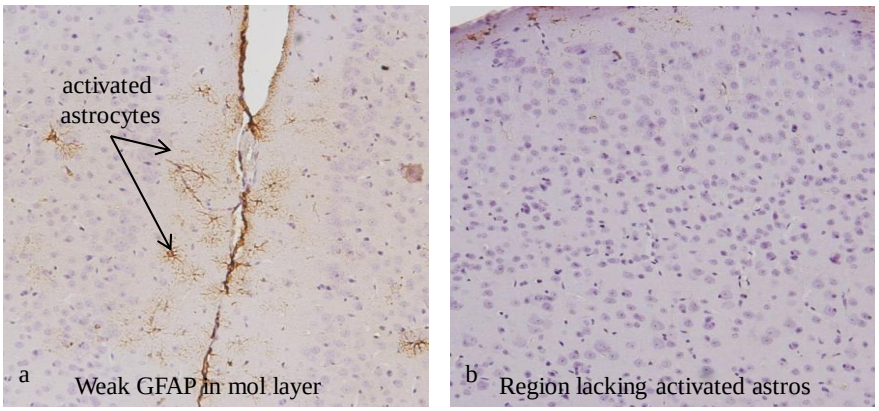

Not all regions of cortex show activated astrocytes

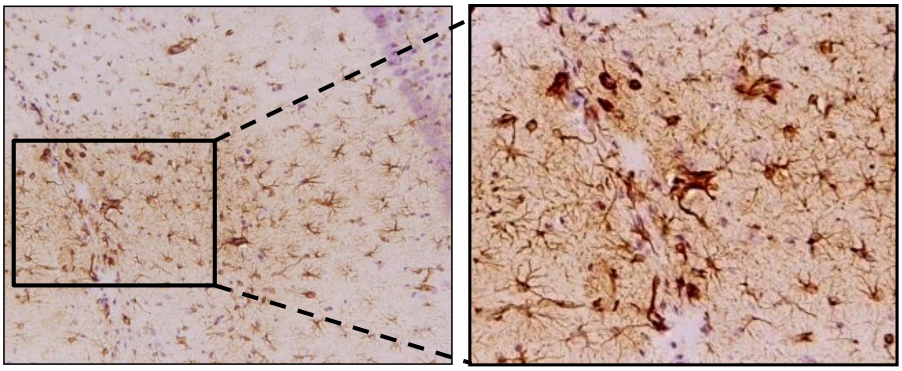

Site of intense activated astrocytes in hippocampus

Note: All immunostained to detect GFAP

Brightfield confirmation of FITC-Aβ42 data: PT-Aβ42

Fig. 24 **PT-Aβ42**: Activated astrocytes are most abundant in the hippocampal region

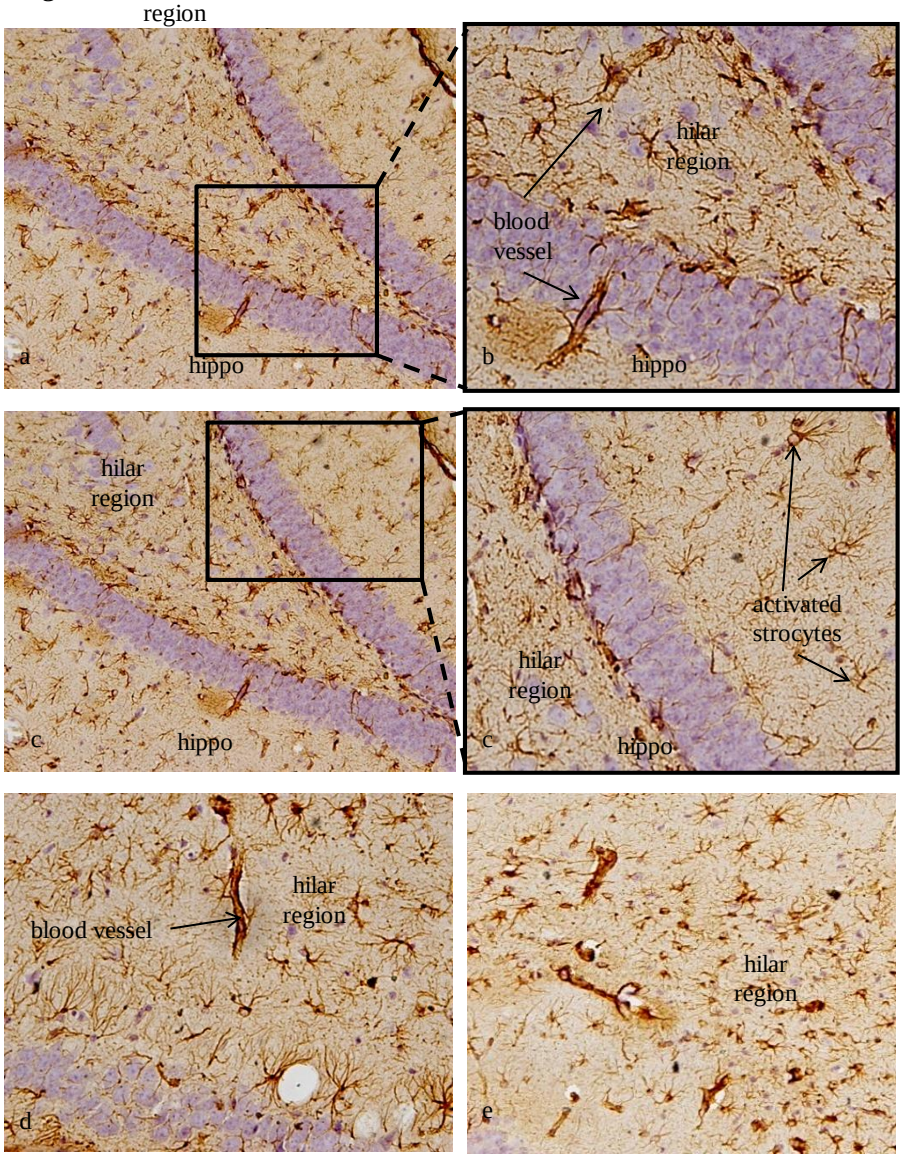

Note: All immunostained to detect GFAP

Brightfield confirmation of FITC-Aβ42 data: PT-Aβ42

Fig. 25 **PT-Aβ42**: Focal sites of activated astrocytes are abundant in the hippocampal region

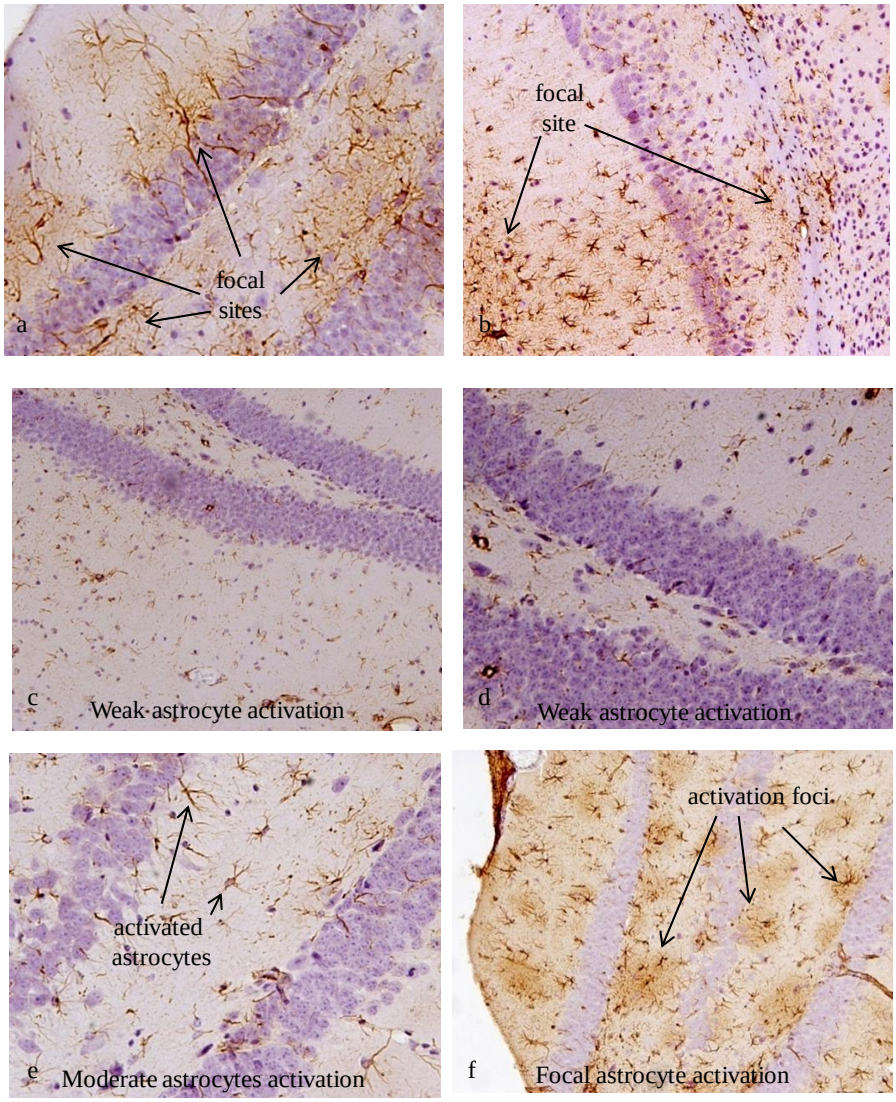

Note: All immunostained to detect GFAP

Brightfield confirmation of FITC-Aβ42 data: PT-Aβ42

Fig. 26 **PT-Aβ42:** Astrocytes are activated focally in the cortex . GFAP is a biomarker for activated astrocytes

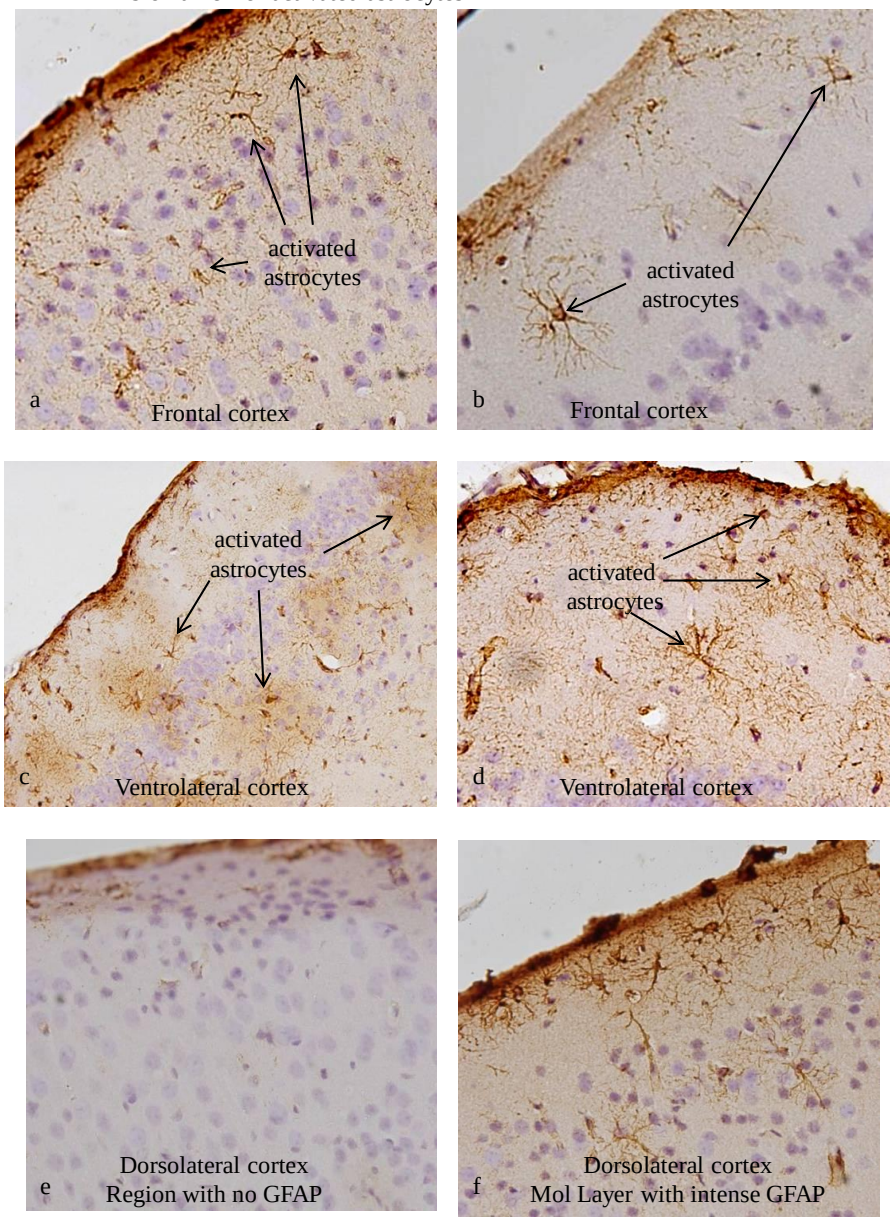

Brightfield confirmation of FITC-Aβ42 data: PT-Aβ42

Fig. 27 **PT-Aβ42**: We found no evidence of F480-positive inflammatory cells within the brain tissue, thus confirming no significant cell death caused by any of the treatments

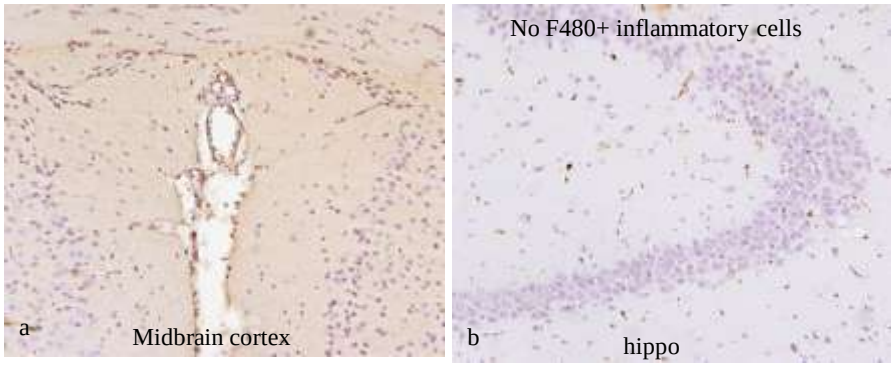

Brightfield confirmation of FITC-Aβ42 data: PT-Aβ42

Fig. 28 **PT-Aβ42:** MAP2 expression is weakly upregulated in the cortex, but often intensely upregulated in the hippocampus

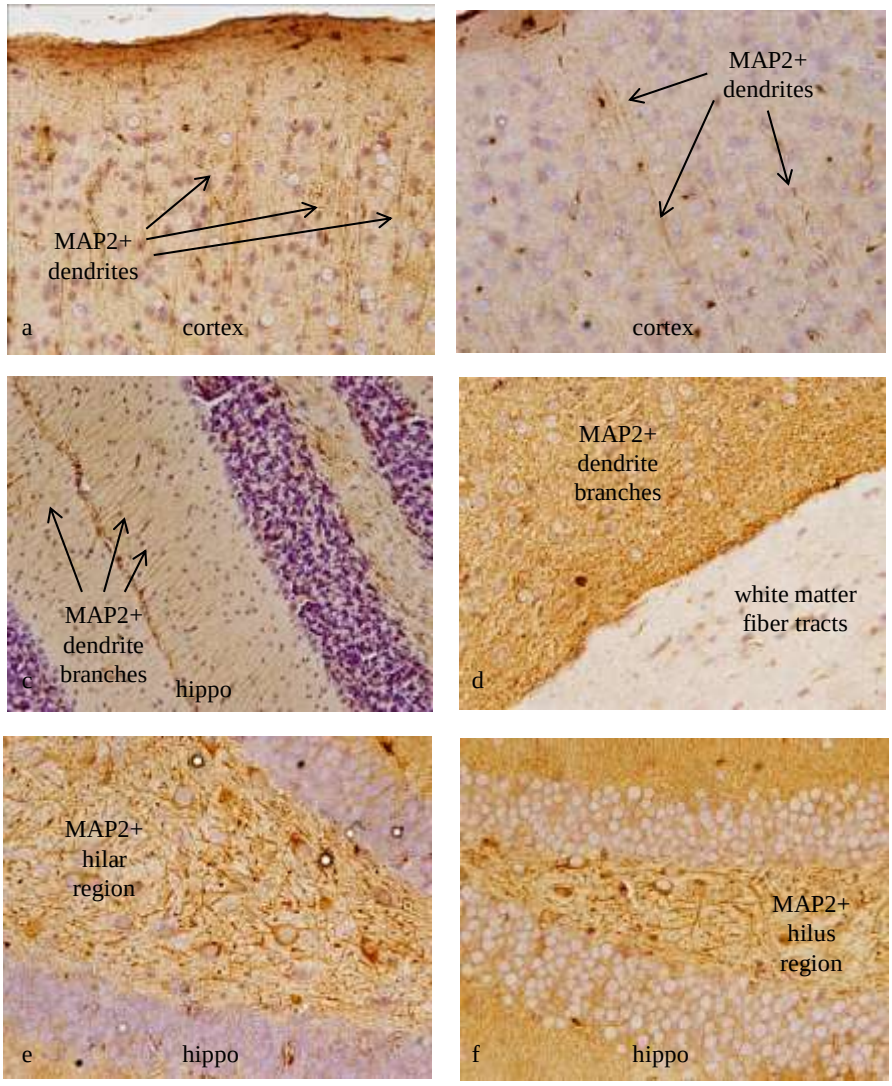

Brightfield confirmation of FITC-Aβ42 data: PT-Aβ42

Fig. 29 **PT-Aβ42:** MAP2 expression is weakly upregulated in the cortex, but often intensely upregulated in the hippocampus

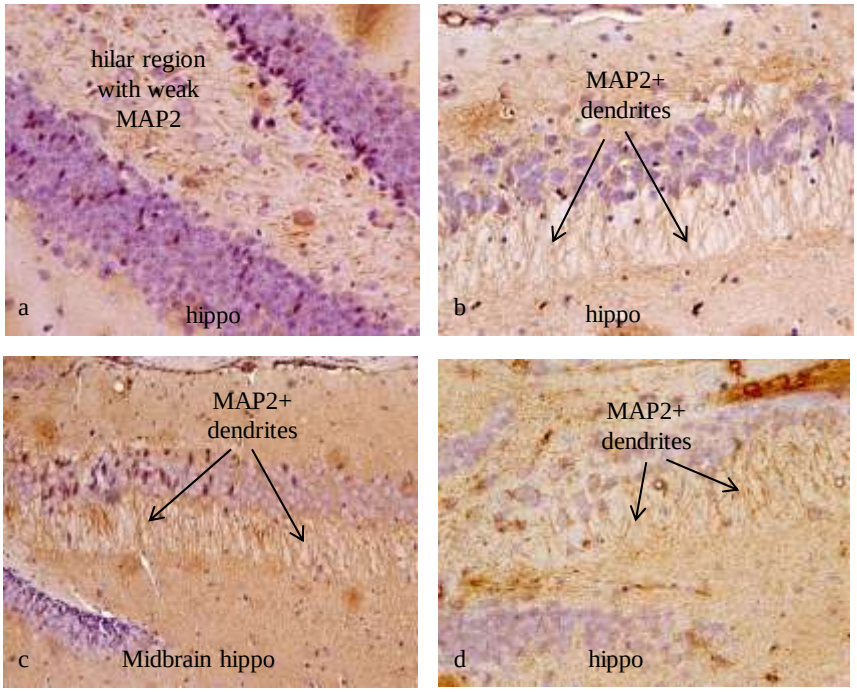

Brightfield confirmation of FITC-Aβ42 data: PT-Aβ42

Fig. 30 **PT-Aβ42:** Changes in synaptic density visualized by synapatophysin immunostaining were not consistently detectable

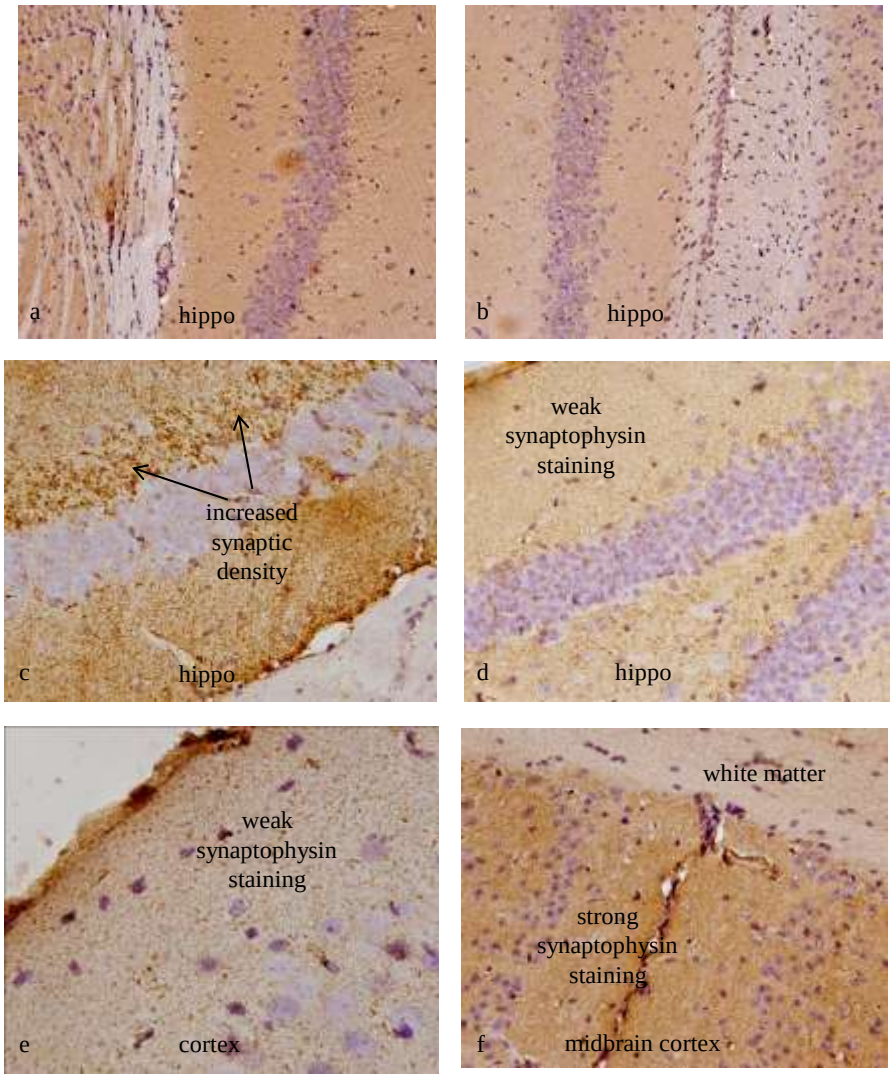

Brightfield confirmation of FITC-Aβ42 data: PT-Aβ42

Fig. 31 **PT-Aβ42:** Changes in neurofilament protein expression visualized by neurofilament immunostaining were not consistent

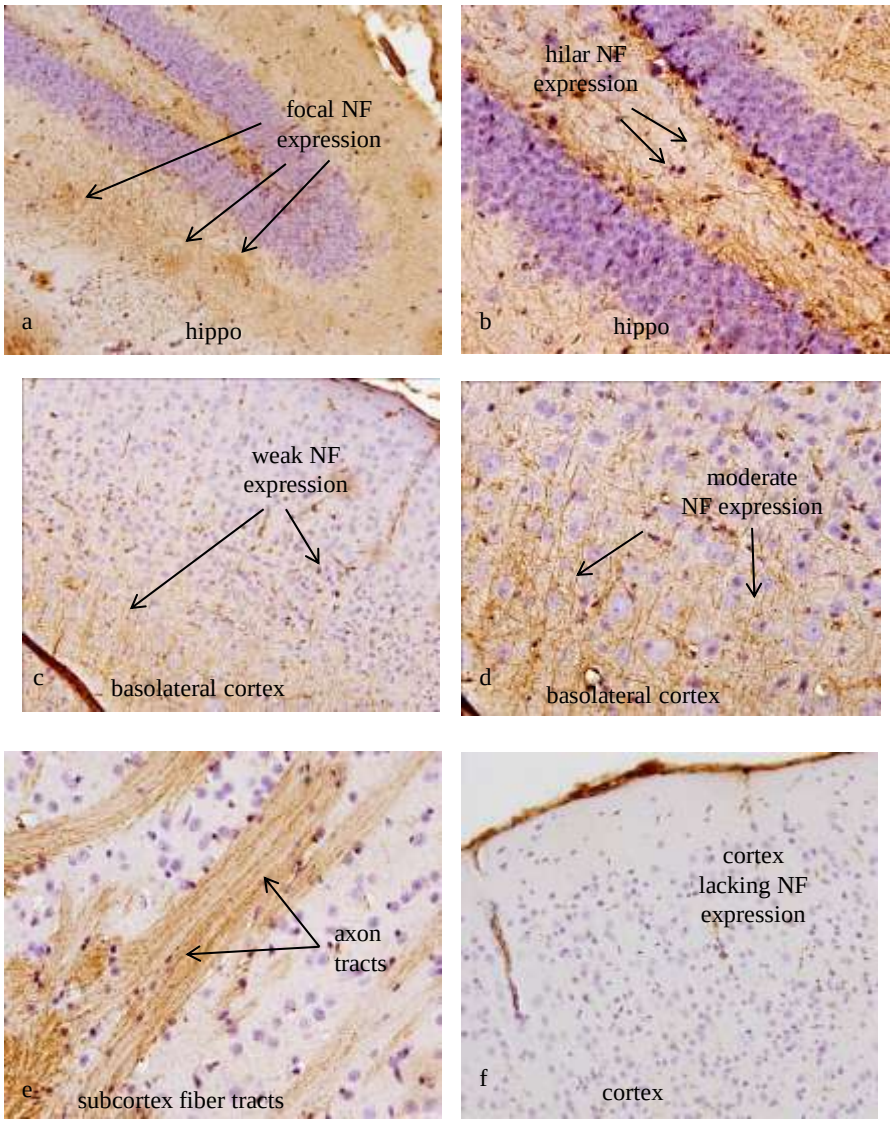

Note: All immunostained to detect NF proteins

Fig. 32

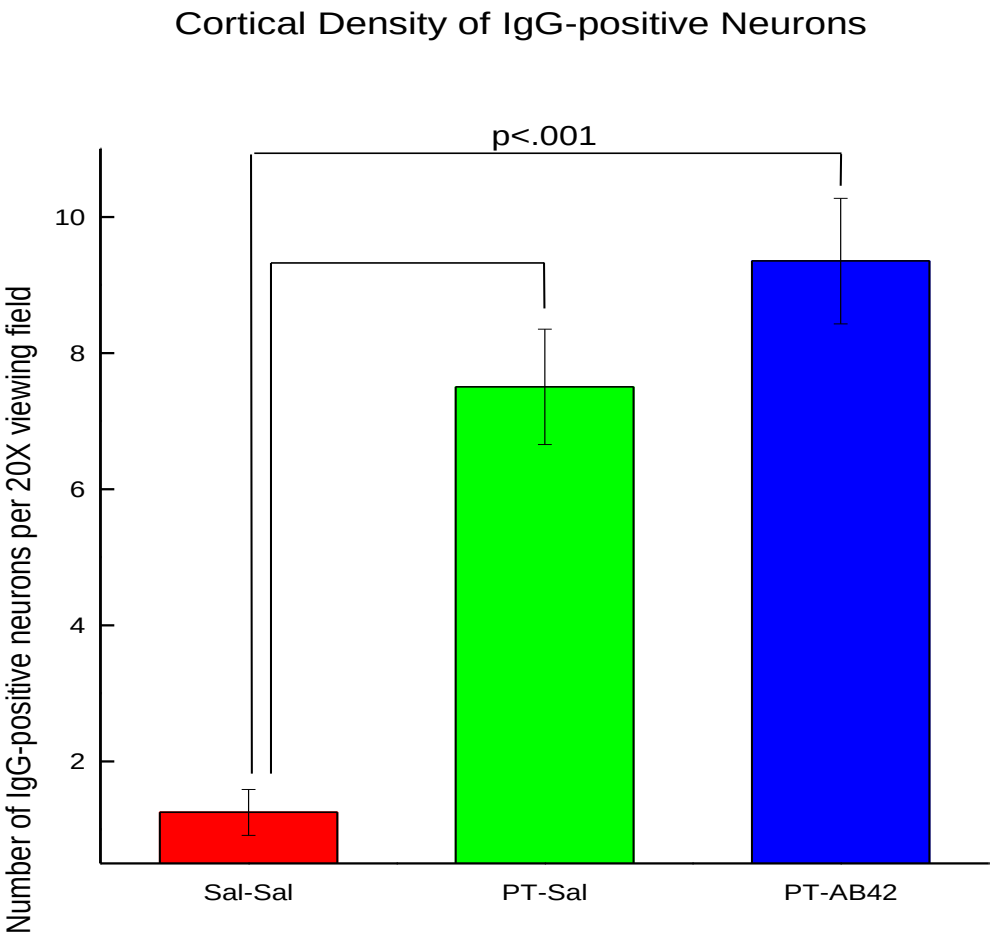
Cortical Density of IgG-positive Neurons
p<.001
Number of IgG-positive neurons per 20X viewing field
10
8
6
4
2
Sal-Sal
PT-Sal
PT-AB42

Fig. 33

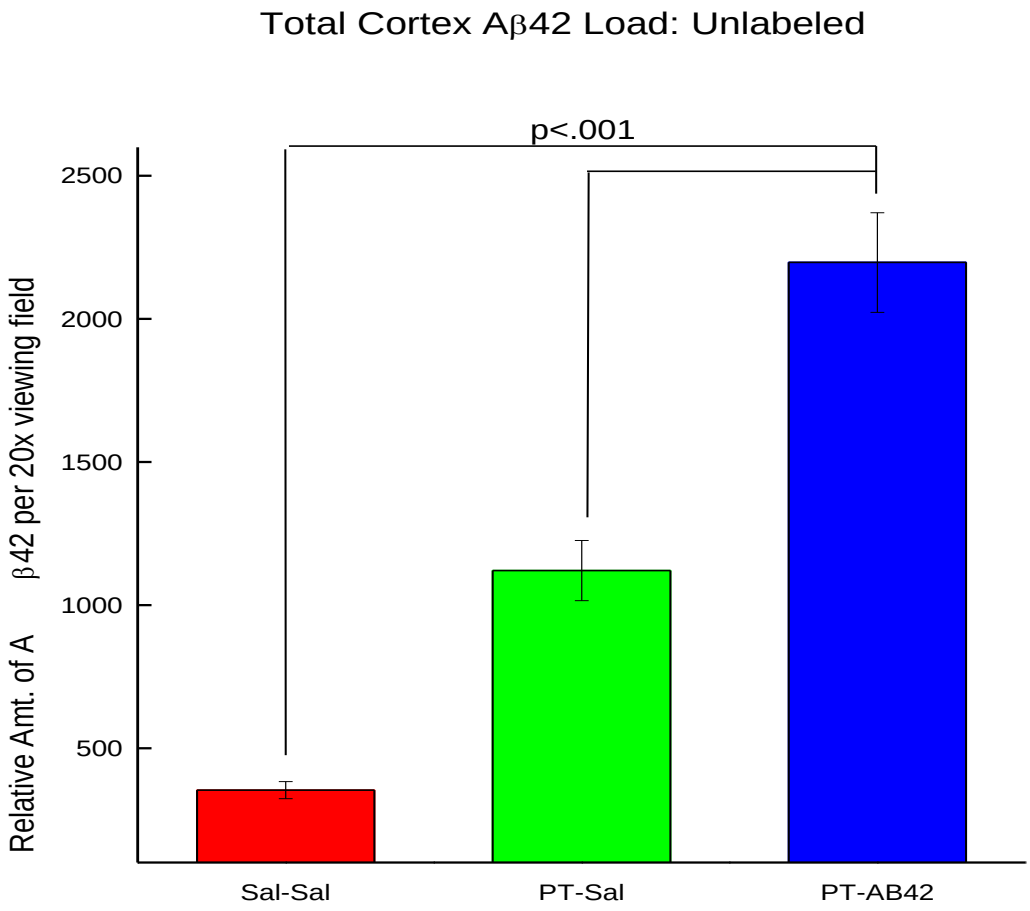
Total Cortex Aβ42 Load: Unlabeled
p<.001
Relative Amt. of Aβ42 per 20x viewing field
2500
2000
1500
1000
500
Sal-Sal
PT-Sal
PT-AB42

Fig. 34

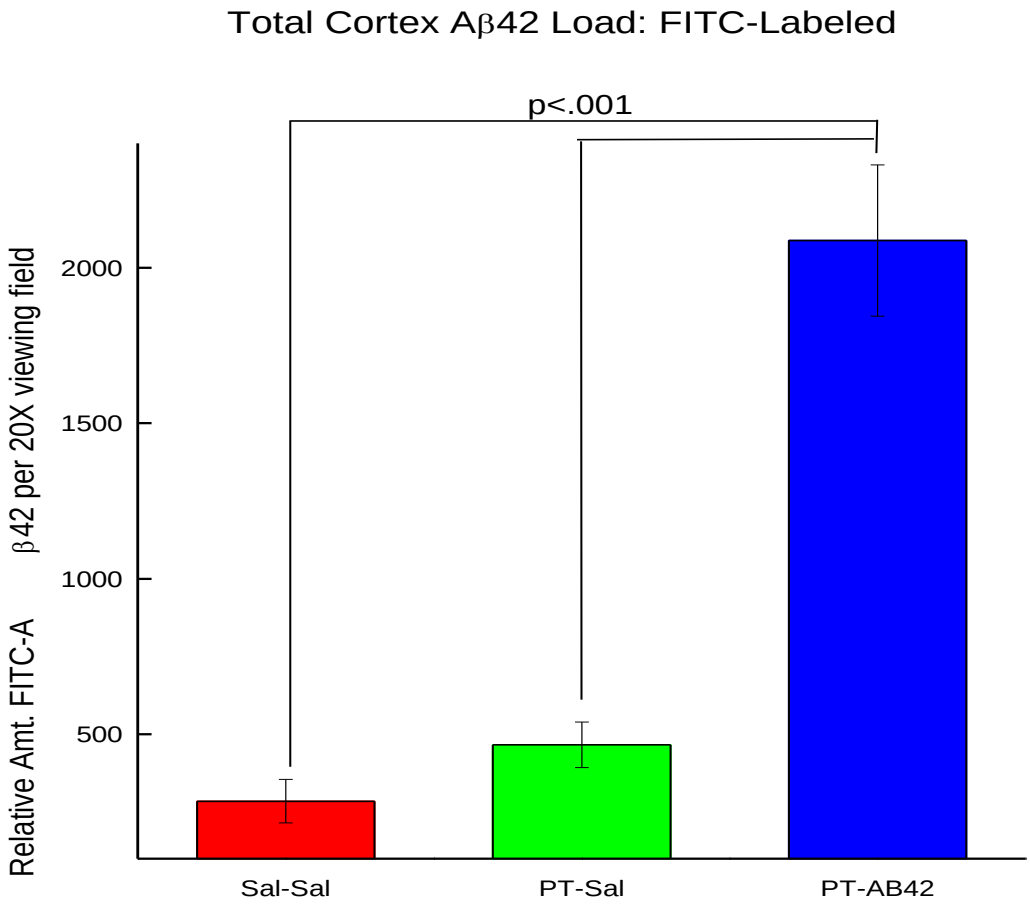
Total Cortex Aβ42 Load: FITC-Labeled
p<.001
Relative Amt. FITC-A β42 per 20X viewing field
2000
1500
1000
500
Sal-Sal
PT-Sal
PT-AB42

Fig. 35

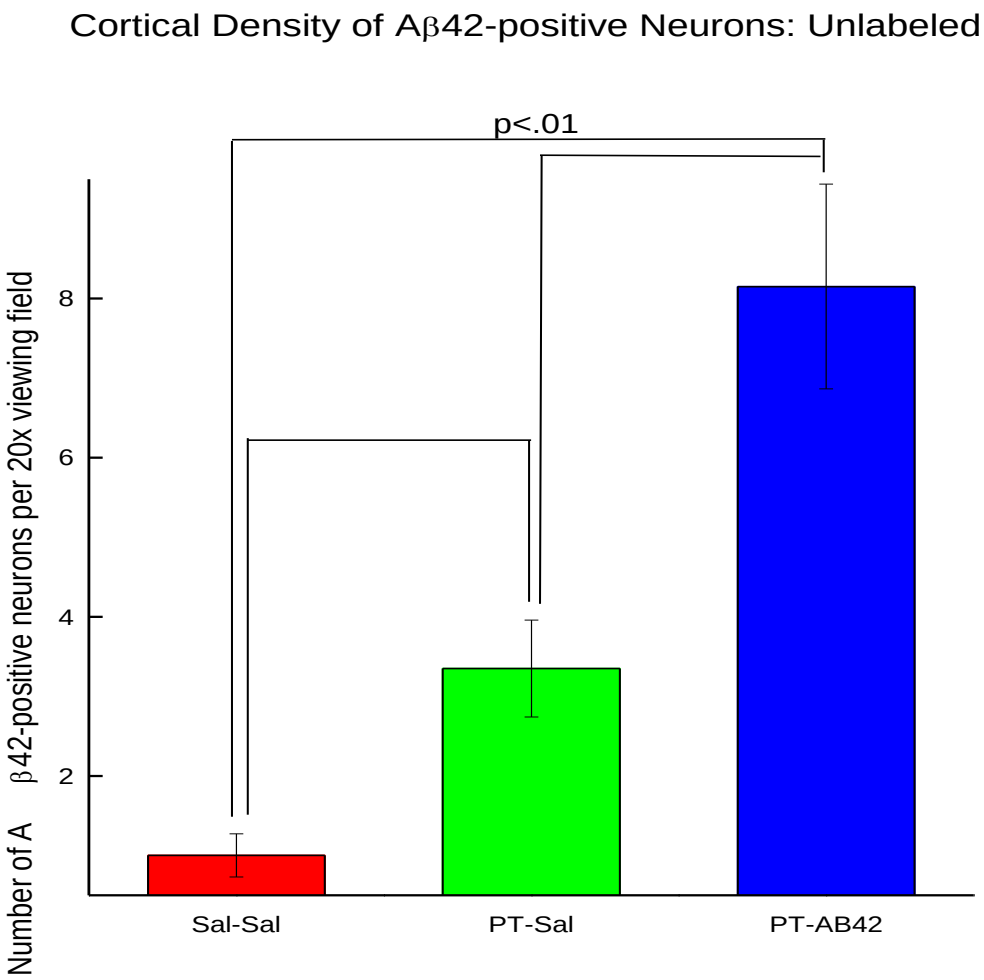
Cortical Density of Aβ42-positive Neurons: Unlabeled
p<.01
Number of Aβ42-positive neurons per 20x viewing field
2
4
6
8
Sal-Sal
PT-Sal
PT-AB42

Fig. 36

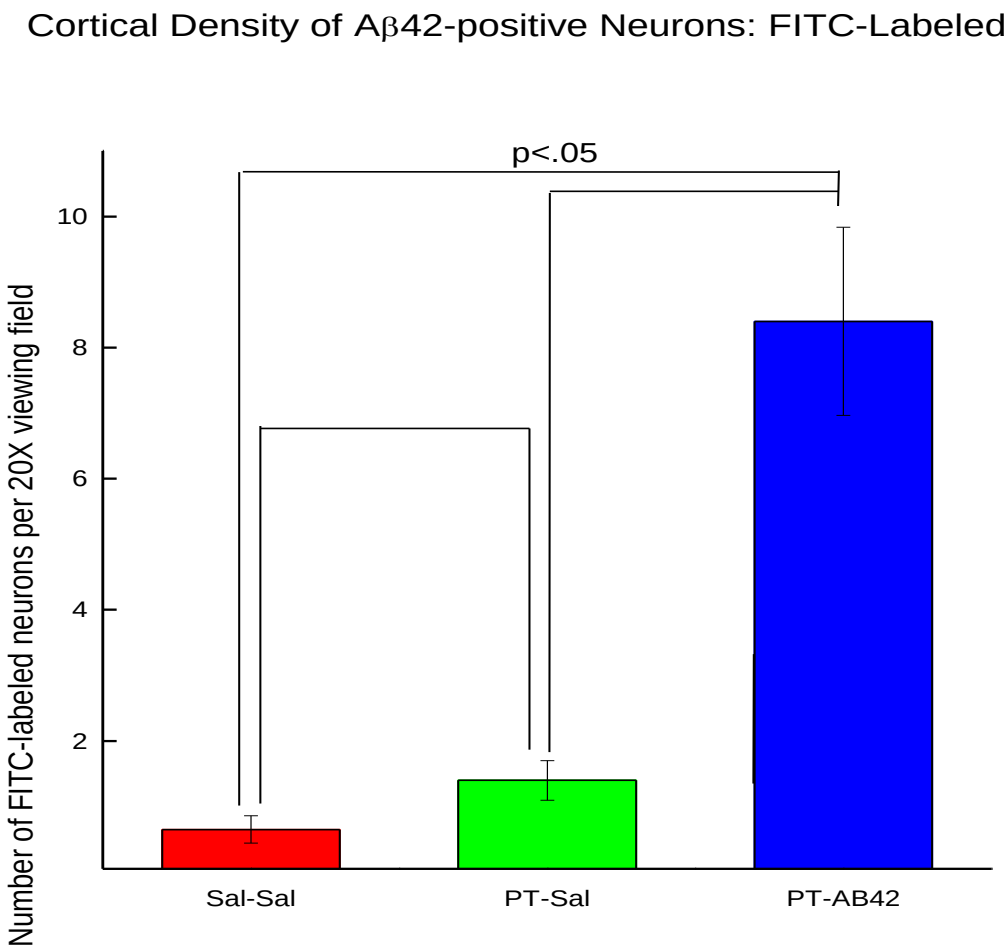
Cortical Density of Aβ42-positive Neurons: FITC-Labeled
p<.05
Number of FITC-labeled neurons per 20X viewing field
10
8
6
4
2
Sal-Sal
PT-Sal
PT-AB42

Fig. 37

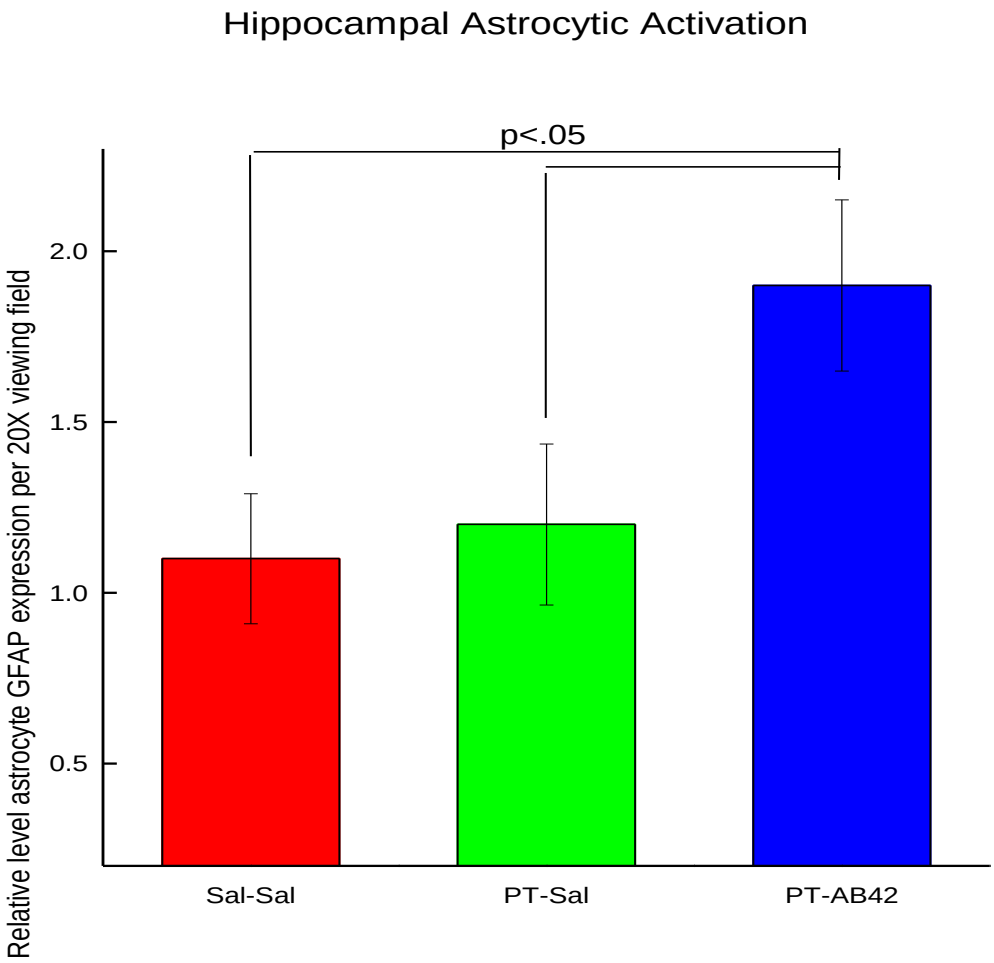
Hippocampal Astrocytic Activation
p<.05
Relative level astrocyte GFAP expression per 20X viewing field
2.0
1.5
1.0
0.5
Sal-Sal
PT-Sal
PT-AB42

Fig. 38

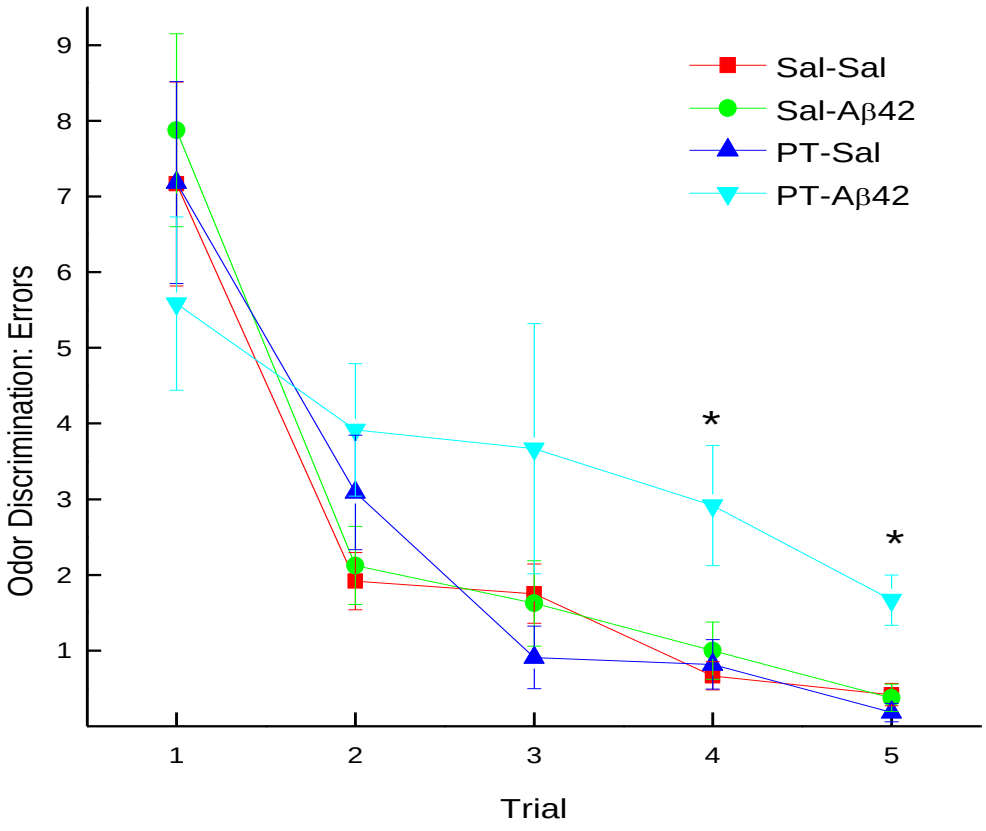
Odor Discrimination: Errors
Trial
Sal-Sal
Sal-Aβ42
PT-Sal
PT-Aβ42
*
*
1
2
3
4
5
1
2
3
4
5
6
7
8
9

Fig. 39

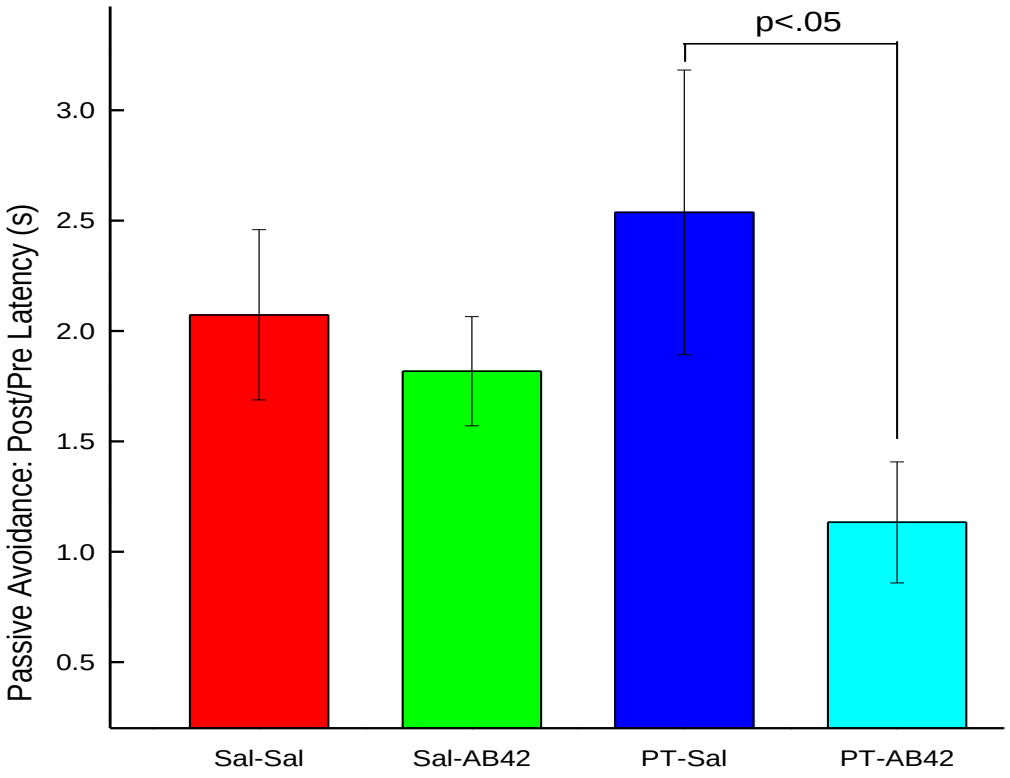
p<.05
Passive Avoidance: Post/Pre Latency (s)
3.0
2.5
2.0
1.5
1.0
0.5
Sal-Sal
Sal-AB42
PT-Sal
PT-AB42

Fig. 40

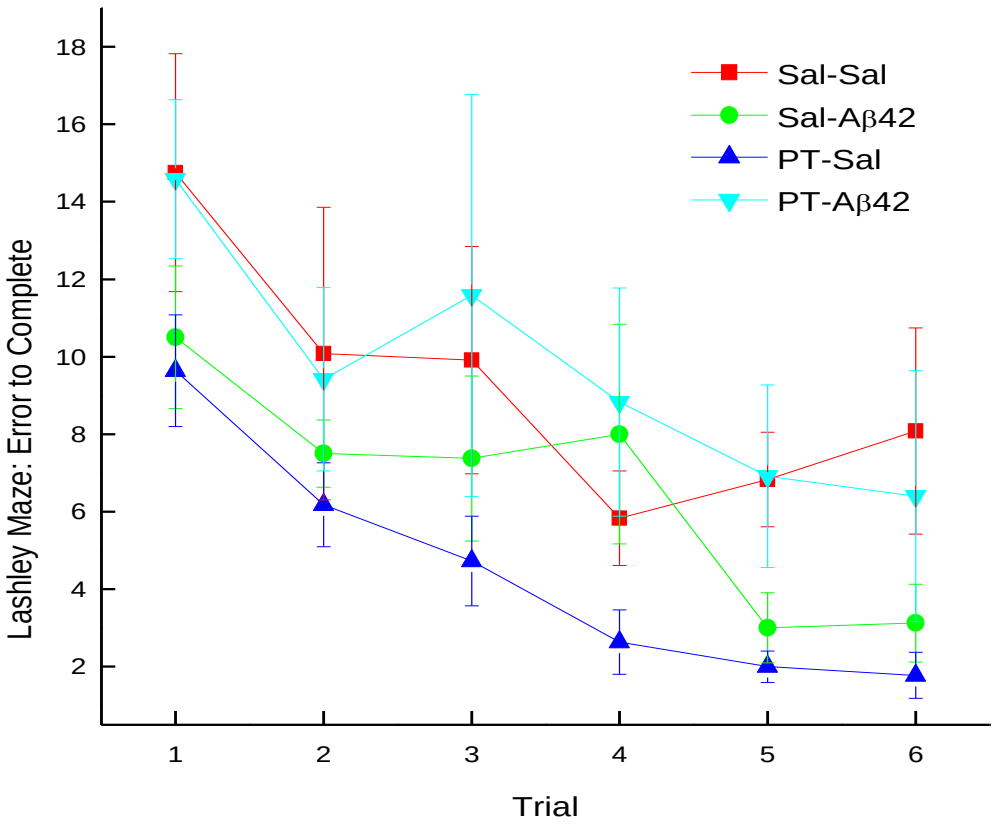
Lashley Maze: Error to Complete
18
16
14
12
10
8
6
4
2
1
2
3
4
5
6
Trial
Sal-Sal
Sal-Aβ42
PT-Sal
PT-Aβ42

Fig. 41

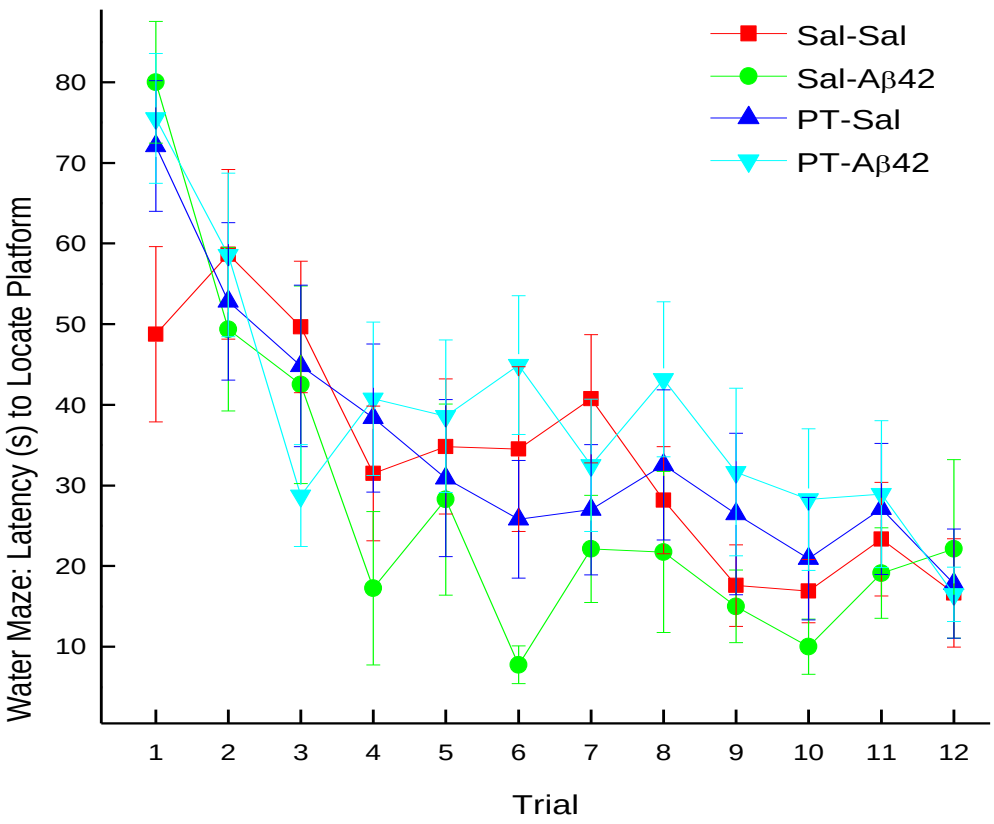
Sal-Sal
Sal-Aβ42
PT-Sal
PT-Aβ42
Water Maze: Latency (s) to Locate Platform
10
20
30
40
50
60
70
80
1
2
3
4
5
6
7
8
9
10
11
12
Trial

Fig. 42

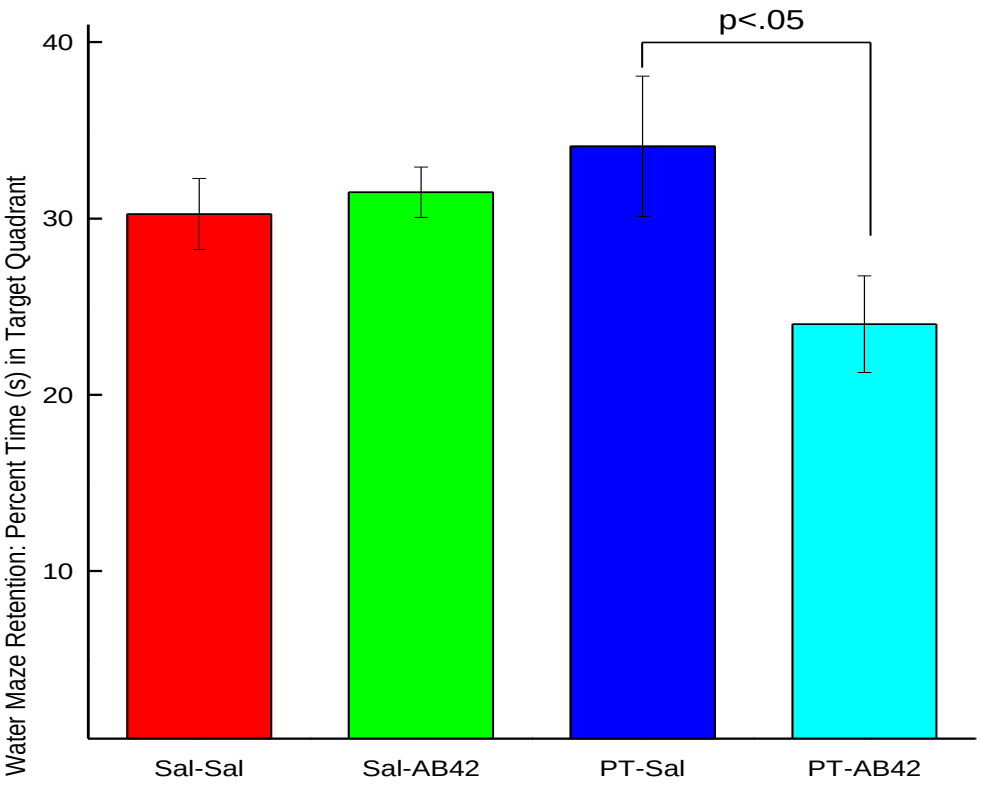
p<.05
40
30
20
10
Water Maze Retention: Percent Time (s) in Target Quadrant
Sal-Sal
Sal-AB42
PT-Sal
PT-AB42

Fig. 43

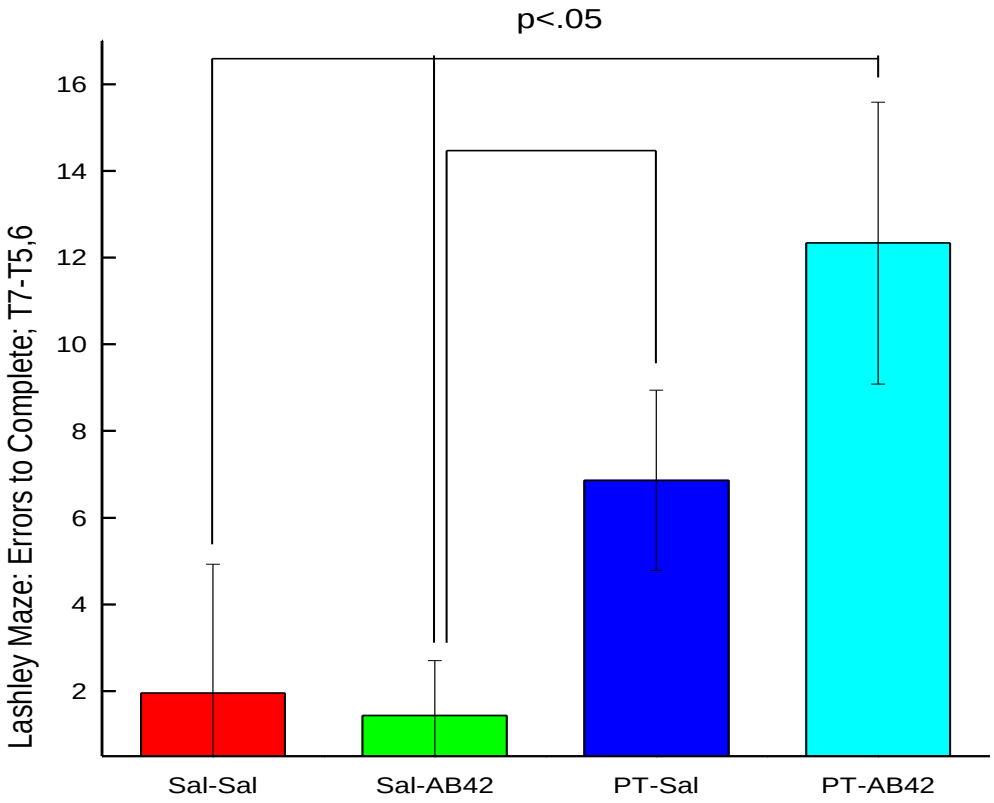
p<.05
Lashley Maze: Errors to Complete; T7-T5,6
16
14
12
10
8
6
4
2
Sal-Sal
Sal-AB42
PT-Sal
PT-AB42

Fig. 44

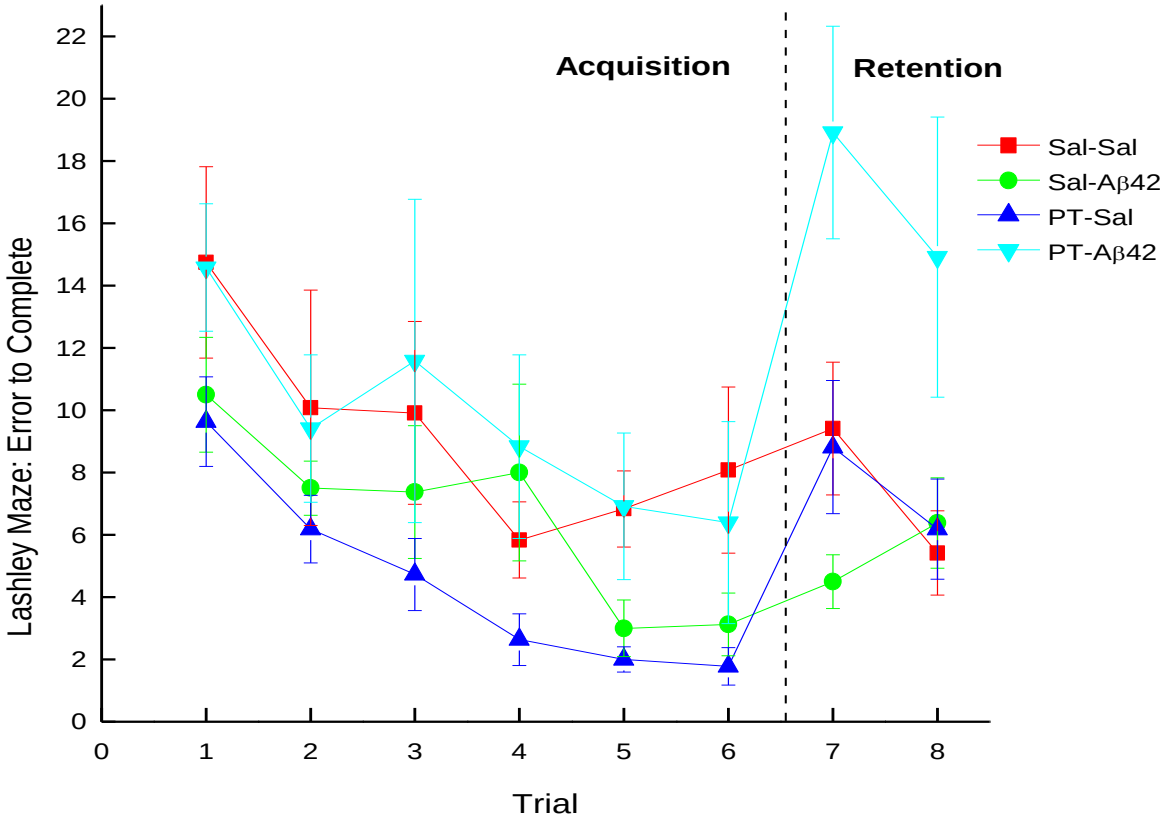
Acquisition
Retention
Sal-Sal
Sal-Aβ42
PT-Sal
PT-Aβ42
Lashley Maze: Error to Complete
Trial
0
2
4
6
8
10
12
14
16
18
20
22
0
1
2
3
4
5
6
7
8

Fig. 45

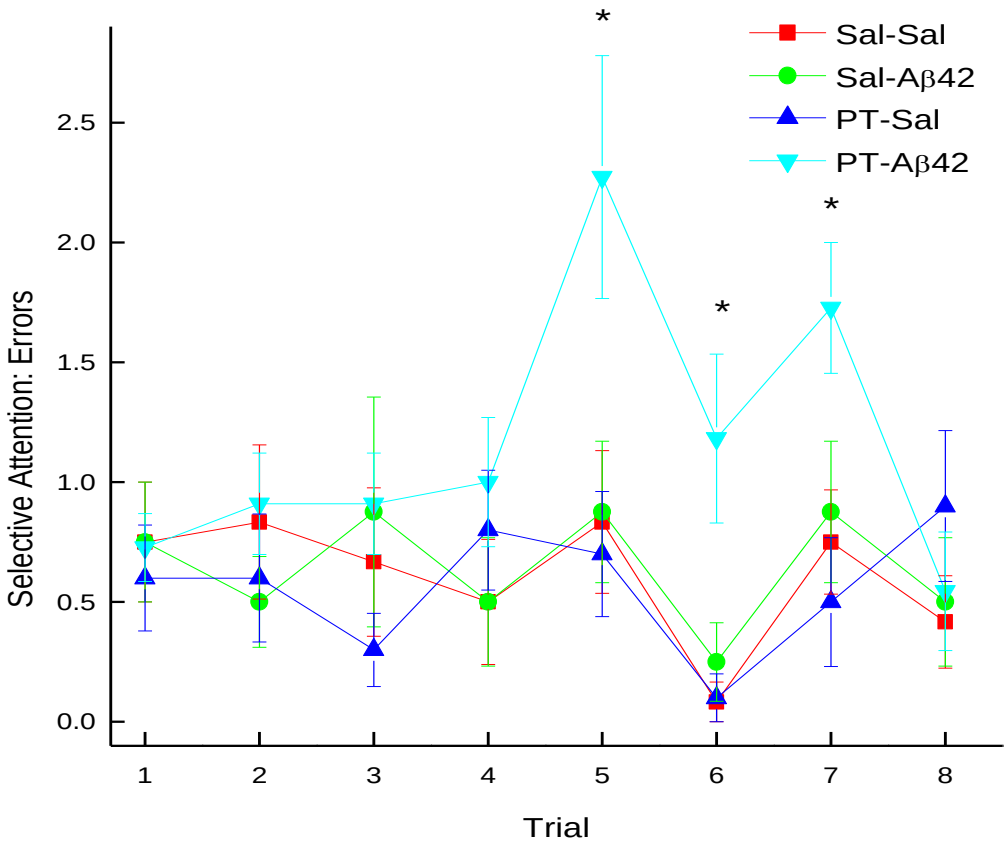
Sal-Sal
Sal-Aβ42
PT-Sal
PT-Aβ42
Selective Attention: Errors
Trial
0.0
0.5
1.0
1.5
2.0
2.5
1
2
3
4
5
6
7
8
*
*
*

Fig. 46

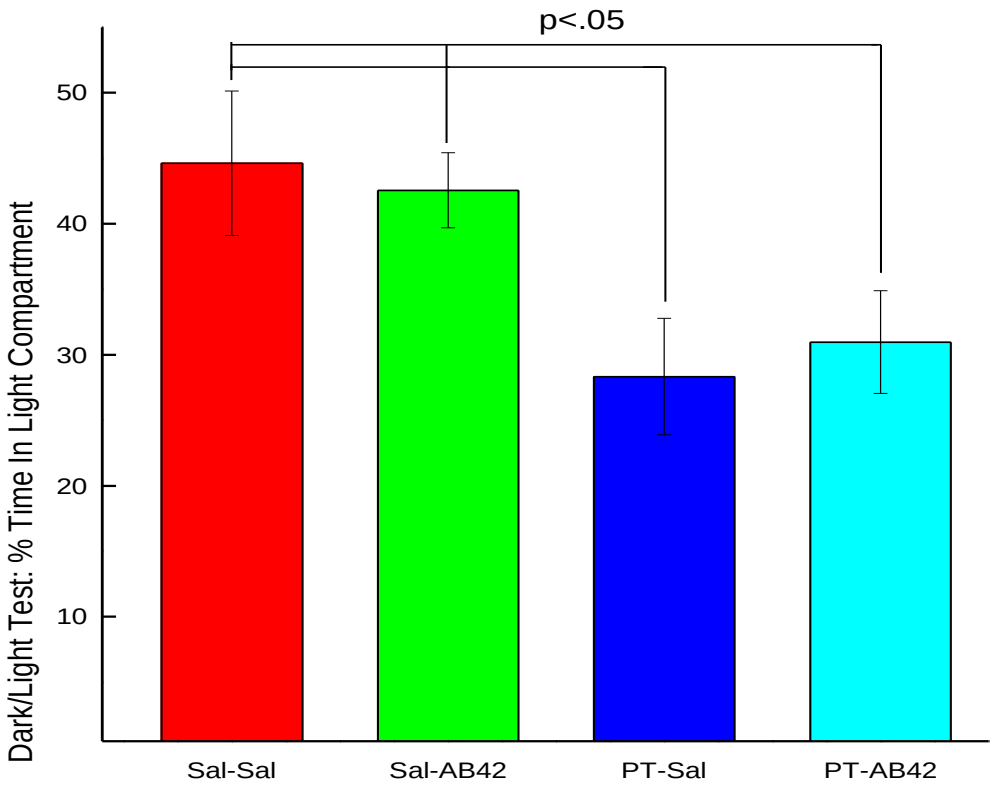
p<.05
Dark/Light Test: % Time In Light Compartment
50
40
30
20
10
Sal-Sal
Sal-AB42
PT-Sal
PT-AB42

Fig. 47

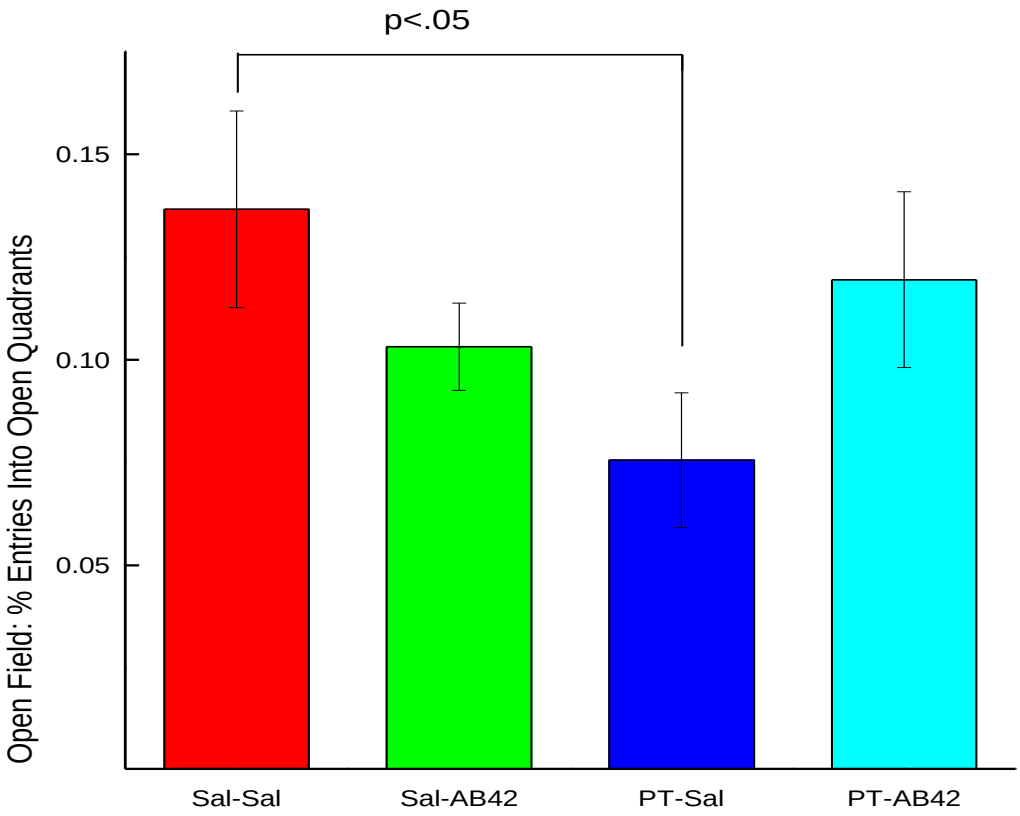
p<.05
0.15
0.10
0.05
Open Field: % Entries Into Open Quadrants
Sal-Sal
Sal-AB42
PT-Sal
PT-AB42

Fig. 48

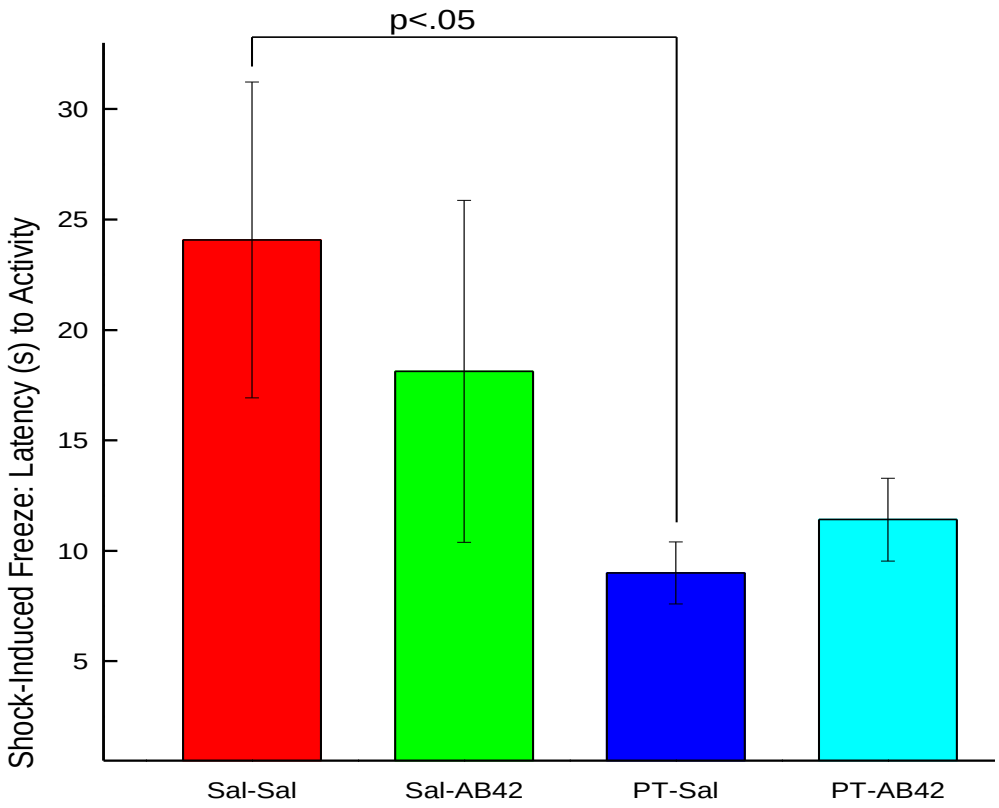
p<.05
Shock-Induced Freeze: Latency (s) to Activity
30
25
20
15
10
5
Sal-Sal
Sal-AB42
PT-Sal
PT-AB42

Fig. 49

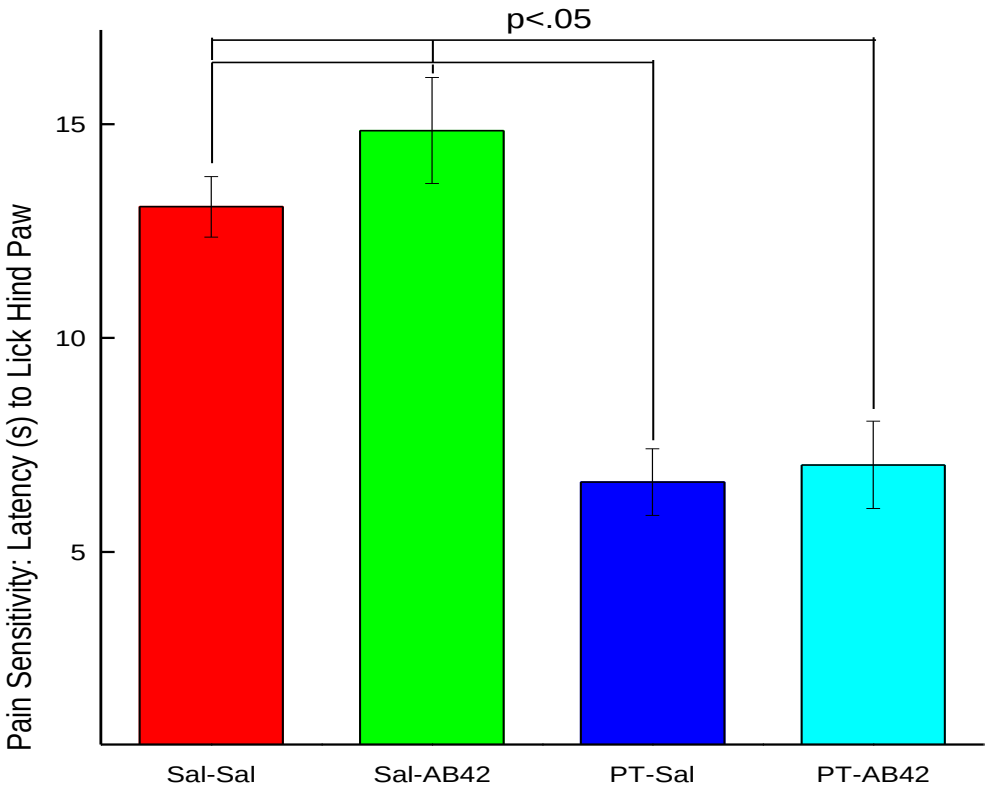
p<.05
Pain Sensitivity: Latency (s) to Lick Hind Paw
15
10
5
Sal-Sal
Sal-AB42
PT-Sal
PT-AB42

Fig. 50

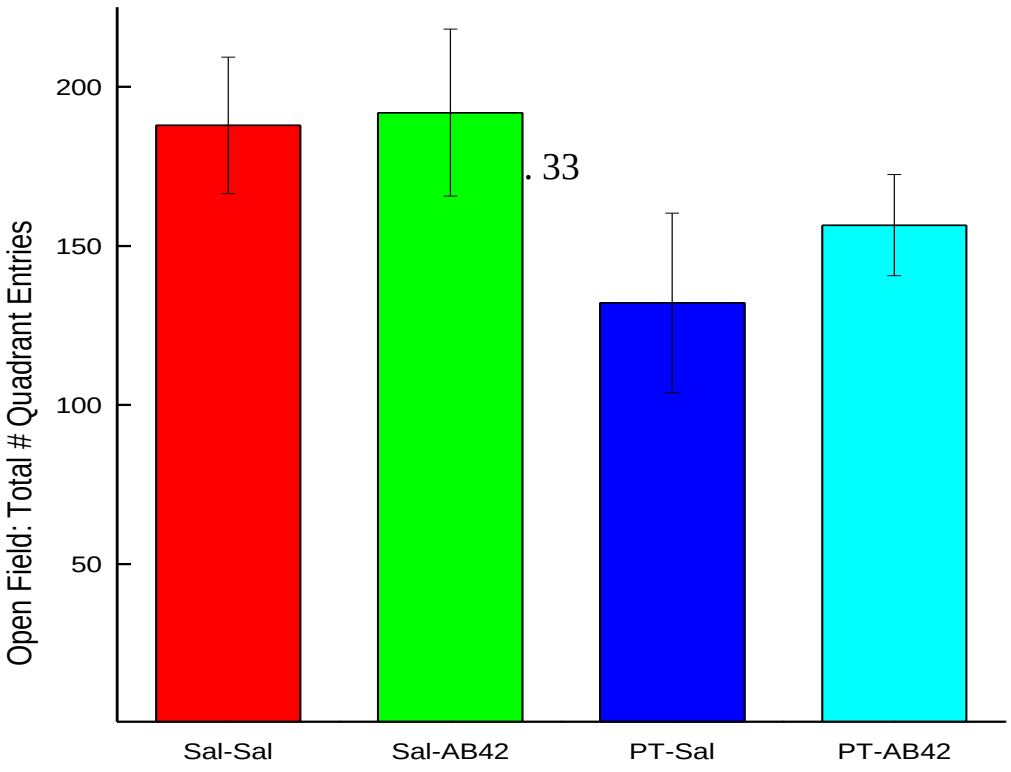
Open Field: Total # Quadrant Entries
200
150
100
50
. 33
Sal-Sal
Sal-AB42
PT-Sal
PT-AB42

Fig. 51

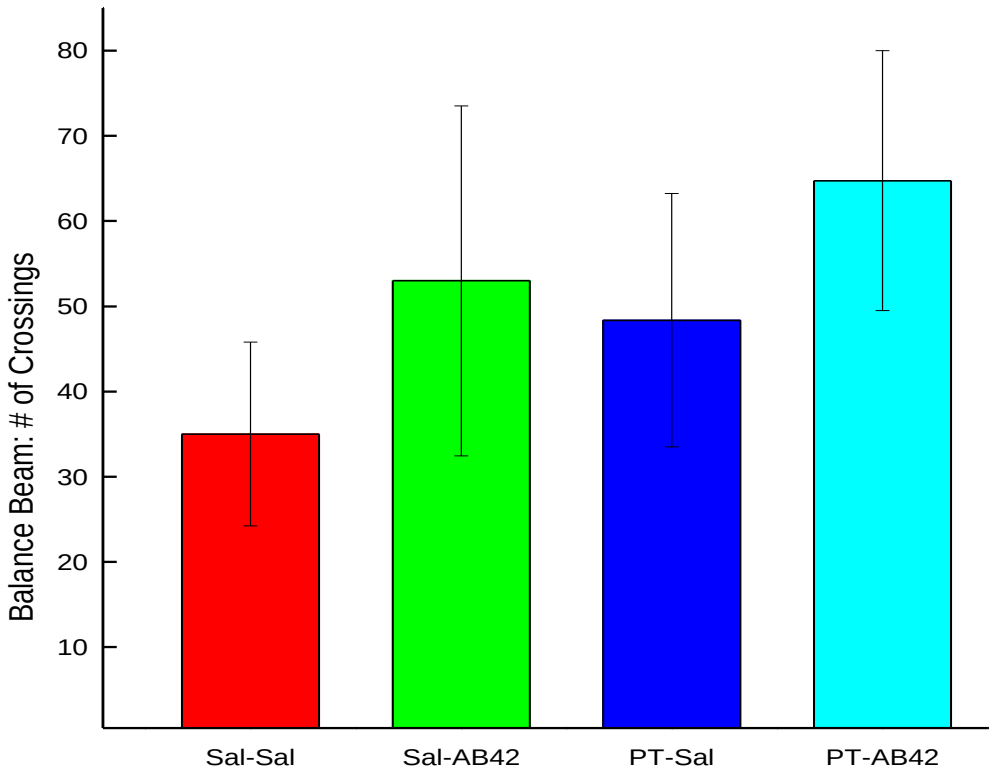
Balance Beam: # of Crossings
80
70
60
50
40
30
20
10
Sal-Sal
Sal-AB42
PT-Sal
PT-AB42

Fig. 52

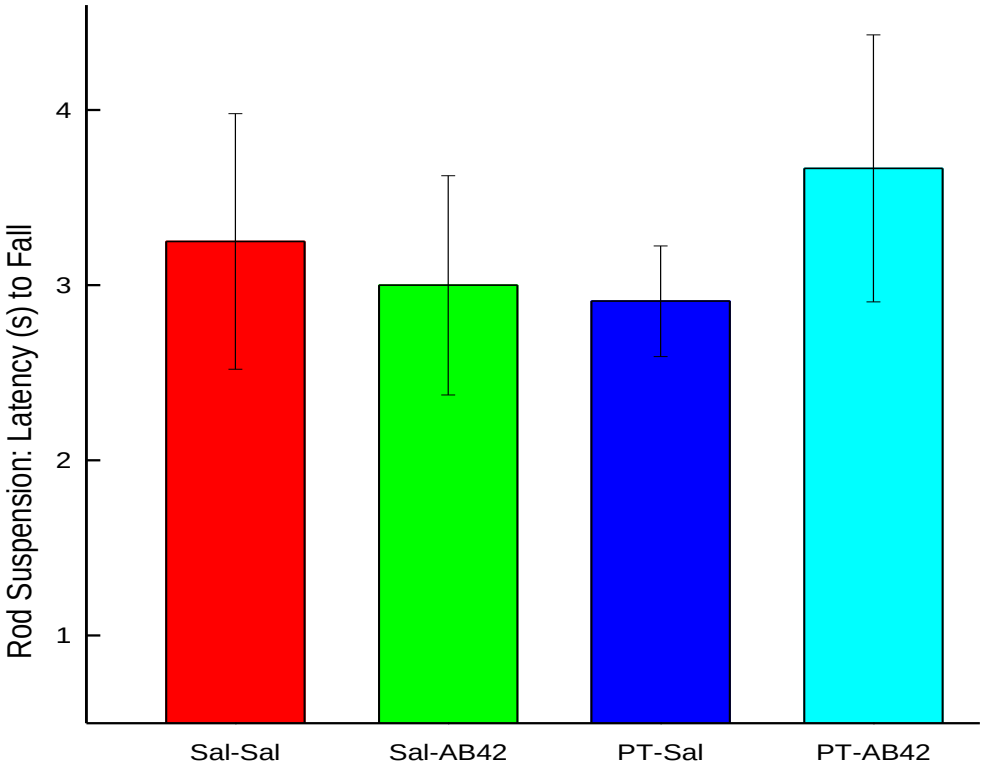
Rod Suspension: Latency (s) to Fall
4
3
2
1
Sal-Sal
Sal-AB42
PT-Sal
PT-AB42

Fig. 53

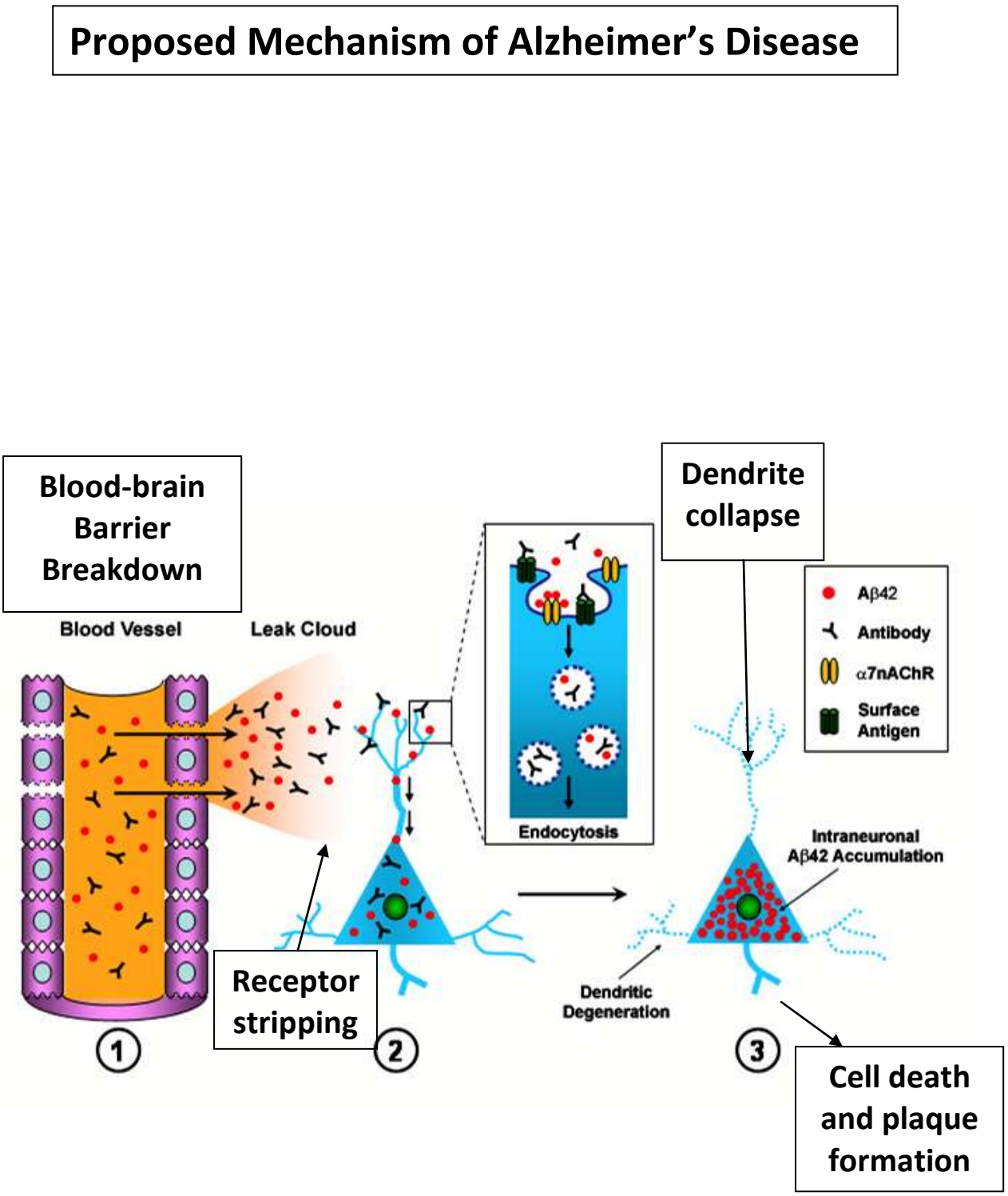
Proposed Mechanism of Alzheimer's Disease
Blood-brain Barrier Breakdown
Blood Vessel
Leak Cloud
Dendrite collapse
Aβ42
Antibody
α7nAChR
Surface Antigen
Endocytosis
Intraneuronal Aβ42 Accumulation
Receptor stripping
Dendritic Degeneration
1
2
3
Cell death and plaque formation

CURRICULUM VITAE

Henya C. Grossman

Education

Rutgers University, New Brunswick, NJ
M.S., Psychology, 2006

Queens College, City University of New York, Queens, NY
B.A., Psychology, Linguistics, 2002

Employment

Fellow, Department of Neurology, University of Pennsylvania, 2009 – 2010

Intern, Department of Neurology, Memorial Sloan-Kettering Cancer Center & New York Presbyterian-Weill Cornell Medical Center, 2008 – 2009

Graduate Teaching Assistant, Rutgers University, 2003 – 2007

Publications

Grossman, H.C., Clifford, P., Kumar, S., Kolata, S., Light, K., Libon, D., Nagele, R., Matzel, L.D. Blood-brain barrier compromise is associated with cognitive deficits and neuropathology characteristic of Alzheimer's disease. (in preparation)

Grossman, H.C., Libon, D., Matzel, L.D., Nagele, R. Vascular mechanisms underlying AD pathogenesis: A critical review and novel model for intraneuronal amyloid deposition. (in preparation)

Panyavin, I., **Grossman, H.C**., Libon, D.J. The cortical vs. subcortical controversy: Memory and executive function in Alzheimer's Disease, subcortical vascular dementia, and Huntington's Disease. (in preparation)

Matzel, L.D., **Grossman, H.,** Light, K., Townsend, D., Kolata, S. (2008). Age-related declines in general cognitive abilities of Balb/C mice are associated with disparities in working memory, body weight, and general activity. *Learning & Memory, 15(10), 733-46.*

Light, K.R., Kolata, S., Hale, G., **Grossman, H.,** Matzel, L.D. (2008). Up-regulation of exploratory tendencies does not enhance general learning abilities in juvenile or young-adult outbred mice. *Neurobiololgy of Learning & Memory, 90(2), 317-29.*

Matzel. L.D., Townsend, D., Babiarz, J., **Grossman, H**., Grumet, M. (2008). Nr-CAM deletion induces a cognitive and behavioral phenotype reflective of impulsivity. *Genes, Brain, & Behavior,7(4), 470-480.*

Grossman, H.C., Hale, G., Light, K., Kolata, S., Goldfarb, Y., Kusnecov, A., Flaherty, C.,Matzel, L.D. (2007). Pharmacological modulation of stress reactivity dissociates general learning ability from the propensity for exploration. *Behavioral Neuroscience, 121, 949-964.*

Kolata, S., Light, K., **Grossman, H.C**., Hale, G., & Matzel, L. (2007). Selective attention is a primary determinant of the relationship between working memory and general learning ability in otubred mice. *Learning & Memory,14, 22-28.*

Matzel, L.D., Townsend, D.A., **Grossman, H.C**., Han, Y.R., Hale, G. Light, K., Kolata, S. (2006). Novelty-seeking in outbred mice covaries with general learning abilities irrespective of stress reactivity, emotionality, and physical attributes. *Neurobiology of Learning & Memory, 86, 228-240*.

Kolata, S., Light, K., Townsend, D., Hale, G., **Grossman, H.C.**, Matzel, L.D. (2005) Variations in working memory capacity predict individual differences in general learning abilities among genetically diverse mice. Neurobiology of Learning & Memory, 84, 241-246.

Matzel, L.D., Han, Y.R., **Grossman, H.C**., Karnik, M.S., Patel, D., Scott, N., Specht, S.M., Gandhi, C. (2003) Individual differences in the expression of a "general" learning ability in mice. J Neurosci., 16, 6423-33.

Grossman, H.C., Hadjimarkou, M.M., Silva, R.M., Giraudo, S.Q., Bodnar, R.J. (2003) Interrelationships between mu opioid and melanocortin receptors in mediating food intake in rats. Brain Res, 991, 240-4.

Silva, R.M., **Grossman, H.C.**, Rossi, G.C., Pasternak, G.W., & Bodnar, R.J. (2002) Pharmacological Characterization of Beta-Endorphin and Dynorphin A(1-17)-induced feeding using G-protein alpha-subunit antisense probes in rats. *Peptides*, 23, 1101-6.

Silva, R.M., **Grossman, H.C.**, Hadjimarkou, M.M., Rossi, G.C., Pasternak, G.W., & Bodnar, R.J. (2002) Dynorphin A(1-17)-induced feeding: pharmacological characterization using selective opioid antagonists and antisense probes in rats. *J Pharmacol Exp Ther.*, 301, 513-8.

Presentations

Grossman, H.C., Libon, D., Nagele, R., Matzel, L.D. (2010) The effects of blood-brain barrier breach on amyloid deposition and cognitive function: A vascular model for

intraneuronal amyloid deposition in Alzheimer's Disease. International Neuropsychological Society.

Grossman, H.C., Libon, D.J. (2008). Differentiation of MCI subtype using a conceptual composite score on the Clock Drawing Test. International Neuropsychological Society.

Panyavin, I., **Grossman, H.C.,** Libon, D.J. (2006) Neuropsychological performance in Alzheimer's disease, subcortical vascular dementia, and Huntington's disease: the cortical vs. subcortical dementia controversy. American Academy of Clinical Neuropsychology, 4, and The Clinical Neuropsychologist, 20(2).

Grossman, H.C., Hale, G., Light, K., Kolata, S., Townsend, D. Matzel, L.D. (2005) The role of information processing rate in the relationship between general learning abilities and exploratory tendencies among genetically diverse mice. Society for Neuroscience, 30.

Kolata, S., Light, K., **Grossman, H.C**., Hale, G., & Matzel, L. (2005). Selective attention is a primary determinant of the relationship between working memory and general learning ability in otubred mice. Society for Neuroscience, 30.

Townsend, D., Hale, G., Light, K., Kolata, S., **Grossman, H.C**., Matzel, L.D. (2004) Age and sex influence on individual differences in domain-specific and general learning abilities in mice. Society for Neuroscience, 29.

Light, K., Kolata, S., Hale, G., **Grossman, H.C**., Townsend, D., Matzel, L.D. (2004) Effects of adaptation to novelty on general learning abilities in outbred mice. Society for Neuroscience, 29.

Kolata, S., Light, K., Townsend, D., Hale, G., **Grossman, H.C.**, Matzel, L.D. (2004) Variations in working memory capacity predict individual differences in general learning abilities among genetically diverse mice. Society for Neuroscience, 29.

Townsend, D., Hale, G., Light, K., Kolata, S., **Grossman, H.C**., Matzel, L.D. (2004) Age and sex influence on individual differences in domain-specific and general learning abilities in mice. Pavlovian Society.

Kolata, S., Light, K., Townsend, D., Hale, G., **Grossman, H.C**., Matzel, L.D. (2004) Individual differences in general learning abilities among genetically diverse mice are predicted by variations in working memory capacity. Pavlovian Society.

Light, K., **Grossman, H.C**., Townsend, D.A., Kolata, S., Hale, G., Matzel, L.D. (2004) The covariance of exploratory tendencies and general learning abilities is independent of variations in stress reactivity, emotionality, and sensory/motor function. Eastern Psychological Association.

Kolata, S., **Grossman, H.C.**, Townsend, D., Hale, G., Light, K., Matzel, L.D. (2004) Individual differences in stress reactivity do not account for variations in general learning ability in outbred mice. Eastern Psychological Association.

Grossman, H.C., Hadjimarkou, M.M., Silva, R.M., Giraudo, S.Q., Bodnar, R.J. (2002) Propopiomelanocortin gene products: interaction of feeding responses mediated by beta-endorphin and alpha melanocyte-stimulating hormone, *Society for Neuroscience*, 28.

Silva, R.M., **Grossman, H.C.**, Liu, P., Rossi, G.C., Pasternak, G.W., & Bodnar, R.J. (2001) Pharmacological and molecular characterization of dynorphin-induced feeding, *Society for Neuroscience*, 27.

Bodnar, R.J., Silva, R.M., Hadjimarkou, M.M., **Grossman, H.C.**, Liu, P., Rossi, G.C., & Pasternak, G.W. (2001) Beta-endorphin induced feeding: modulation by opioid receptor and g-protein antisense oligodeoxynucleotide probes, *Society for the Study of Ingestive Behavior*, 11.